Electrospinning piezoelectric fibers for biocompatible devices

Bahareh Azimi,

Dept. of Civil and Industrial Engineering, University of Pisa, Pisa, 56122, Italy.

Laboratory for Atomistic and Molecular Mechanics (LAMM), Massachusetts Institute of Technology, Cambridge, MA, 02139, USA.

Mario Milazzo,

Laboratory for Atomistic and Molecular Mechanics (LAMM), Massachusetts Institute of Technology, Cambridge, MA, 02139, USA.

Andrea Lazzeri,

Dept. of Civil and Industrial Engineering, University of Pisa, Pisa, 56122, Italy.

Stefano Berrettini,

Dept. of Surgical, Medical Molecular Pathology and Emergency Care, University of Pisa, Pisa, 56124, Italy

M. Jasim Uddin,

Dept. of Chemistry, Photonics and Energy Research Laboratory, University of Texas Rio Grande Valley, Edinburg, TX 78539, USA

Zhao Qin,

Laboratory for Atomistic and Molecular Mechanics (LAMM), Massachusetts Institute of Technology, Cambridge, MA, 02139, USA.

Markus J. Buehler,

Laboratory for Atomistic and Molecular Mechanics (LAMM), Massachusetts Institute of Technology, Cambridge, MA, 02139, USA.

Serena Danti

Dept. of Civil and Industrial Engineering, University of Pisa, Pisa, 56122, Italy.

Laboratory for Atomistic and Molecular Mechanics (LAMM), Massachusetts Institute of Technology, Cambridge, MA, 02139, USA.

Abstract

The field of nanotechnology has been gaining great success due to its potential in developing new generations of nanoscale materials with unprecedented properties and enhanced biological

responses. This is particularly exciting using nanofibers, as their mechanical and topographic characteristics can approach those found in naturally occurring biological materials. Electrospinning is a key technique to manufacture ultrafine fibers and fiber meshes with multifunctional features, such as piezoelectricity, to be available on a smaller length scale, thus comparable to subcellular scale, which makes their use increasingly appealing for biomedical applications. These include biocompatible fiber-based devices as smart scaffolds, biosensors, energy harvesters and nanogenerators for human body. This paper provides a comprehensive review of current studies focused on the fabrication of ultrafine polymeric and ceramic piezoelectric fibers specifically designed for, or with the potential to be translated towards, biomedical applications. It provides an applicative and technical overview of the biocompatible piezoelectric fibers, with actual and potential applications, an understanding of the electrospinning process and the properties of nanostructured fibrous materials, including the available modeling approaches. Ultimately, this review aims at enabling a future vision on the impact of these nanomaterials as stimuli-responsive devices in the human body.

Graphical Abstract

Electrospinning enables the production of smart fibers, including piezoelectric, with a length scale comparable to subcellular scale, therefore relevant for biomedical applications. This paper provides a comprehensive review on the fabrication of piezoelectric ultrafine fibers by providing an understanding of the electrospinning process, the obtained piezoelectric properties, the available modeling approaches, and their current and future applications in healthcare field.

Keywords

1. Introduction

The evidence of the piezoelectric effect was demonstrated in 1880 by the Curie brothers. They first used the term "piezoelectricity" since its original Greek meaning relates to pressure, namely "pressure electricity".[1] Since then, with the term piezoelectricity, scientists have been referring to the generation of electrical charges induced by mechanical stress (i.e., direct effect) and vice versa (i.e., indirect or converse effect).[2] Although piezoelectricity is a phenomenon widely found in nature, some synthetic and natural materials that belong to the family of ceramics and polymers have shown significant piezoelectric effects. Perovskite-structured ceramics, such as lead titanate (PT), lead zirconate titanate ceramics (PZT), lead lanthanum zirconate titanate (PLZT), and lead magnesium niobate (PMN) possess the highest piezoelectric properties.[3] However, the concerns about the toxic effects of lead oxides have driven the research seeking other piezomaterials for biomedical uses.[4–6] Consequently, in the last few years, researchers have focused on lead-free piezoelectric materials, aiming to obtain properties comparable to their lead-based counterparts.[7,8] The most important lead-free piezoceramics still possess perovskite-like structures and are barium titanate ($BaTiO_3$), alkaline niobates $(K,Na,Li)NbO_3$, alkaline bismuth titanate $(K,Na)_{0.5} Bi_{0.5} TiO_3$, barium zirconate titanate-barium calcium titanate (BZT-BCT) and $(Ba,Ca)(Zr,Ti)O_3$(BCZT).[9–11] In contrast to the

intrinsic fragility of these ceramics, with brittleness manifesting also at low tensile strains, piezoelectric polymers have lower density and are more flexible, stretchable, spinnable and, thus, ideal for wearable or implanted devices.[12,13]

Polymers entitled with piezoelectric properties and usable in contact with the human body include polyvinylidene fluoride (PVDF), polyamides, polyvinyl chloride (PVC), liquid crystal polymers (LCPs), Parylene-C, and some polyhydroxyalkanoates, such as poly-b-hydroxybutyrate (PHB),[14] (poly-3-hydroxybutyrate-3-hydroxy valerate) PHBV [15] and some natural biomaterials, such as silk, elastin, collagen and chitin.[16] Owing to their macromolecular nature, semi-crystalline polymers behave similarly to piezoelectric inorganic materials with the advantage of being much more processable and lightweight than piezoelectric ceramics.[4,17] Among the abovementioned polymers, PVDF and its copolymers, such as polyvinylidene fluoride-trifluoroethylene [P(VDF-TrFE)] and poly(vinylidene fluoride-*co*-hexafluoropropylene) (PVDF-HFP), show a high piezoelectric effect.[18] This character derives from the oriented molecular dipoles formed by a combination of mechanical deformation and electrical poling of the crystallographic phase β.[19] Indeed, the β-phase, which has fully trans-planar zig-zag conformation, is responsible for most of the obtained piezoelectric response due to its polar structure with oriented hydrogen and fluoride unit cells along with the carbon backbone. In addition, the remarkable properties of PVDF-based polymers (i.e., flexibility, transparency, good mechanical strength, and high chemical resistance due to the C-F bond) provide many advantages in a number of relevant healthcare applications, since PVDF is stable under the gamma radiation commonly used for sterilizing medical devices. Finally, similarly to piezoelectric ceramics, PVDF boasts chemical stability, biocompatibility and durability in the human body. Other less studied piezoelectric polymers such as PHB and PHBHV, are still biocompatible, but are biodegradable in the human body, thus being potentially ideal for transient bioimplants. PVDF, but also parylene-C for coating,PVC, Nylon, P4HB are among the ones already approved by the U.S. Food and Drug Administration (FDA).[4,20] P(VDF-TrFE) is a multifunctional copolymer of PVDF in which the β phase is promoted, and therefore the piezoelectricity, with respect to the homopolymer. In addition to the piezoelectric effect, P(VDF-TrFE) displays ferroelectric, pyroelectric and electro-cooling effects as well as superior dielectric permittivity. P(VDF-TrFE) can be handled to fabricate solid parts, films, textiles, and coatings. PVDF-HFP has a lower crystallinity when compared with PVDF, yet presents good ferroelectric and piezoelectric behavior. As the piezoelectric properties are highly dependent on the concerted organization of piezoelectric domains in the bulk materials, ceramics and polymers must be poled with approximately 2 kV·mm^{-1} to maximize their performance.[21]

Owing to their specific characteristics, piezoelectric materials have been used in several fields: ultrasonics, robotics, energy harvesters, energy conversion, aerospace, domestic industries, damage detection, automotive engines, sensors and actuators. Yet they still represent a valuable class of materials for bioengineering.[22–25] Furthermore, driven by the growing interest in nanofabrication, researchers have been studying piezoelectric materials at the nanoscale in order to make them a real option for diverse and high performance applications. [26] In particular, piezoelectricity has become very attractive for new generation biomedical nanodevices, as the length scales at which the biological interactions take place

approach those of cellular and extracellular components, thus revealing interesting modes for controlling and activating electro-mechanically sensitive cells and enabling innovative tools for nanomedicine. [27] Piezoelectric nanoceramics are being widely used and investigated, and consequently, the assessment of their possible toxic effects, is still a topic of debate. [28]

In view of this and due to the concerns over using toxic lead in health-related applications, scientists have been focused on how to apply new fabrication techniques to the production of lead-free and sustainable piezoelectric nanofibers.[23,29–31] Electrospinning, hence, is a relevant and flexible approach to easily manufacture one-dimensional (1D) nanostructures with a precise tuning of the main parameters (i.e., diameter, composition, and morphology). Electrospun piezoelectric fibers offer excellent properties as a consequence of their surface area-and size-dependent properties, so their employment in a large number of applications has been strongly encouraged.[32,33] However, it is noteworthy that the electrospinning of piezoelectric ceramics is more challenging if compared to their polymer counterparts because of the involvement of hydrolysis, condensation, and gelation reactions.[18] These issues have led to the development of a hybrid process combining electrospinning and sol-gel. This synergic approach allows different sizes, compositions, and morphologies of ceramic nanofibers to be exploited.[34] Similarly, piezoelectric polymers have received notable attention for numerous applications [13,35,36], including the case of electrospun composite fibers made of piezoelectric polymer matrices with nanoceramics as fillers, which can be obtained in a single-step process.[33]

The biomedical field has been taking advantage of these new approaches and scientific progress towards lead-free piezoelectric nanofibers: as examples, self-powered wearable or bio-implantable devices (e.g., nanosensors, energy harvesters, nano-generators), and bioactive scaffolds in tissue engineering.[22,37–40] New interesting approaches employing self-powered bio-implantable systems have also been investigated by integrating piezoelectric nanofiber-based devices inside the human body to convert biomechanical actions (i.e., cardiac/lung motions, muscle contraction/relaxation, and blood circulation) into electric power.[41–43]

Moreover, piezoelectric nanofibers have catalyzed interest for tissue engineering purposes due to their capability of providing electrical stimulation to promote tissue regeneration, thus acting as stimuli-responsive (known as "smart") scaffolds.[40,44] Indeed, piezoelectric electrospun fibers can provide a number of stimuli for cell growth, cell differentiation, and ultimately tissue function repair, including mechano-electrical, topographical, and physico-chemical stimuli. Submicrometric fibers as obtained via electrospinning can mimic the architecture of extracellular matrix fibrous proteins, thus enabling contact signals and mechanical support for the cells. New researches are focusing on implementing nanodevices able to combine piezoelectricity with biocompatibility to produce piezoelectric scaffolds for electro-mechanically responsive cells.[45]

The first patents of the electrospinning process date back to the early 1900s.[46,47] However, its use has become popular in the 20th century, in particular in the biomedical sector.[48] Therefore, electrospinning is considered a relatively young technique that allows the

fabrication of fibers offering specific properties useful in many fields (e.g., high surface area to volume ratio and tunable porosity). So far, more than 200 polymers have been processed for a large number of applications.[49,50] With this process, a polymeric solution is extruded from a needle in the presence of an electric field: once this latter overcomes the surface tension of the liquid, a continuous jet is projected onto a collector with a simultaneous evaporation of the solvent. A number of parameters (e.g., solvent properties, solution concentration and viscosity, applied voltage, geometrical and many other parameters) are thus implied in the final outcome, which make this technique as much versatile as complex. Depending on the collector used to deposit the material, it is possible to fabricate fibrous membranes with good mechanical properties such as high elasticity and high strain tolerance and both randomly oriented or aligned fibers, with diameters usually in the range of a few micron down to tens of nanometers, namely ultrafine to nanofibers.[51] These features make electrospun piezoelectric fibers key players health and human body, where such constructs can be used for self-powered wearable or implantable devices for environmental sensing, stimulating/rehabilitating and regenerating tissues, up to sustaining energy needs of any devices.

Highlighting and explaining the recent progress in electrospinning of different biocompatible piezoelectric materials, with a focus on their applications related to the human body, are the intent of this review (Figure 1). After a comprehensive review of biomedical applications of polymeric and lead-free ceramic electrospun piezoelectric fibers, the experimental procedures and techniques to clarify how the electrospinning process affects morphology and piezoelectric properties of the fiber mesh are presented and discussed. Then, mathematical and computational modeling to fabricate and optimize the properties of piezoelectric fibers and fiber meshes are reported. In the last section, this review encompasses the future prospects of electrospinning biocompatible piezoelectric fibers for biomedical applications.

2. Bio-applications of electrospun polymer-based piezo-fibers

Within the biomedical field, the applications of piezopolymers are much better developed and differentiated according to various tissues and devices than those of piezoceramics, in particular in the form of ultrafine fibers (Figure 2). In particular, the use of the fluoropolymers belonging to the PVDF family in human body application is largely approved for their chemical inertia and stability, as well as their processability. It is a fact that PVDF is not a biodegradable polymer: as a consequence, its natural uses concern flexible permanent devices, recently including those where a transduction function is requested. In fact, due to its piezoelectric properties and biocompatibility, PVDF has become a potential material also as a stimuli-responsive scaffolds for tissue engineering.

2.1. Tissue engineering scaffolds

Because of some specific functional properties, piezoelectric materials have found many current and potential bio-applications. Tissue engineering approach aims to restore faulty organs and tissues which cannot self-regenerate by developing biomaterial-aided biological substitutes. Biocompatible scaffolds are key components for tissue engineering, because

they can guide tissue growth and regeneration across a three dimensional (3D) space. As many parts of the human body, such as bone, dentin, tendon, ligaments, cartilage, skin, collagen, deoxyribonucleic acid (DNA), conceivably have bioelectrical activity and even piezoelectricity, new and challenging research fields are emerging based on the application of biocompatible piezoelectric polymers in active tissue engineering, so as to properly regenerate these specific tissues or heal/support injured functions by giving physiologically relevant bio-signals, such as the electric ones.[52–54]

Under the application of mechanical stress, piezoelectric biomaterials generate transient surface charge variations and subsequently electrical potential variations to the material without the requirement of additional energy sources or wired electrodes. PVDF and its co-polymers (e.g., PVDF-HFP, PVDF-TrFE) in the form of 3D scaffolds can thus provide electrical stimulation to cells to promote tissue regeneration. Since topography of the scaffold has a significant effect on cell behavior and cell morphology, selecting the most suitable design is essential.[55] Several piezoelectric structures including films, nanofibers, porous membranes and 3D porous bioactive scaffolds have been used for bone, muscle and nerve regeneration.[56] In these cases, electrospun piezoelectric nanofiber webs have shown great advantages due to the high surface to volume ratios, high porosity, but reduced pore size with respect to other scaffolding techniques.[57] Because of the fibrous nature of these meshes, pore interconnectivity is maximal; moreover, the internal and external morphology of fibers can be adjusted by controlling the processing parameters. Table 1 shows a comprehensive list of piezoelectric polymer-based fiber meshes fabricated by conventional and customized electrospinning techniques, which have been used or proposed for tissue engineering applications, as grouped by tissue type.

Orthopedic surgery accounts for an increasing market, as over two million bone grafting procedures are annually performed worldwide. However, the optimal bone regeneration and repair remains a challenge, especially in the cases of complicated healing and large defects. Innovative approaches try to mimic tissue physiology with new materials or growth factors. Bone is a tissue with piezoelectric constants similar to those of quartz, primarily by virtue of collagen type I, the main component of the bone organic extracellular matrix (ECM). For this reason, the application of piezoelectric materials in bone tissue engineering has been invoked to support tissue function. [81] Since the role of electric signals in bone is still poorly understood, several studies have investigated the effect of piezoelectric materials, by their properties and structure, in the osteogenic process.

For example, Timin et al. demonstrated that piezoelectric properties of PHB and polyaniline (PANi)-loaded PHB scaffolds promoted adhesion of human mesenchymal stem cells (MSCs) compared to that of the non-piezoelectric polycaprolactone (PCL) scaffolds.[65] Ribeiro et al. [58] investigated the osteogenic properties of PVDF fiber meshes, and poled and non-poled β-PVDF films by analyzing new bone formation in vivo. They concluded that bone regeneration does require mechano-electrical stimuli. In comparison to the film, the piezoelectric fibrous structure enhanced bone regeneration with evidence of inflammatory cell infiltration. The process parameters of electrospinning may also affect the piezoelectric output and thus biological response. Damaraju et al. [36] have prepared PVDF fibers by electrospinning at different voltages (12 kV and 25 kV) for bone tissue engineering. Human

MSCs cultured on PVDF produced at −25 kV scaffolds revealed the maximum alkaline phosphatase activity, an early marker of osteogenesis, in comparison to PVDF produced at −12 kV scaffolds and the tissue culture polystyrene (TCP) and also showed early mineralization by day 10, thus clearly indicating its potential for bone regeneration. 3D fibrous scaffolds of P(VDF-TrFE) with the greatest piezoelectric activity have also been shown to stimulate cell function in a variety of cell types.[62]

Moreover, different cells and tissues have revealed different sensitivity to piezoelectric signals. By mimicking the physiological loading conditions in structural tissues through dynamic loading of piezoelectric P(VDF-TrFE) fibrous scaffolds cultured with MSCs, it was interestingly demonstrated that lower levels of piezoelectricity promoted chondrogenesis (i.e., cartilage formation), whereas higher levels promoted osteogenesis (i.e., bone formation). This work is meaningful as it would allow stem cell fate to be controlled in difficult body settings, such as the osteo-chondral interface, by acting on the differential piezo-properties of the scaffolds. Scaffold topography, including surface texture, is also very important as it enhances the surface area for cell adhesion and ECM deposition, including bone matrix. Shifting from smooth to nanoporous surface in P(VDF-TrFE) ultrafine fibers can be obtained during electrospinning by changing the environmental conditions, such as relative humidity [82]. By using methyl ethyl ketone (MEK) as a solvent, the nanoporous structure of ultrafine fibers was obtained (Figure 3).

The cell culture results revealed that this piezoelectric polymeric scaffold induces human MSC growth and accelerates osteogenic differentiation. PVDF is a hydrophobic polymer. To improve the epiezoelectric properties and wettability of PVDF, Kitsara et al. [59] employed electrospinning and oxygen plasma post-modification for obtaining PVDF nanofibrous scaffolds. Osteoblast cultures showed better cell spreading and scaffold colonization in plasma-treated electrospun scaffolds with highly piezoelectric and hydrophilic properties (Figure 4). They also induced intracellular calcium transients and could stimulate excitable cells, namely, osteoblasts, without the need for an external power source, thus demonstrating the versatility of these devices for biological interactions. [59]

The electric properties of the scaffold surface also give signals influencing cell behavior, therefore several scientists are studying diverse ways to improve them. By applying positive and negative voltage polarities during electrospinning, Szewczyk et al. prepared two types of scaffolds, i.e., PVDF(+) and PVDF(−), to control their surface potential. They demonstrated that surface potential has a significant effect on cell shape and adhesion via filopodia and lamellipodia formation. Increased cell viability/proliferation was found in the PVDF(−) samples and they also exhibited a much higher cellularity in comparison with the PVDF(+) samples, since their surface potential (i.e., −95 mV) was very close to the membrane potential of MG63 osteosarcoma cells (−60 mV). Collagen mineralization was enhanced by tuning the surface potential of the fibers. After 7 days in osteoblasts culture, PVDF(−) scaffolds showed well-mineralized osteoid formation, therefore, it is entitled for the most efficient application in bone regeneration.[60]

Wang et al. investigated the effect of dynamic electrical stimulation on mouse osteoblastic cell (MC3T3-E1) adhesion and proliferation on annealed P(VDF-TrFE) and electrically

poled P(VDF-TrFE) scaffolds. The results highlighted that the cells were elongated and oriented along the direction of nanofibers. Electrical poling led to a higher β-phase content of the fiber meshes (69.2%) than annealing (46%) and subsequently higher cell proliferation rate [64]

To improve antioxidant and anti-inflammatory properties which are important for the regeneration of damaged bone, Jeong *et al.* developed composite PVDF nanofibers including polyhedral oligomeric silsesquioxane–epigallocatechin gallate (POSS–EGCG) conjugate. The presence of POSS–EGCG conjugate led to formation of 3D interconnected porous structures with improved piezoelectric and mechanical properties, which in turn enhaced the proliferation and differentiation of osteoblasts (MC3T3-E1) on the scaffold. [61]

As a part of the musculoskeletal system, also muscles can be affected by several damages. Among them, heart is a semi-striated muscle that plays a vital role, thus being the leading cause of death together with cancer. Electroactive polymers displayed an innovative potential for muscle tissue regeneration, since muscle reacts to electrical and/or mechanical stimulation and retains a hierarchical fibrillar structure.[83] Accordingly, Martins *et al.* [74] investigated the effect of polarization and morphology of electroactive PVDF nanofibers on the biological response of myoblasts. It has been shown that the negative surface charge on aligned PVDF scaffolds provided suitable stimuli for proper muscle regeneration.

Hitscherich *et al.* [77] demonstrated the potential application of electrospun P(VDF-TrFE) scaffold for cardiovascular tissue engineering. Their outcomes showed the desirable adhesion of cells that initiated spontaneous contraction within 24–48 h post seeding. Live/ dead assay also revealed 99.90% cell viability on day 3 and 99.70% cell viability on day 6 with no significant changes. To improve cell adhesion, Augustine *et al.* [79] generated a novel nanocomposite scaffold composed of ZnO NPs and P(VDF-TrFE) fibers to elicit hMSC proliferation and angiogenesis by exploiting the piezoelectric properties of its components and the reactive oxygen species (ROS)-mediated proliferation induced by ZnO NPs. By applying 2% w/w ZnO, the scaffolds were cytocompatible and supported cell adhesion. *In vivo* studies in rats have confirmed the nontoxicity of the P(VDF-TrFE)/ZnO scaffolds and their ability to promote angiogenesis. In another study, [67] Fe_3O_4 magnetic NPs have been added into P(VDF-TrFE) nanofibers. Under optimal conditions, the incorporated NPs were homogeneously dispersed inside the fibers without altering the piezoelectric crystalline phase of the P(VDF-TrFE) nanofibers. The results of a preliminary cell culture showed a good cytocompatibility of these composite fibers.

Gouveia *et al.* produced scaffold based on a PCL magnetic nanofilm (MNF) covered with P(VDF-TrFE) microfibers to preserve the contractility of cardiomyocytes and promote cell– cell communication. The maximum piezoelectric constant that was reached is $d_{14} = 11.1$ pm V^{-1}. The scaffold indeed promoted rat and human cardiac cell attachment and the presence of MNF increased contractility of the cardiac cells cultured in the scaffold.[84]

Piezoelectric fibrous scaffolds have also received considerable interest for neural tissue engineering, where electric signals are of utmost importance for nerve function.[66–72] Indeed, it is widely known that nerve damage, by traumatic, congenital and degenerative

diseases, often has a dismal prognosis for which many efforts are currently in place. Neural tissue engineering aims to restore nerve function by reducing the fibrous scar and connecting nerve segments, also aided by transplantation of neural stem cells. The particular micro/nanofibrous architecture of electrospun scaffolds, together with electrical activity, has appeared of great importance for such a challenge. Electrospun scaffolds can have random up to aligned fibers to simplify neurite extension via contact guidance. It has been verified that PVDF nanofibers may serve as instructive scaffolds for monkey neural stem cell (NSC) survival and differentiation, thus disclosing great potential for neural repair. Fiber alignment, which governs the stiffness and piezoelectric character of the scaffolds, had a significant effect on the growth and differentiation capacity of NSCs into neuronal and glial cells. This study also indicates that fiber anisotropy plays an important role in designing desirable scaffolds for tissue engineering.[66] Moreover, Lhoste *et al.*[67] demonstrated that the neurons cultured on aligned and plasma treated PVDF nanofibers showed an enhanced outgrowth of neurites in comparison to that observed on random nanofibers or aligned fibers without plasma treatment, which concur to support the fact that PVDF hydrophobicity/hydrophilicity ratio should be balanced to improve cell ingrowth within the fibers. [59]

The importance of fiber alignment in neural tissue engineering was confirmed by other studies, which have investigated the effect of fiber orientation and annealing process on neurite outgrowth.[70,71] Lee *et al.*[70] demonstrated that P(VDF-TrFE) aligned fibers directed the neurite outgrowth, while they extended radially on the randomly oriented P(VDF-TrFE) fibers. Annealing the scaffolds above the Curie temperature led to an increase of the amount of β-phase crystals, thereby enhancing their piezoelectric properties. Annealed aligned P(VDF-TrFE) fibers revealed the maximum neurite extension in comparison with annealed and as-spun random P(VDF-TrFE) scaffolds. Arinzeh *et al.*[71] concluded that the differentiation of human neural stem/precursor cells (hNSC/NPC) on electrospun piezoelectric fibrous scaffolds mostly induced the expression of neuron-like β-III tubulins, while on nonpiezoelectric laminin-coated plates, mainly nestin. Fiber morphology and contact guidance, crystallinity and consequently the piezoelectricity of the P(VDF-TrFE) scaffolds, alignment, and annealing of the microfibers had a significant effect on neurite extension and differentiation of hNSC/NPCs to neuron-like β-III tubulins.

In another study, Motamedi *et al.*[68] successfully prepared fully aligned PVDF nanofibrous high-surface area mat with enhanced piezoelectric properties by doping laser ablated Au nanoparticles (Au NPs) and investigated the application of these fibers in nerve tissue engineering. Their results showed that Au NPs/PVDF composite nanofibers have the ability to encourage the growth and adhesion of cells without any toxicity. Results also demonstrated normal proliferation beside elongated and spread out morphology after culturing for 24 h.

Differently, Lee *et al.*[72] reported that fiber alignment had no significant effect on the differentiation of neural stem/progenitor cells (hNPCs) into the neuronal lineage while annealing led to enhancement of neuronal differentiation which displays higher piezoelectricity, as indicated by the higher fraction of cells expressing β-III tubulin.

Recently, Wu *et al.* demonstrated aligned PVDF-TrFE fibrous scaffolds supported Schwann Cells (SCs) growth and neurite extension and myelination. SCs were oriented and neurites extended along the length of the aligned fiber. They concluded that aligned PVDF-TrFE fibers might play a significant role in directional axon regeneration and they might be a promising scaffold to restore the aligned anatomical structure of damaged spinal cord tissue. [73]

To improve piezoelectric properties, which could be useful in cochlear nerve stimulation in deaf persons, Mota *et al.* [69] added $BaTiO_3$ NPs inside the ultrafine PVDF fibers and showed that piezoelectric coefficients proportionally increased with $BaTiO_3$ concentration, namely about 2 times with 20% $BaTiO_3$ weight content (Figure 5). Preliminary *in vitro* tests using SHSY-5Y neural cells displayed increased viability under physiology-simulated culture conditions, thus implying efficiency of these composite as a suitable interface for neurites. The potential use of fibrous P(VDF-TrFE) as a scaffold for nerve stimulation is thus suggested.

Skin is a tissue rich in collagen type I fibers, which also contains mechanoceptors as sensorial cells. Therefore, it was considered for tissue engineering using electrospun piezoelectric polymers. Skin is in fact our main barrier towards the external world and can be damaged by wounds, burns and sores, which hamper its protective effect from infections, water content and temperature control in the human body. Human skin fibroblasts were cultured on a 3D fibrous scaffolds of P(VDF-TrFE), observing perfectly spindle shaped cells on day 7, which may hold promise for skin regeneration (Figure 6). [75] The efficacy of electrospun polyurethane/PVDF piezoelectric composites for wound healing application has been investigated. [76] The scaffolds were exposed to alternative deformation and shown higher migration, adhesion, and secretion in comparison to the pure polyurethane which led to faster wound healing. *In vivo* assays indicated that mechanical deformation of scaffold induced by animal movements led to enhancement of fibroblast activities due to the piezoelectric stimulation.

As shown, the applications of polymeric piezoelectric fibers in tissue engineering are many and include non-bioresorbable piezoelectric polymers, such as those of PVDF family, to take advantage of the highest piezoelectric properties. Electrospinning approaches are being developed to this purpose, in order to downscale electric signals to cellular level by means of ultrafine and nanometric fibers. In tissue engineering, the fiber orientation and surface properties may play key aspects, which are still under investigation. On the other hand, the importance of piezoelectric and electric signals in normal and pathologic states and their presence in biologic tissues is a topic of recent studies. As a consequence, even though the applications of piezoelectric fibrous materials have not reached the bedside yet, they are tremendously helping in comprehending the role of bioelectricity and the possibility to use it to induce, control, inhibit and accelerate tissue regeneration. It is expected that this topic would greatly increase, and even become dominant in the research of the near future.

2.2. Biosensors

A transducer is a device that can convert two different forms of energy due to its inherent properties. If energy is transformed to measure or detect a signal or stimulus in the

environment, the transducer properly functions as a sensor.[85] A biosensor is an analytical device, which is able to detect the chemical substance that incorporates a biological component with a physicochemical detector. Recently, novel biosensors that are based on biocompatible piezoelectric materials have received considerable attention. Polymer-based piezoelectric materials are flexible and can deform under smaller applied forces which makes them suitable candidate for detecting many mechanical-like signals in the human body, such as pressure sensing applications.[86] They are also able to detect and react to an electrical stimulus that can be used to perform a correction by deformations generated by mechanical actions (e.g., forces from pressures or vibrations).[87] Some outstanding applications include healthcare, health monitoring, motion detection, among others,[88–91] since they can detect human physiological signals, such as pulse and breathing.[92] Such signals will give information enabling vital function monitoring and life style awareness. For their flexibility, piezoelectric polymers are, indeed, suitable candidates for mechanical (pressure) sensors if applied onto skin or integrated inside wearable/portable electronics. Moreover, due to their piezoelectric effect, the polymer is able to change its polarization state under small external stimulation, and the response of the sensor is sufficiently fast.[93]

Biosensors using surface acoustic waves (SAWs) are also used to perform detection activities to find dangerous agents, both infectious and poisonous agents. [87] Piezoelectric polymeric devices with different structures have been proposed to get high sensitivity, flexibility, repeatability, and wide working range. In recent years, nano-/micro-structures, such as nanofibers, have been implemented into the basic polymeric structure to improve the performance of these transducers. Electrospun piezoelectric fibers have been reported to be biocompatible and have been considered promising for biological sensor applications (Table 2).

For their durability, chemical inertia and piezoelectric response, PVDF and its copolymers have easily found application as sensors. The key advantage of electrospinning relies on the possibility of maximizing the surface area within a flexible support, suitable for being in contact with the human body.

By using a mixture of DMF and acetone as solvents, Wang *et al.* [94] developed a force sensor based on electrospun PVDF nanofibers, meeting high flexibility and breathability, able to be exploited as a dedicated human-specific sensor. Furthermore, by adding a solvent with a low boiling point (e.g., acetone), it was observed also an increase of the β-phase structures. It has been demonstrated that electrospun PVDF fibrous membranes with high β-phase content and excellent piezoelectricity may be used as nanosensors.[95]

In another study,[97] a highly durable PVDF nanofiber-based sensor was fabricated on printed electrodes with silver nanostructures without any additional poling processes. Results revealed that the voltage and current were strongly influenced by the actual contact areas between the electrodes themselves and the PVDF nanofibers. Lang *et al.* [98] produced high-sensitivity acoustic sensors from PVDF nanofiber webs and results showed a sensitivity of 266 mV·Pa^{-1}, which was five times higher than the sensitivity of a commercial PVDF film device. In another research,[117] the assembled PVDF piezoelectric nano/micro-fibers

were used to develop a sensor-embedded garment able to identify specific human motions (e.g., skin wrinkle/eye blink and knee/elbow bending) (Figure 7).

Ren et al. [99] fabricated a pressure sensor using a P(VDF-TrFE) nanofiber web with several different concentrations of TrFE in the copolymer. As a result, the authors improved sensitivity reaching 60.5 mV·N^{-1} with the P(VDF-TrFE; 77/23) specimen. Finally, they also demonstrated that a P(VDF-TrFE; 77/23) sensor based allows a reliable measure for dynamic forces up to 20 Hz.

Beringer et al. [100] used aligned P(VDF-TrFE) nanofibers interfaced with a flexible plastic substrate to create a device able to evaluate the voltage response. This biosensor was capable of producing from –0.4 V to +0.4 V when loaded by cantilever force of 8 mN at 2 Hz and 3 Hz. This equipment can be also used to assess the electromechanical behavior of cellular-powered nanodevices. In another work, Persano et al. [101] developed bendable piezoelectric sensors based on P(VDF-TrFE) electrospun aligned nanofibrous arrays in a flexible piezoelectric nano-generator (PENG). The device had special piezoelectric properties and enabled high sensitivity to measure pressures up to about 0.1 Pa. Mandal et al. [102] studied the piezoelectricity in an electrospun P(VDF-TrFE) web by using polarized FTIR spectroscopy and electric signals from the pressure sensors based on the electrospun mesh. Furthermore, the feasibility of the electrospun P(VDF-TrFE) mesh was demonstrated for applications concerning both sensors and actuators.

Park et al. [103] have proposed a bendable and stretchable P(VDF-TrFE) sensor able to identify the movement of the skin on the neck induced by the pulsed behavior of the carotid, with a resolution of about 1 mm. P(VDF-TrFE) nanofiber meshes were drowned into an elastomeric matrix of polydimethylsiloxane (PDMS), which ensured the bendability and stability of the apparatus (Figure 8). Besides single PVDF and its copolymer P(VDF-TrFE), the polymeric nanofiber may be developed with other nanostructures, such as salts [105], ceramic nanoparticles [106–108,118], nanowires [109] and carbon nanotubes [110], aiming at boosting the piezoelectric properties. Accordingly, Dhakras et al. [105] studied the effect induced by the addition of a hydrated salt, $NiCl_2.6H_2O$, to an electrospun PVDF on the piezoelectricity. By using hydrated salt, the authors found an increase of the polar β-phase of about 30% and the device exhibited also a remarkable enhancing of the dynamic response.

Lee et al. [106] reported an electrospun uniaxially-aligned matrix of PVDF nanofibers (average diameter of 200 nm) with $BaTiO_3$ nanoparticles. It was noticed that the alignment enhanced remarkably the piezoelectricity. Moreover, the addition of the nanoparticles showed an increase in the output voltage when loaded with similar loads. In another attempt, the authors characterized $(0.78Bi_{0.5}Na_{0.5}TiO_3–0.22SrTiO_3)$ (BNT-ST) ceramic particles loaded in P(VDF-TRFE) nanofibers with various BNT-ST concentrations (from 0 to 80 w %), highlighting that contents of 60 w% of BNT-ST had improved homogeneity and enhanced piezoelectric performances.[107]

Augustine et al. [108] deposited ZnO loaded P(VDF-TrFE) nanofibers on $LiNbO_3$ surface acoustic wave (SAW) device to identify and estimate the cell proliferation in cultures used as

acoustic biosensors (Figure 9). Their results showed that the dispersion of ZnO NPs increased the β-phase in the electrospun biomaterials.

Another example of force sensor application used silver nanowires (AgNWs) that were dispersed in PVDF nanofibers to enrich the β-phase. [109] The AgNWs showed a good dispersion due to the good matching between the polymeric chain and the AgNW surfaces. This interaction led to an increase of the polar β-phase during electrospinning, which was imputed to the local field-dipole close to the AgNW surfaces inducing TTT structure stabilization.

Composite of the PVDF and carbon nanotubes (MWCNTs) have been electrospun on a hollow cylindrical near-field electrospinning (HCNFES) without any further treatment. [110] The improvement on the mechanical properties and on the piezoelectric features of the PVDF/MWCNT nonwovens revealed that the connection between the PVDF structures and MWCNTs can make the nucleation of β-phase content easier. The PVDF nanofibers owing high crystallinity have been manufactured into a highly long-life bendable wearable transducer, to be exploited for long-term care. In a similar fashion, Lou *et al.* [111] used graphene oxide (rGO) inside P(VDF-TrFE) nanofibers to form a pressure transducer, which can be used to monitor human pulse waves and muscle movements. They demonstrated that a platform where several aligned sensors can be used as a device to finely mapping pressures on a surface. Some further studies have used the composition of different polymers to produce nanofibers for biosensors applications.[112–115] For instance, Manesh *et al.* [112] developed a transducer composed of nanofibers of PVDF and poly(aminophenyl boronic acid) (PAPBA) able to detect little concentrations of glucose (1 – 15 mM) in less than 6 s.

Sharma *et al.* [113] have developed pressure sensors by using P(VDF-TrFE) nanoweb fibers for endovascular applications validating them *in vitro* with dedicated physiological conditions. By using core–shell electrospun fibers, significant improvements in signal intensity gain were observed when compared to PVDF nanofibers and, also, nearly 40-fold higher sensitivity was achieved with respect to P(VDF-TrFE) thin-film structures. They reported that these flexible nanofibers have a great potential to fabricate more durable and bendable pressure sensors for innovative treatments in surgery (e.g., catheters).

Abreu *et al.* [114] reported the fabrication of P(VDF-TrFE) nanofibers embedding a water-soluble polyaniline mixed with polystyrene sulfonic acid (PANi-PSSA) owing fibers up to ~ 6 nm in diameter. Furthermore, by adding the conducting polymer PANi-PSSA the surface tension can be reduced and, at the same time, the charge density of the solution increased. This addition allowed the uniformity of the fabrication and bead-free nanofibers at lower P(VDF-TrFE) concentrations which are more desired for sensor applications. In another attempt,[115] P(VF2-TrFE)/poly(3,4-thylenedioxthiophene)-poly(styrene sulfonate), composite nanofibers were generated by electrospinning with fibers up to ~15 nm in diameter. The use of conducting PEDOT-PSS for the fabrication of slender PVF2-TrFE nanofibers, with reduced concentrations of polymeric chains, makes these constructs ideal candidates for supersensitive biosensor applications.

Liu *et al*. fabricated a wearable self-powered sensor based on a flexible piezoelectric PVDF nanogenerator and placed it in different parts of body to monitor human respiration, subtle muscle movement, and sound frequency (i.e., voice) recognition. A physiological signal recording system was used to measure the electrical signals of the sensor corresponded to the respiration signals with good reliability and feasibility. Results showed that this active sensor has promising applications in evaluating the pulmonary function, monitoring of respiratory, and detecting of gesture and vocal cord vibration for in the recovery of stroke patients who have suffered paralysis.[116]

The diversified and high performing biosensor applications of electrospun fibrous meshes all in all disclose the great versatility of piezopolymer-based nanoscale approaches for detecting human body signals and/or molecules of interest. Wearable and personal technologies have become emerging scenarios for monitoring patient's vital functions and life style. Indeed, the ultimate purpose of wearable sensor devices is to connect via smartphone to domotics and telecommunication facilities for point-of-care medicine. Pervasive, miniaturized and smart sensing applications will thus represent the future of personalized healthcare and rehabilitation.

2.3. Energy harvesters

Implantable medical electronics (IMEs) can improve the quality of human life as diagnostic tools (e.g., heart beat, temperature monitoring, and blood pressure) for different pathologies affecting body organs, while supporting treatment (e.g., stimulation of brain and muscles). There is a strong interest to design smaller, lighter and more flexible IMEs to minimize the impact on human activities. One oft the most important features is flexibility such IMEs can be applied and the cyclic expansion–contraction movements of human body can be easily matched. Batteries are the most common power source for IMEs but they face some limitations such as achieving the maximum miniaturization and limited lifetime.[119]

Harvesting energy from intrinsic human body motions has been intensely studied in the recent years: furthermore, self-powered implantable devices able to scavenge energy from different natural sources have been developed to convert biomechanical energy into other usable energies.[42] Piezoelectric polymers are the most widely used generators to collect human-related biomechanical energy. Unlike electrostatic and electromagnetic materials, piezoelectric materials permit simple architectures for energy harvesters to be obtained, which, in turn, are desirable for micro-electromechanical system (MEMS) electronic devices. Accordingly, different piezoelectric harvesters have been developed.[20,120] However, only few attempts have been made to develop bulky piezoelectric energy-harvesters for implantable energy sources, due to specific requirements to meet when coupled with the human organs (e.g., non-regular and rough surfaces).[121]

Recently, some advancement for harvesters based on piezoelectric nanofibers has significantly helped to fix such issues. To meet the requirements of wearable electronics, flexible and large surface area PVDF and P(VDF-TrFE) fibers were obtained via electrospinning technology (Table 3). These fiber-based electronics are capable of being woven into textiles and integrated into cloths to harvest energy during human activities. [19,122–129]

The effect of electrospinning parameters on the β-crystal phase of the PVDF structures and piezoelectric energy conversion of randomly-oriented PVDF nanofiber constructs have been investigated by different studies.[122,123] In general, PVDF fibers with a uniform and fine structure displayed a higher β-crystal phase content and better piezoelectric performances. Liu *et al.* [125,126] demonstrated a cell-pattern method on random and aligned PVDF nanofiber meshes for energy harvesting applications (Figure 10). This study showed that PVDF nanofibers, when aligned, could be shaped into a bendable monolayer by using a dedicated collector which ultimately enriched the piezoelectric β-content without any other post-processing. This device gave rise to a remarkable contractile response at cardiac level. It was reported that this cell-based energy harvester is versatile to several applications concerning biomechanical energy scavenging from, for instance, heartbeat, blood flow, muscle stretching, or irregular vibrations.

Baniasadi *et al.* [12] quantitatively investigated how the annealing process affects the piezoelectric features of P(VDF-TrFE) nanofibers performing dedicated experimental tests on both meshes of nanofibers and on individual nanofibers.

Results revealed that the annealing process enhances the stiffness (i.e., Young modulus) and the piezoelectric constants of single nanofibers up to 50% - 60%, which may have relevant consequences for these applications. Furthermore, they showed the fabrication of highly deformable piezoelectric P(VDF-TrFE) polymeric constructs through twisting electrospun P(VDF-TrFE) nanofibers (Figure 11), finally getting a noticeable boost of the mechanical properties. The application of twisted fibers in piezoelectric constructs has also been demonstrated in other publications.[128,129]

He *et al.* [127] used electrospinning and subsequent hot pressing to produce P(VDF-TrFE) porous membranes for energy harvesting employment. Despite the high quantity of β-crystallites, the P(VDF-TrFE) electrospun membranes have not shown any piezoelectric behavior because of the random distribution of dipoles. As a matter of fact, the alignment of the dipoles in the crystallites, due a poling process, leads to the effective piezoelectricity. A recent study demonstrated that a hot pressed P(VDF-TrFE) electrospun membrane with beads revealed higher piezoelectric constant value ($d_{33} = 24.7$) if compared to bead-free membrane before hot-pressing ($d_{33} = 3.2$) which may be related to the easier poling of beads with respect to nanofibers. There have been several attempts to improve energy harvesting efficiency of PVDF and its copolymers nanofibers. In some previous work, some additives like inorganic salt,[130] inorganic piezoelectric nanoparticles and nanowires,[118,131–133] cellulose nanocrystals,[135] and multi-walled carbon nanotubes,[136] have been used into polymer solutions to form composites with attractive properties for energy harvesting devices.

Kato *et al.* [118] generated novel vibration energy harvester by using lead-free piezoelectric $(Na_{0.5}K_{0.5})NbO_3$ (NKN) ceramic particles dispersed in PVDF nanofibers. They demonstrated that this energy harvester can be used as power sources for transducers in omnipresent networks. The piezoelectric coefficient d_{33} of the harvester increased by using the highest amount of NKN particles (50%) and after corona poling which demonstrated that the particles were sufficiently polarized.

In one report, [130] twenty-six inorganic salts were doped into the PVDF nanofibers and their piezoelectric properties were studied to investigate the positive and negative influences of the salts on the electrospinning process. The obtained outcomes indicated that the optimum amount of unionized salt molecules with low dipole moments induced amorphous polymer phases to be transformed into a piezoelectric phase. The optimized piezoelectric voltage of a device made of $FeCl_3 \cdot 6H_2O$ doped nanofibers was 700% higher than that of a device with undoped nanofibers. Pereira et al. [134] have prepared electrospun PVDF, P(VDF-TrFE) and composite fibers of P(VDF-TrFE) with different sizes of $BaTiO_3$ on top of an interdigitated circuit in order to investigate the effect of ceramic filler on the efficiency of the scavenging process. Another study showed that the best energy scavenging performances were reached for pure P(VDF-TrFE) fibers which had less mechanical stiffness if compared to the copolymers and the composites. An average piezo-potential of 100 mV could be measured for constructs made of fibers and $BaTiO_3$ particles. This value is higher than the one achieved for the pure polymer matrix, along with a strong decrease in the piezo-potential by applying bigger fillers which acted as a defect and led to damping of the composite fibers. They have demonstrated that the reduction of the electromechanical efficiency affected by the intensification of the damping had a stronger implication with respect to the positive effect of the larger coupling coefficient of the fillers: the global result is a reduction of the power output.

Many studies have reported their flexible piezoelectric energy scavengers, i.e., nano-generators (PENGs), which have used lead-free piezoelectric nanofibers. [137,139–145,149] Due to their shape and their structural properties, PVDF nanofibers are excellent candidates as active building blocks in such nano-generators. Both single PVDF nanofibers and uniaxially aligned arrays can be used to produce these nano-generators. Single fibers can be directly positioned between pre-defined metal electrodes with high precision by near-field electrospinning.

Discussing the PVDF nano-generators, manufactured using conventional far-field electrospinning, Gheibi et al. [140] showed a direct manufacturing process for piezoelectric PVDF nanofiber meshes able to convert mechanical into electrical energy. In this case, the outputs are directly proportional to the technical features of the electronic devices used to store the electrical energy. They reported that many factors (e.g., polymer solution characteristics, shape of the collector) affect the fabrication of the electrospun constructs for wearable electronic textile applications. Fang et al. [141] developed nano-generators based on PVDF electrospun fibers, which achieved voltage output between 0.43 V and 6.3 V when subjected to vibrations with frequency content from 1 Hz to 10 Hz. Hansen et al. [142] published an energy scavenger, developed from the combination of a PVDF nano-generator and a biofuel cell, capable of collecting biomechanical energy from breathing or heartbeat. Moreover, they developed a compliant enzymatic biofuel cell to harvest energy from glucose/O_2 in biofluids. Results showed 20 mV and 0.3 nA with a fixed strain rate of 1.67%/s.

Wang et al. [143] proposed a bendable triboelectric and piezoelectric coupling a nano-generator based on P(VDF-TrFE) nanofibers with excellent flexibility. The sandwich-shaped nano-generator delivered peak output voltage, energy power, and energy volume power

density at 30 V, 9.74 µW, and 0.689 mW·cm^{-3} when stressed with a load of 5 N, respectively. The nano-generator has itself several advantages such as bendability, thickness tuning, and double coupling mechanisms. Mokhtari *et al.* [144,145] have introduced a compliant and lightweight nano-generator device based on PVDF nanofibers containing various additives (ZnO, CNT, LiCl, PANi). Researchers studied the influence of each different addition to the matrix to maximize the mechanical and piezoelectric properties, highlighting that the LiCl is definitely the best option.

In some studies, authors have fabricated a piezoelectric fiber-based nano-generator and energy harvesters by using a direct-write technique via near-field electrospinning (NFES). [146–150] A direct-write and in situ poled PVDF nanofiber-based nano-generator was developed and validated for wearable applications[147]. Wide PVDF nanofiber arrays were manufactured on a compliant PVC substrate via NFES. When the piezoelectric device was coupled on a human finger, the electrical results reached 0.8 V and 30 nA under bending-releasing at ~ 45°C. Moreover, a hybrid energy cell-based on the nanofibers was also generated to scavenge mechanical energy. This device could provide a renewable energy source with the ability of energy collecting from human-based mechanical motion. In another study [148], the researchers developed a flexible PVDF/PMLG [poly (γ-methyl L-glutamate)] energy harvester with the power of 637.81 pW and an efficiency of 3.3% generated by NFES process. Results showed that NFES process had a positive influence on the piezoelectric and mechanical properties of composite fibers.

Liu *et al.* [146] published a modified hollow cylindrical near-field electrospinning (HCNFES) to make PVDF energy harvesters with outstanding output properties. The advantage of HCNFES relies on both the strong mechanical stress generated from the rotation of the collector and the high voltage that synergistically promoted the alignment of the dipoles along a single direction, thus assuring the PVDF fibers good piezoelectric properties. Repeated mechanical strain of 0.05% at 7 Hz on PVDF nonwoven fiber fabric with a strain of 0.05% at 7 Hz produced a 76 mV and 39 nA (maximum peaks).

3. Bio-applications of electrospun ceramic-based piezo-fibers

The Restriction of Hazardous Substances Directive 2002/95/EC, namely, RoHS-1, adopted by the Member States in 2006, limited the use of some hazardous substances, such as lead, in electrical and electronic equipment. The life cycle assessment of lead-containing electronics is a subject of current studies, for example by the United States Environmental Protection Agency (EPA).

In addition to the high-tech waste problem, RoHS reflects the contemporary research in biological toxicology assessing the long-term effects of low-level chemical exposure on population, which has been associated with neurological, developmental, and reproductive changes. Therefore, there is much concern about the use of lead-containing ceramics in biomedical applications. In fact, even if the lead atoms are fixed in the crystalline structure, the possibility of debris, contact toxicity and, most of all, occupational diseases for workers, are discouraging the practical use of such ceramics, which are entitled with the best piezoelectric properties. Lead-free piezoelectric ceramics can be processed in the form of

fibers and also obtained as meshes by using specific technologies. This exciting possibility renders them versatile for many applications where membrane-shape devices are suitable to exploit target properties, such as filtration, support for catalysts, sensing, storage, or bioactive scaffolding. For their fully crystalline structure, ordered at atomic level, ceramics possess the best piezoelectric properties if compared with polymers. However, electrospun ceramic fibers are less known and for this reason their bio-application are still limited. A comprehensive panel of piezoelectric ceramic fibers fabricated by electrospinning, with their main employment in the biomedical field is presented in Table 4.

Materials such as $BaTiO_3$, metal oxides with perovskite structure, are widely employed for their excellent piezoelectric properties. Furthermore, the absence of lead and their stability at high temperatures make this material an optimal candidate for bioengineering applications, such as implantable devices.[121] Electrospinning of $BaTiO_3$ fibers has been considerably explored in the last years in the field of sensors[152,153,194], transducers [154,155] and ferroelectric random access memory (FRAM) devices.[30,156–158] However, a careful preparation of the precursors and annealing condition are essential to accurately prepare $BaTiO_3$ nanofibers.

For instance, McCann et al. [151] demonstrated how it is possible to fabricate ribbon-like nanofibers of $BaTiO_3$ with tunable aspect ratio where the topology of the fibers depends only on the concentration of $BaTiO_3$ precursor (Figure 12). At higher concentrations, hence, the solution deposits on the surface, resulting in constructs with double layers ribbon-like fibers: core (solution)/sheath (skin). In contrast, at lower concentrations, the skin formation decreases, with a subsequent isotropic shrinkage leading to a final cylindrical-like shape fiber. However, piezoelectric nanoribbons with rectangular cross-sections have been preferred due to their morphology and greater adaptability more adaptable to design and produce different types of devices.

A remarkable work related to the fabrication of hollow nanofibers for a new generation of sensors and actuators is represented by the work of Zhan et al. who co-electrospun the sol precursor of $BaTiO_3$ xerogel without any further polymer additive.[152] They concluded that the rheology of a spinnable sol is one of the main parameters to be taken into account to tune the diameter and the wall thickness of the nanofibers.

Following this approach, He et al. [153] fabricated an impedance-based humidity sensor with $BaTiO_3$ nanofibers. To prevent any clotting at the spinneret level, a small amount of additives, such as catalysts and salts, are usually employed and mixed with the solution. For instance, acetic acid is often used as a catalyst to regulate both the hydrolysis and gelation rates, stabilizing the electrospinning process. Although humidity sensors do not represent classical biomedical applications, we think that they have potential use in detecting physiological parameters, e.g. in body temperature control through sweating, thus concurring to health monitoring at a point-of-care.

Zhuang et al. [154] prepared $BaTiO_3$ nanofibers for transducer applications and demonstrated that a correct management of both the hydrolysis and the polymerization of the sol solution can be beneficial to the final surface morphology of the processed $BaTiO_3$ nanofibers. The

rheology of the sol-gel precursor was tuned using a proper amount of acetic acid as a catalyst and polyvinylpyrrolidone (PVP), usually dissolved in ethanol. Improved polycrystalline fibers were achieved by regulating the ethanol-to-acetic acid ratio to 8:3 v/v and the annealing temperature at 750°C. Bauer et al. [156] demonstrated a method for obtaining aligned $BaTiO_3$ nanofibers using a rotating copper wire drum collector (Figure 13), in which the alignment was maintained during calcination. The use of a rotating drum collector led to a large scale synthesis of electrospun ceramic nanofibers with enhanced piezoelectric properties, interesting for new devices and applications.

Li et al. [159] investigated the effect of annealing temperature and time on crystal structure and morphology of $BaTiO_3$ nanofibers. They demonstrated that by an annealing temperature at 600 °C for 8 h; it is possible to achieve a full crystallization of $BaTiO_3$, while keeping constant the grain size. On the other hand, some additives, such as ions, also can be introduced into the solution to affect the piezoelectricity of the material.[121,162–169] Zhuang et al. [121] reported on the influence of cerium ion concentration on crystal phase, microstructure, piezoelectricity and elasticity of $BaTiO_3$ nanofibers. By applying 0.6% Ce/Ba atomic ratio, the piezoelectric constant (d_{33}) of the fibers was calculated in about 42 pmV^{-1}, which was approximately two times higher than that of pure $BaTiO_3$ nanofibers. The transmission electron microscopy (TEM) images and nano beam diffraction (NBD) pattern of a single $BaTiO_3$ nanofiber with a diameter of 100 nm are depicted in Figure 14.

Energy harvesting is another application of piezoelectric nanofibers which can be used as one of the building blocks for nano-generators and nano-sensors of potential interest also in the biomedical field.[195]

Jalalian et al. [166,167] used sol-gel assisted electrospinning technique to fabricate very large piezoelectric lead-free $Ba(Ti_{0.80}Zr_{0.20})O_3-0.5(Ba_{0.70}Ca_{0.30})TiO_3$ (BTZ-0.5BCT) and lead free $(Ba_{0.85}Ca_{0.15})(Ti_{0.9}Zr_{0.1})O_3$ (BCTZ) nanofibers with high aspect ratio in morphotropic phase boundary area which can be applied as piezoelectric nano-generators with d_{33} = 180 pmV^{-1}. In another study, Sahoo et al. [168] also successfully prepared lead-free $(Ba_{0.95}Ca_{0.05})(Ti_{0.92}Sn_{0.08})O_3$ (BCTS) piezoceramic nanofibers using acetate precursors of its constituents with piezoelectric constant (d_{33}), dielectric constant (K) and remnant polarization (Pr) of 398 $pC\cdot N^{-1}$, 3485 and 8.1 $pC\cdot cm^{-2}$, respectively.

Lead-free alkaline bismuth titanate $(K,Na)_{0.5}Bi_{0.5}TiO_3$ (NBT) has been considered a good piezoelectric material due to environmental sustainability and biocompatibility.[196,197] Recently, scientists focused on NBT-based material electrospinning for specific applications, such as transducers [170], micro-electro-mechanical systems (MEMS) [31,171,172] and nano-sensors.[173] Chen et al. [31] have demonstrated that loading $Ba_{0.06}TiO_3$ inside $Na_{0.5}Bi_{0.5}TiO_3$ nanofibers led to an increase of piezoelectric properties from d_{33} = 66 pmV^{-1} to d_{33} =102 pmV^{-1}. Excellent piezoelectric properties may be attributed to the composition near the morphotropic phase boundary (MPB) of NBT-BT6 nanofibers which possesses an enhanced number of possible spontaneous polarization directions. In order to improve the humidity sensing of $(Na_{0.5}Bi_{0.5})0.94TiO_3$–$Ba_{0.06}TiO_3$ (NBT–BT6) electrospinning was used to produce nanofibers with the high specific surface area.[173]

By using bismuth nitrate, cerium nitrate, and titanium butoxide as resources, Jiang *et al.* [174] have synthesized cerium-substituted bismuth titanate (BCT) nanofibers with a uniform diameter and good nanocrystalline distribution for energy harvesting application. The Curie temperature of the fibers was higher than that of $Bi_{3.15}Nd_{0.85}Ti_3O_{12}$ nanofibers [175], and the piezoelectric coefficient of the fibers (d_{33}=124 pmV^{-1}), surpasses that of $Bi_{3.25}La_{0.75}Ti_3O_{12}$ (d_{33} = 101)[176], $(NaK)_{0.5}Bi_{0.5}TiO_3$ (d_{33} = 102 pmV^{-1}) [31] and Ce-doped $BaTiO_3$ nanofibers (d_{33} = 42 pm/ V).[121] Zhao *et al.* [180] have successfully prepared lead-free $Bi_5Ti_3FeO_{15}$ (BTF) and $Bi_{5-x}La_xTi_3FeO_{15}$ (x = 0, 1) (BLTF) nanofibers and have assembled the wool keratin-based biocompatible piezoelectric nano-generators (Figure 15).

BLTF nanofibers are biocompatible in biologic environment as confirmed by results with mice pre-osteoblasts MC3T3-E1. Cells grew successfully on the surface of nanofibers and were alive after 48 h. For the single BLTF nanofibers, a piezoelectric coefficient d_{33} = 39.11 pmV^{-1} was obtained, which was higher than that of BTF ceramic (d_{33} = 13.4 $pC \cdot N^{-1}$). [198] The improved piezoelectricity of the nanofibers came from the necklace-like structure by resulting in the counteraction of the clamping effects. Alkaline niobates compositions $(K,Na,Li)NbO_3$ have shown a good potential as biocompatible lead-free piezoelectric ceramics.[199] Jalalian *et al.* [167,183] have produced biocompatible piezoelectric bead-free $(Na,K)NbO_3$ nanofiber meshes with an average diameter of 150 nm which can be used as piezoelectric scaffolds for engineering, repairing and regenerating defective tissue. They concluded that the piezoelectric coefficient is strongly dependent on the orientation of ferroelectric domains in NKN fibers so that the d_{33} coefficients were 75.8 pmV^{-1} and 18.3 pmV^{-1} for out-of-axis and on-axis oriented ferroelectric domains respectively.[183]

Lead-free Mn-doped $(Na_{0.5}K_{0.5})NbO_3$ nanofibers have been used for fabrication of flexible nano-generators. The presence of Mn has improved crystallite growth, leading to the formation of single-particle-chain shaped nanofibers with the considerable enhancement of piezoelectric properties (d_{33}= 7.27 pmV^{-1} to d_{33}=40.06 pmV^{-1}).

ZnO is well-known as a semiconducting, piezoelectric, and photoconductive functional ceramic with a large excitation binding energy (60 meV). Recently, ZnO nanofibers have raised attention, due to their great potential for high-technology applications. [186–189] Chen *et al.* [189] have designed piezoelectric devices based on V–ZnO nanofibers for Micro-Electro-Mechanical Systems (MEMS) application. The average d_{33} of the $Zn_{0.975}V_{0.025}O$ nanofiber that was obtained is 121 pmV^{-1}, which was about one order of magnitude larger than that of pure ZnO bulk and thin films.[200] MEMS is a technology exploiting miniaturized mechanical and electro-mechanical elements obtained via microfabrication, which is becoming central in point-of-care medicine. There are a wide variety of applications for nanotech-aided MEMS devices in biotechnology and medicine, in particular as pressure sensors to monitor the patients' vital signs, like heartbeat, breathing, contactions, kidney dialysis, drug infusion pumps, adiuvants for biochemical analyses and so on.

Titanium and titanium-based nanofibers have a great potential in biomedical applications. They can be used as dental and bone implants since they are sensitive to neighboring bone surface without the creation of any fibrous tissue interface.[201,202] Bioactivated titanium oxide electrospun nanofibers have been produced as a template for the synthesis of

hydroxyapatite (HA) [Ca_{10} $(PO4)_6(OH)_2$] crystals.[190] To increase the biochemical activities, nanofibers were chemically treated with NaOH and HCl solution respectively and then HA was synthesized on their surface. The X-ray diffraction (XRD) results demonstrated the presence of HA crystals on titanate nanofibers.

Core/sheath ceramic nanofibers can be produced by coaxial electrospinning using two immiscible solutions. For creating ceramic hollow fibers, the core material can be removed by the selective method. Traditionally, a mineral oil is used as an inner solution and a conventional spinnable sol-gel solution is used as an outer solution to form the sheath structure.[152,203] During electrospinning, the sheath solution becomes more viscous through the rapid hydrolysis, condensation, and gelation and thus transmits its viscous stress to the core phase. Additionally, the *in situ* formation of a ceramic network can make the wall stronger, and thus prevent the oil core from smearing out during a rapid bending of the coaxial jet. The feeding rate of the inner solution also has a significant effect on the structure and diameter of the hollow fibers. By using a coaxial, two-capillary spinneret, Li *et al.* [191] have successfully fabricated a continuous aligned array of TiO_2 hollow nanofibers with round cross-sections which can be used for energy conversion, drug release and sensing applications (Figure 16).

Two different methods have been used to create hierarchical structures of electrospun ceramic based nanofibers. The first method is based on the *in situ* generation of nanostructures on the surface of nanofibers introducing the desired metal salts or metal alkoxides into the electrospinning solution. Using this method, Oysterman *et al.* [192] introduced V_2O_5 nanorods on the surface of TiO_2 nanofibers to create hierarchical ceramic nanostructures (Figure 17).

The second method is based on the post-treatment of electrospun nanofibers in a aqua based liquid bath to directly put the secondary structure.[204]

Wang *et al.* [193] have successfully produced the hierarchical structure of TiO_2 nanofibers containing high amounts of ZnO nanorods and nanoplates via a combination of electrospinning with a hydrothermal method (Figure 18).

As summarized above, lead-free piezoelectric ceramic nanofibers can be exploited in many fields. However, despite their advantages, few devices have been commercialized so far. The main reason dwells in the complex synthesis needed to build a structure limiting the fragile effects at low tensile strains. To improve usable features of oxide-based microfibers in biomedical applications, such as flexibility, piezoelectric properties and handleability, a deeper understanding of the sol-gel growth of the molecular structures from nucleation to the crystalline phase along with electrospinning process is necessary. This involves the selection of suitable component viscosity, precursors and post-treatments to obtain optimal morphology and piezoelectricity of ceramic fibers.

It has to be noted that, even if electrospinning ceramics is a much more difficult process than using polymers, on the other hand, due to the atomistic structure of ceramics, modeling can be easier to apply than in piezoelectric polymers. Many ceramics are biocompatible, some of them also biodegradable. Ultimately, several options are available to obtain the highest

piezoelectric effect. Therefore, more effort should be placed on the study of piezoelectric ceramic nanofibrous materials.

4. Electrospinning piezoelectric fibers

Although operationally easy, the electrospinning process is based on various working parameters, whose influence on the final properties of the fibers. Since the final properties of piezoelectric electrospun fibrous mesh play an important role in different biomedical device function, an in-depth understanding of electrospinning mechanism and the effects of its parameters on different properties of piezoelectric fibers is necessary. This section provides a comprehensive summary of electrospinning of piezoelectric polymeric and lead-free ceramic ultrafine fibers and describes how different processing parameters affect the final properties of the fibers.

4.1. Polymeric fibers

In the fifties, Fukada found piezoelectricity in various polymers, [205] but because of the weak electromechanical response, such polymers did not receive much attention. Among few synthetic polymers entitled with piezoelectric properties, PVDF and its copolymers have shown superior piezoelectric properties, which make them a desirable candidate for particular applications.[206] PVDF is a polymorph polymer with four crystalline phases: α, β, γ, and δ (Figure 19). The most piezoelectric configuration of PVDF is related to the polar structure of the β-phase with oriented hydrogen and fluoride (CH_2–CF_2) unit cells along with the backbone. [207,208] To increase the amount of the β-phase, dipoles should be aligned in the crystalline PVDF structures during the manufacturing process. [4,209] By providing both effects of mechanical stretching and electrical poling simultaneously, electrospinning may be a versatile method to increase the percentage of polar β-phase. [36,138,209–211] P(VDF-TrFE), a PVDF co-polymer, is also a semi-crystalline polymer with several stable crystalline forms which regardless of processing method always contains polar β-crystalline phase. This is related to the steric hindrance of TrFE in the copolymer, which forces PVDF into all-trans (TTTT) configuration (β-phase).[207]

Most dipoles of P(VDF-TrFE) are aligned in the transverse direction with respect to the fiber axis, during the electrospinning process. In aligned nanofibers, ordered crystallites are embedded within the ordered amorphous phase. The piezoelectric, ferroelectric, and mechanical properties of P(VDF-TrFE) nanofibers can be affected by the amount of crystalline phase and alignment of dipoles.[12] Then, near-field and far-field electrospinning have been used to produce PVDF single fiber, [117,149,212] as well as nano-fibrous structure of PVDF meshes, respectively.[213–219] It has indeed been demonstrated that aligned PVDF nanofiber arrays possess superior piezoelectric properties compared to random nanofibers meshes.[220–223] Hence, a very promising research topic is how the molecular configuration of piezoelectric polymers and their polymorphic states relate to the nanofiber geometry and how piezoelectric properties can be induced by electrospinning.

So far, it has been pointed out that a fine control of the morphology and amount of the different phases of electrospun piezoelectric nanofibers through the electrospinning parameters is essential. For example, polymer molecular weight and concentration of the

polymer solution, solvent type, electrospinning methodologies, applied voltage and flow rate, and needle-to-collector distance can all affect the morphological and piezoelectric properties of electrospun fibers. Different research groups have been investigating the effect of electrospinning parameters on the final properties of piezoelectric nanofibers (Table 5).

Solution viscosity has a fundamental role on the electrospun fiber morphology and on the limiting boundaries for the formation of fibers, including PVDF-based polymers. Solution viscosity is a function of both polymer concentration and molecular weight, which play similar roles on the morphology and diameter of electrospun fibers, based on the assumption that an elastically deformable entanglement network develops above a critical value of these two parameters. Indeed, during the electro-processing of polymer solutions, it has been observed that an increase in polymer concentration results in a morphology change, following the progression: *(i)* beads only, *(ii)* beads with incipient fibers, *(iii)* beaded fibers of different shapes, *(iv)* homogeneous, continuous fibers, until the concentration is raised at a certain critical value, beyond which the flow of the polymer solution through the needle tip is hampered, ultimately resulting in *(v)* defective nanofibers.[235,236] The increase in viscosity of the polymer solution has been acknowledged as the primary effect in this progression is sketched in Figure 20.

Zhao et al. [216] also reported that solution concentration and type of solvent had a significant effect on the morphology of the electrospun PVDF membranes. [218] The effect of concentration on the morphology and diameter of PVDF electrospun fibers has also been investigated by Matabola *et al.* who have observed that at PVDF concentrations below 22 w %, a combination of beads and fibers was generated by the electrospinning process. Increasing concentration up to 28 w% led to the formation of fibers with more consistent fibrous morphology and increasing fiber diameter consistently from 98 nm to 397 nm.[232]

Liao *et al.* [237] demonstrated that viscosity and conductivity of PVDF solution has a significant effect on fiber morphology. They showed that the presence of LiCl in the solution as an additive increased solution viscosity as a result of higher affinity between the salt and DMF/acetone than PVDF and improved polymer solution conductivity, which may manage the electrostatic interaction between DMF/Acetone and PVDF. A higher conductive polymer solution can generate a higher charge density on the surface of charged jet; higher charges thus result in a larger self-repulsion force, therefore, the fiber diameters become thinner as the fibers are ejected faster.

Proper additives have also been used in the electrospinning solutions to obtain pure β PVDF nanofibers. For example, Yu and Cebe showed that ion–dipole interactions between the PVDF chains and the organic modified nanoclay platelets as additive eliminate the non-polar α crystal conformers in the electrospun nanofibers.[238]

Li *et al.* also changed polymer solution conductivity using different kind of organic and inorganic salts. Salt-free PVDF nanofibers exhibited a common circular structure and had a uniform diameter with an average of 180 nm. Using organic branched salts in the polymer solution led to formation of tree-like nanofibers with a trunk fiber diameter of 100–500 nm and branch fibers diameter of 5–100 nm (Figure 21).

These authors deduced that the increased conductivity of the solution was the primary factor to form tree-like nanofibers and the organic branched salts, with longer carbon chains, had better effect on the tree-like structure than the inorganic salts.[239] The results also showed that incorporation of the tetrabutylammonium chloride (TBAC) in PVDF nanofiber increased the amount of β-phase, the degree of crystallinity and mechanical strength. TBAC as hygroscopic salt could maintain water in the fibers, thus resulting in hydrogen bonding between the fluorine atoms of PVDF and the water molecules and increasing the Trans conformers.

The evaporation rate of solvent strongly influences dimension, crystallinity, and homogeneity of the final polymeric fibers. For this reason, it is important to balance flow rate, tip-to-collector distance, applied voltage and choose the proper solvent mixture to obtain an optimal evaporation. N,N-dimethylformamide (DMF) has been demonstrated to be a good solvent for PVDF and P(VDF-TrFE) due to its high dielectric constant.[240]However, to promote faster solvent evaporation (due to its lower boiling point), and improve spinnability, the proper amount of MEK is usually added to DMF. [235]

Sencadas *et al.* [57] investigated the effect of applied solvents (DMF/MEK) on the morphology of electrospun P(VDF–TrFE) fibers. They concluded that inclusion of MEK to the solvent system promotes faster solvent evaporation allowing polymer crystallization in the jet traveling between the tip and the grounded collector, thus avoiding the presence of beads in the fiber mats. Wei *et al.* have reported the optimum solution concentration and the ratio of DMF/MEK for electrospinning of homogeneous PVDF fibers which are 19 w% and 8:2, respectively.[235]

The flow rate of the solution during the electrospinning strongly affects the evaporation rate of the solvent. The higher the flow rate, the lower the evaporation rate of the solvent and the larger the fiber diameter. This also causes the formation of beads and concurs to a broader distribution of fiber diameters.[57] Costa *et al.* [220] showed that high solvent evaporation rates favor the formation of α-phase. At slower evaporation rate, the forming fibers undergo higher elongation and strain rates which can align polymer chains, causing the transformation of α-phase to β-phase. [241]

Cozza *et al.* [215] used a different ratio of DMF/acetone as solvents for PVDF and obtained that low concentration of polymer, increasing content of DMF in the starting solution and a low flow rate are factors leading to large α-phase content during electrospinning.

By varying the needle-to-collector distance, both the flight time and the electric field strength are affected. At small distances, the jet has a reduced travelling time and the electric field will increase the acceleration of the jet. Accordingly, larger and wetter fibers are formed because of the insufficient time for solvent evaporation. As the distance is increased, fibers become thinner and drier, due to the longer time available for solvent evaporation and to the greater stretching of the fiber. Therefore, an optimum distance is required to allow the evaporation of solvent from the fibers and prevent bead formation. Motamedi *et al.* observed that the mean fiber diameter of PVDF nanofibers decreased with an increase of needle-to-collector distance.[241]

The applied voltage is the driving force of the electrospinning process. However, there is a dispute about the effect of applied voltage on PVDF fiber diameter. Some researchers have reported that increasing the applied voltage led to an increase in the fiber diameter (Figure 22). They concluded that at higher voltage, the polymer jet becomes highly unstable and produces thicker fibers with higher size distribution.[241] Other studies have reported that the formation of fine fibers is mainly achieved by the stretching and acceleration of jets in a high electric field. [36,211,242] The higher voltage applied can therefore result in a higher charge density on the surface of the jet. As a consequence, jet velocity is increased and increaded elongation forces are imposed to the jet. Consequently, the diameter of the final fibers becomes gradually smaller with increasing the applied voltage (Figure 22).

There is also no clear relationship between the applied voltage and the β-phase fraction. Some studies reported an ascending trend of β-phase content with increasing applied voltage. [243,244] In other reports, the fraction of β-phase was found to be enhanced by decreasing the applied voltage.[211] There are also a few studies which suggested that there is no voltage dependence. [215]

Jiyong *et al.* [221] indicated that the flow rate has the most significant effect on the β-phase fraction and the crystallinity with respect to applied voltages and needle tip diameter.

Temperature and relative humidity are also key environmental parameters playing an important role in the final properties of electrospun fibers. Increasing the relative humidity leads to the formation of nanofiber with a uniform diameter.[215] Huang *et al.* have investigated the effect of temperature on the formation, morphology, diameter, structure, and crystallinity of PVDF nanofiber via electrospinning. The FE-SEM and atomic force microscopy (AFM) observations revealed a decrease in nanofibers diameter with rising in temperature. They demonstrated that the surface morphology and crystalline structure of the electrospun PVDF nanofibers were significantly affected by the environmental temperature during electrospinning and improvement of crystallinity of the fibers could be attributed to the crystallization rate and solidified time. They observed that through an ambient temperature changing, the crystalline structure can be altered from a single structure, β, to multiple structures, α and β demonstrating the sensitivity of molecular chains movement to the ambient temperature.[245]

Besides the conventional electrospinning techniques, needleless disc electrospinning [19], centrifugal electrospinning, [225] and melt-electrospinning, [224] have also been used to fabricate piezoelectric nanofibers. PVDF nanofiber meshes fabricated by needleless technique have shown greatly enhanced energy conversion yield in comparison to the conventional needle-based nanofibers. Using centrifugal electrospinning at 200 rpm led to an increase of the piezoelectric response by ~27 times through fiber alignment and molecular poling alignment (Figure 23).[225]

In the electrospinning technique, the type of collector significantly influences the final characteristics of the fibers. The fibers diameter and alignment are markedly affected by the collector type and its rotation speed. The collectors are broadly classified in rotating and static collectors. Considering PVDF, many studies suggested that an increase of nanofiber

orientation leads to an optimized piezoelectric output. For this reason great efforts were made to control the arrangement of electrospun fiber.[2] It is important to point out that there are also some drawbacks associated with the use of different type of collectors. For rotating collectors, air turbulence generated by the fast motion is a limiting factor to produce aligned fibers. Using air shield can reduce air turbulence which leads to improvement of fiber alignment.

In some studies, a rotating ring or water bath have been used as a collector to produce piezoelectric nanofibers and yarns.[226–230] By using a modified rotating disk, Yee *et al.* [226] produced aligned PVDF fibers with the majority of β-phase crystallites along the axial direction of the nanofibers. The modified rotating disks had separate, parallel electrodes attached on the rotating disk, which can stretch the fibers in the air gap between the electrodes. They demonstrated that the electric field had more significant effect on the formation of the β-phase in comparison to the mechanical shear force while by using a modified rotating disk collector shown in Figure 24, they concluded that the effective stretching by the rotation disk led to the formation of highly oriented β-phase which is entirely different from their previous report.[227] Through this modification, the electric field between the separate electrodes and the mechanical force of rotational disk assist the fiber alignment. Polymer chains undergo tensile stress between the electrodes because of fast solvent evaporation and, simultaneously, crystallize via "sliding diffusion" to form extended chain β crystal.

Clearly, these findings indicate a shortage in the substantial understanding of the piezoelectric effects of nanofibers, which still deserve more empirical and theoretical efforts to be fully mastered.

Co-electrospinning has also been used to produce core-shell piezoelectric nanofibers made of different materials.[113,231] By using the co-electrospinning method, non-spinnable materials such as ceramics can be loaded into the polymer shell.

To improve the piezoelectric effects of nanofibers, several studies have been carried out aiming at adjusting the quantities of solvents and/or adding other nanomaterials. Some additives such as carbon nanotubes (CNTs),[212,222,227] ionic salts, [223,226,232,233] and ionic surfactant, [234] have been used in the solution to modify the piezoelectric properties of the fibers. For example,

Huang *et al.* [222] showed that the interfacial interaction between the single-walled carbon nanotubes (SWCNTs) and PVDF polymer chain can significantly increase the amount of oriented β form crystallites at a very low SWCNT concentration. By using only 0.00133 w% of the LiCl, Mokhtari *et al.* [223] fabricated PVDF nanofibers with piezo-response ability (8 V) four times higher compared to that of the pure nanofiber (1.89 V). Clarke *et al.* [233] reported that dispersion of ferrite ($Ni_{0.5}Zn_{0.5}Fe_2O_4$) NPs in a PVDF solution induced the arrangement of the polymeric chains in a fully extended configuration, thus enhanced the β-phase fraction. Nasir *et al.* [234] used an anionic surfactant in solution to produce PVDF nanofibers by electrospinning. All these findings corroborate the hypothesis that an interaction between the charge group of surfactant and the hydrogen atom or fluorine atom

of PVDF have the significant effect on the formation of the β phase structure during the electrospray process.

4.2. Ceramic fibers

At a glance, ceramics are considered materials suitable for electrospinning but, actually, it is possible to electrospin them after a pre-processing at high temperature, or via the sol-gel technique. Like other conventional spinning techniques to fabricate ceramic fibers, [246] electrospinning takes advantage of spinnable precursors.[247] To approach the electrospinning of ceramic materials, conventional sol-gels are mixed with other polymers to improve the viscosity of the mean with a subsequent calcination at higher temperatures to remove the organic components and allow the formation of the ceramics.[34,174,209] Some polymers, like Polyvinylpyrrolidone (PVP), poly(vinyl alcohol) (PVA), poly(vinyl acetate), polyacrylonitrile (PAN), poly(acrylic acid) (PAA), or poly(ethylene oxide) (PEO) have been used to act as a matrix to host inorganic precursors.[151,185,187,194,248–253] Sol-gel based electrospinning has become popular for its high purity and easy chemical doping.[174] In this process, the sol-gel reactions (i.e., hydrolysis, condensation, and gelation) take place in a confined environment, namely, the spinning jet and the final nanofiber. Moreover, the solvent rapidly evaporates due to the jet conditions and is quickly fixed in the fibers.

This process affects significantly the phase separation of the different parts of the final product. This unique feature is at the basis for the preparation of complex oxide ceramics, ceramic/polymer nanocomposites, and uniformly doped ceramics. The procedure consists of three main steps: *1)* preparation of a sol with appropriate inorganic precursors and polymers to get the correct viscosity of the material; *2)* spinning the material to get nanofibers; *3)* calcination, sintering, or chemical conversion of the precursor into the desired ceramic at high temperature, with simultaneous removal of all the organic components.[194] However, generating piezoelectric ceramic nanofibers by electrospinning is more challenging than their polymeric counterparts. Beside the needed evaporation of the solvents, all physico-chemical reactions occur in the air once the liquid jet is projected from the needle.

Consequently, it is important to correctly manage the process to have high-quality outcomes. [194,254] Only few studies have been carried out without any addition of polymers and by using only inorganic precursors (i.e., metal alkoxides or metal salts) and a solvent. [152,255–257] However, the inappropriate rheological properties and the rapid hydrolysis rates of metal alkoxides or metal salts make the control of the electrospinning process very difficult. [151] Finally, high-temperature post treatments, like calcination, can mobilize the dipoles putatively oriented during the electrospinning process, thus decreasing the final piezoelectric properties. A poling effect can be necessary, which in turn may result in increased fabrication costs. As a consequence, polymer/ceramic composite devices provided with specific surface modifications which enable higher piezoelectric effects without using poling treatments are under development.[258]

5. Modeling in electrospinning

As many parameters act on the final result, in the electrospinning process as well as in piezoelectric phenomena, the number of experiments to achieve an optimal result can be

high, thus leading to laborious and expensive trials. Aimed to facilitate the next progress in piezoelectric nanofiber fabrication, this review discloses the prime efforts and the potential role of mathematical and computational modeling. The complex structures get introduced at several different scale levels during the entire electrospinning process, including the self-assembly process of the ceramics and polymers that happens at the nanoscale (atomistic scale) under the shear stress within the microfluidic flow, as well as the fully guided spinning process of the fibers that happens at the micrometer scale that controls the fiber diameters and the architecture of the fibrous mat (topology).[259] The structure of the fibrous mat from electrospinning becomes very different from the piezoelectric crystal, as well as its physical properties. The physical properties, specifically for how its constitutive relation between electrical response and stress changes with the structural features at multiple length scales, will be quite different from the ceramics material *per se*.

Due to the structural complexity and the span of different scales, modeling at a single length scale will not be sufficient but it can be fully solved by developing its multiscale models. [260,261] Former study of silk materials has established a multiscale paradigm for learning the material physics of the silk network all the way from the silk sequence to the mechanics of the entire network structure.[262–265] The modeling includes the full atomistic structure of each silk peptide that studies how silk builds from single amino acids (at the length scale of 0.1 nm) to the β-sheet molecular structure (at 10 nm length scale) to achieve the high strength by using classical molecular dynamics with full atomistic description [265], the mesoscopic structure that studies how different silk molecules assemble into porous microfibril (at μm scale) of different structure and mechanics within the microfluidic environment by using the coarse-grained model[264,266], the further coarse-grained model that studies how microfibrils assemble into their bundles as individual silk fibers (at 10~100 μm scale) during wet spinning [263], and how silk fibers interconnected to form an entire network structure (at meter scale) with certain optimized mechanical functions.[262] For the study toward the rational design of the electrospinning of piezoelectric fibers, we can follow the same strategy and develop a series of finer-trains-coarser models at multiple length scales to investigate the full structure-function relations of the material.

5.1. Modeling the electrospinning process

Even though electrospinning emerges as a simple and easy fabrication approach, the influence of the process parameters is still not fully understood.[267] In fact, electrospinning is a complex process in which many physical factors concur to create the final fibrous structure: mechanics, electro-statics/dynamics and fluid dynamics. This latter, influenced by the others, plays a fundament role since the main process consists in producing solid fibers, whose diameters are in the order of magnitude of tens-of nanometers to few micrometers called "ultrafine"), from a liquid solution pouring out from a capillary tube with a millimetric nozzle.

The main parameters of this process can be roughly divided into three groups: solution parameters (concentration, molecular weight, viscosity, surface tension, conductivity/surface charge density), process parameters (voltage, flow rate, collector geometry, working distance, which is the distance as measured between the collector and the tip of the syringe

where the electrodes are placed), and environmental parameters (humidity, temperature)[268]. The electrospinning process includes three main steps [269]: 1) jet initiation, 2) jet elongation, and 3) jet solidification into fibers. The understanding of these different stages has required both experimental and modeling approaches.[270–272]

As for the first stage, one of the main achievements has been represented by the definition of the geometry of the cone which the fluid comes out from as a jet. Taylor *et al.* demonstrated that the optimal semi-vertical cone angle is about 49° and many further studies have independently demonstrated that the jet can be possible only with an angle close to 50° . [273–275] In addition to this, Taylor *et al.* also studied analytically the critical voltage V_c [kV] to get the jet fluid, represented by the following equation [272]:

$$V_c^2 = 0.117\pi r\eta\left(\frac{2h}{l}\right)^2\left(\ln\frac{2L}{R} - 1.5\right) \tag{1}$$

where *h* is the distance between the electrodes, *r* and *l* are the radius and the length of the capillary tube respectively and η the surface tension of the fluid in dyn·cm^{-1}.

The physical phenomena during the jet elongation are still a subject of investigation: in particular, many studies have been carried out to demonstrate the role of the nozzle geometry during this stage.[276–281] Concerning the last phase, the jet solidification, Yarin and his team described this stage with a quasi-one-dimensional equation on the mass/volume decrease due to the evaporation/solidification of the fluid.[282]

5.2   Modeling piezoelectric materials

A reliable and exhaustive model represents a useful tool for a better understanding of physical phenomena, including the prediction of the electro-mechanical behavior of a material. Scientists have been modeling piezoelectricity aiming at understanding the roles of the several players involved in the phenomenon by employing techniques that differ by time and length scales. The first approach concerns the atomistic/molecular scale in which the materials properties are investigated through the motion analysis of each atom composing the system. Mesoscale models (or coarse-graining models) aim, instead, at reducing the degrees of freedom of the samples by exploiting a simplified representation of the material. Finite Element models (FEM), eventually, are devoted to studying materials at the macroscale, by solving algebraic equations on a finite number of elements in which the system is discretized. Within the recent years, a new multi-scale approach aims to overlap the different scales in order to overcome the intrinsic limitations and reduce the computational cost, namely the amount of resources or time required to process a specific study.

From the molecular point of view, several attempts have been performed to evaluate how the deformation of primitive cells can affect the piezoelectric constants. Many atomistic studies have thus modeled primitive cells of ferroelectric materials, such as $BaTiO_3$ shown in Figure 25, [283] and III-nitrides (i.e., AlN, GaN, and InN).[284]

Other studies have focused on piezoelectric chains presenting molecular dynamics approaches to study nanowires of oxides (e.g., zinc oxide (ZnO)) by associating electric

charges to the atoms/molecules of interest.[284,286–290] However, the built models could reach sizes up to 5 nm to contain the computational costs.[291] Coarse graining models, trying to bridge the molecular scale to the macro scale, have been considered more complicated due to the difficulty in defining the correct inputs.

The constitutive equations of a piezoelectric material can be expressed through the Gibbs free energy, where the stress T and the electric induction D are functions of the magnetic field H, the temperature θ, the electric field E and the strain tensor S through appropriate constants.[292] Such a complex relation can be significantly simplified according to specific cases. In biomedical applications, the body temperature almost constant at 37°C and the absence of significant magnetic fields allow for a simplification of the equations as follows:

$$\begin{cases} T_p = c_{pq}^E S_q - e_{kp} E_k \\ D_i = e_{iq} S_q + \varepsilon_{ik}^S E_k \end{cases} \tag{2}$$

where the physic fields are coupled through constants that represent the elastic moduli (c_{pq}^E), the clamped permittivities (ε_{ik}^S) and piezoelectric coefficients (e_{kp}, e_{iq}).[293]

Eq. 2 can be also re-written in other three different forms, by deciding in advance which couple of the four fields (T, S, E, D) is to be considered unknown. Furthermore, for macro-applications it is possible to write Eq. 2 under strict approximations as follows:

$$\begin{cases} F_P = k_{PE} z + \alpha V \\ I_p = \alpha \dot{z} - C_p \dfrac{dV}{dt} \end{cases} \tag{4}$$

In this case, the restoring force F_P of the piezoelectric material and the outgoing current I_p are bonded to the displacement z, the velocity $\dot{z}$ and the voltage across the electrodes V through mechanical and electrical coefficients.[294]

5.3. Modeling single piezoelectric fibers

In the literature, only few papers have been published on the modeling of a single electrospun piezoelectric fiber[294] and the approaches pursued can be classified based on the analysis scale. Two techniques have been proposed for modeling on the molecular scale: the stochastic Monte Carlo method and the deterministic molecular dynamics method.[295] The first one leads to the static properties of the structure through a random sampling of the configurational space, while the second brings to the static/dynamic properties of the nanofibers using specific trajectories of the molecules in the configurational space. For both methods, the key point of the modeling approach relies on the evaluation of the intermolecular potential of the structure, which usually requires a significant computational effort.[296]

On the contrary, by approaching the problem at the macro-scale, it is crucial to understand which working principle has to be studied: for instance, concerning the specific case study in

which stress and electric fields dwell along the fiber axis direction (usually defined by the subscript *33*), Eq. 2 can be written as:

$$\begin{cases} T_3 = c_3^E S_3 - e_{33}E_3 \\ D_3 = e_{33}S_3 + \varepsilon_{33}^S E_3 \end{cases} \tag{5}$$

Assuming that the analysis is to be performed on a fixed-fixed fiber, as represented in Figure 26, subjected to an input voltage V_{in} at one end, it is possible to observe that the structure will be deformed transversally with the highest displacement in correspondence of the middle of the fiber ( ).

By choosing, for instance, the PVDF material, which owns a negative piezoelectric constant (e_{33}), a tensile/compressive strain ($\pm S_3$) occurs by considering a negative/positive voltage applied at one end. An interesting side effect also proved experimentally, consists on the buckling effect happening with a positive voltage that causes a repulsive force and a torque close to the fix end as well as a relevant electrostatic force on the lateral surface of the fiber. [212]

Other interesting considerations can be made by considering how the topology of the single fiber affects the piezoelectric response. Persano *et al.* modeled a single P(VDF-TrFE) piezoelectric fiber thus highlighting how a variation of the main geometrical features affects the output voltage with the same boundary conditions. The first case study involved a comparison between two fibers with distinct cross-sections (i.e., squared and circular with the same maximum diameter). FEM results obtained with a circular cross-section showed that the output voltage is more than two times higher with respect to the squared case. In both cases, the output voltage was found proportional to the length of the single fiber.[297]

A second case study, proposed by the same authors, relies on the sensitivity of the output voltage with respect to the ellipsoidal axes of the cross-section (Figure 27). Here, the variation of the output voltage is compared to the baseline represented by the circular cross-section, where the two axes are the same. The piezoelectric effect is definitely larger when the b-axis is longer of the a-axis rather than the opposite case.

5.4. Modeling meshes of piezoelectric fibers

In the case of aligned arrays of piezoelectric fibers, it has been shown that dense meshes own better performances than the single piezoelectric fibers. For instance, for the specific case of P(VDF-TrFE), a thick array can show an output voltage higher up to two orders of magnitude than that of single fibers.[101,149,298,299] In an interesting study, the authors pursued a FEM approach to study the cooperativity of P(VDF-TrFE) piezoelectric fibers organized in a mesh, considering two different cross sections (circular/squared) and two different packing strategies (horizontal/vertical) under the same boundary conditions. [297]

As depicted in Figure 28a, the horizontal packing showed a remarkable increment ratio for the output voltage (V_{out}) in the case of circular cross-section in contrast to the rectangular one, achieving performances about three times higher than the one of a single fiber reaching.

A saturation of the piezoelectric effect has been noticed after using more than four coupled fibers. On the contrary, using a rectangular cross-section, a horizontal packing does not change significantly the piezoelectric effect. A difference between the two cross-sections was observed also for the vertical packing where a quasi-linear trend was found as the number of fiber increases but without a clean-cut saturation (Figure 28b).

6. Conclusions and future perspectives

Piezoelectric nanomaterials are gaining significant attention in the healthcare field for their high biocompatibility and the related mechano-electrical properties usable in new and intriguing ways to repair, cure and enhance body functions. Electrospinning enables the production of piezoelectric fiber meshes with submicrometric size made of ceramics, polymers and composites. A number of parameters affect the sensitivity of piezo-transducers in general and nanofiber meshes in particular, including material choice, fabrication, post-treatment, and activation modes, whose extensive study requires large and expensive research efforts. As an *in silico* platform, material modeling is currently gaining an attracting interest being a tool with the high potential to describe physical phenomena, therefore to design and tune new materials generations. However, research studies are still looking to fill the gaps between different length scales, from molecular-to-macro scale, which is mainly due to the not full understanding of the physical phenomena as well as the limitations imposed by computational costs. Moreover, focusing on the macroscale applications, several attempts have still to be pursued in modeling the interactions of multiple fibers when embodied in randomly oriented meshes, as well as how the electrospinning process and composite materials may affect their piezoelectric properties. Forced electrospinning is one of the most versatile methods for preparing nanofibers with a wide range of parameters. Through the application of the sol–gel method, the capability of the electrospinning process has been successfully used to make different types of lead-free piezoelectric ceramic nanofibers. Long-term prospects in this area should look forward to the investigation of specific properties for biomedical applications. Although the advantages of lead-free piezoelectric nanofibers in some biomedical applications have been shown, only a few devices have been commercialized so far. For example, ceramic nanofibers for applications as biomedical implants, drug delivering, as transducers and as purification tools are still in their early stages and the potential advantages are still to be quantitatively evaluated. This is probably due to difficulties in the manufacturing process. Since on the nanoscale, many material properties drastically change if compared to those of macroscale counterparts, it has been shown with other ceramics including SiC that nanofibers can become flexible. [300] Researchers expect that, by further improving the process, and with a profound investigation of fiber properties, the lead-free piezoelectric ceramic nanofibers will have a brighter future in their biomedical applications.

Moreover, owing to the versatility, spin ability and biocompatibility of piezoelectric polymers, the use of piezoelectric polymer nanofibers is spreading in fields like tissue engineering to fabricate scaffolds, self-power implantable devices and electric clothing as well as some other general applications such as distillation membranes, [237,301–304] detection membranes,[305] and sound absorption devices.[306,307] Performing cell cultures on piezoelectric nanofibers might open a new landscape for regenerative medicine and tissue

engineering aided by electrical stimulation. The field of pressure sensors is also converging on piezoelectric wearable devices, which, being in contact or in proximity with a movable tissue or organ, can detect in a non-obstructive fashion, vital signs for telemedicine. As a matter of fact, wearable piezoelectric devices can take advantage of human body vibrational and mechanical energy to supply current battery-assisted medical devices (i.e., working as energy harvesters), such as hearing devices and pacemakers. The excellent differentiation in possible fields for piezoelectric nanofiber-based nano-generators makes them an attractive topic of research. A further application concerns the use of piezoelectric nanofibers as barrier membranes or in smart drug delivery systems or artificial pores wherein permeability of the drug across the membrane is triggered by an external electric field.[54] For each application, it would be advisable to master the key parameters for a uniform characterization of the piezoelectricity of electrospun nanofibers. To reach this goal, fundamentals of the piezoelectricity of nanofibers have to be studied methodically in all their aspects, including a multiscale modeling, to fabricate nanofibers with high piezoelectricity. Within the recent years, different studies have remarkably made the electrospinning process more usable: for example, some interesting new morphologies such as ribbon-like and multi-core cable-like of piezoelectric fibers have recently been outlined as a result of a detailed study on the electrospinning mechanisms.

Although several questions have still to be clarified, it is expected that a deeper understanding of piezoelectric phenomena in biomaterials, the improved ability in controlling the final properties via a better knowledge of the their relation with the fabrication process and a fine comprehension of the piezoelectric effects on cells and tissues will enable a relevant increase in using smart devices and scaffolds in healthcare, including, but not limited to, cancer treatment, green energy generation and Tissue Engineering.

Acknowledgments

References

[1]. Srinivasan A, Advances in polymer materials and technology. CRC Press; 2016.

[2]. Kázmierski TJ, Beeby S, Energy harvesting systems: Principles, modeling and applications; 2011.

[3]. Haertling GH, Journal of the American Ceramic Society 1999.

[4]. Kim TH, Thesis of Master 2015, 29.

[5]. Aksel E, Jones JL, Sensors 2010, 10, 1935. [PubMed: 22294907]

[6]. Liu W, Ren X, Physical Review Letters 2009, 103.

[7]. Safari A, Abazari M, 2010, 57.

[8]. Zheng L, Wang J, Wang C, Zang G, Ferroelectrics 2010, 404, 134.

[9]. Shrout TR, Zhang SJ, Journal of Electroceramics 2007, 19, 111.

[10]. Rödel J, Webber KG, Dittmer R, Jo W, Kimura M, Damjanovic D, Journal of the European Ceramic Society 2015, 35, 1659.

[11]. Panda PK, Sahoo B, Ferroelectrics 2015, 474, 128.

[12]. Baniasadi M, Xu Z, Hong S, Naraghi M, Minary-Jolandan M, ACS Applied Materials and Interfaces 2016.

[13]. Bowen CR, Kim HA, Weaver PM, Dunn S, Energy and Environmental Science 2014, 7, 25.

[14]. Fukada E, Ando Y, International Journal of Biological Macromolecules 1986.

[15]. Jacob J, More N, Kalia K, Kapusetti G, Inflammation and Regeneration 2018.

[16]. Pisignano D, Polymer Nanofibers: Building Blocks for Nanotechnology; 2013.

[17]. Ramadan KS, Sameoto D, Evoy S, Smart Materials and Structures 2014, 23.

[18]. Preumont A, Responsive Systems for Active Vibration Control NATO Science Series; 2001.

[19]. Fang J, Niu H, Wang H, Wang X, Lin T, Energy and Environmental Science 2013, 6, 2196.

[20]. Zheng Q, Shi B, Li Z, Wang ZL, Advanced Science 2017, 4, 1.

[21]. J. O. H. N. M. R. Eid, 2006.

[22]. Bystrov VS, Bdikin I, Heredia A, Pullar RC, Mishina E, Sigov AS, Kholkin AL, In Nanomedicine and Nanotoxicology; 2012.

[23]. Mokhtari F, Latifi M, Shamshirsaz M, Journal of the Textile Institute 2016, 107, 1037.

[24]. Coondoo I, Panwar N, Kholkin A, Journal of Advanced Dielectrics 2013, 03, 1330002.

[25]. Li F, Liu W, Stefanini C, Fu X, Dario P, Sensors 2010.

[26]. Wang ZL, Song J, Science 2006, 312, 242. [PubMed: 16614215]

[27]. Ciofani G, Danti S, Ricotti L, D'Alessandro D, Moscato S, Mattoli V, In Piezoelectric nanomaterials for biomedical applications; Springer, 2012; pp. 213–238.

[28]. Ciofani G, Danti S, Genchi GG, Mazzolai B, Mattoli V, Boron nitride nanotubes: Biocompatibility and potential spill-over in nanomedicine. Small 2013.

[29]. Chang J, Dommer M, Chang C, Lin L, Nano Energy 2012, 1, 356.

[30]. Sahoo PK, Panda B, Ceramics International 2012, 38, 5189.

[31]. Chen YQ, Zheng XJ, Feng X, Zhang DZ, Dai SH, Physica Status Solidi - Rapid Research Letters 2009, 3, 290.

[32]. Dong Z, Kennedy SJ, Wu Y, Journal of Power Sources 2011, 196, 4886.

[33]. Nunes-Pereira J, Sencadas V, Correia V, Rocha JG, Lanceros-Méndez S, Sensors and Actuators, A: Physical 2013, 196, 55.

[34]. Ramaseshan R, Sundarrajan S, Jose R, Ramakrishna S, Journal of Applied Physics 2007, 102.

[35]. Baniasadi M, Xu Z, Hong S, Naraghi M, Minary-Jolandan M, ACS Applied Materials and Interfaces 2016, 8, 2540. [PubMed: 26795238]

[36]. Damaraju SM, Wu S, Jaffe M, Arinzeh TL, Biomedical Materials (Bristol) 2013, 8.

[37]. Hannan MA, Mutashar S, Samad SA, Hussain A, BioMedical Engineering Online 2014, 13, 1. [PubMed: 24410918]

[38]. Ramsay MJ, Proceedings of SPIE 2001, 4332, 429.

[39]. Platt SR, Farritor S, Garvin K, Haider H, IEEE/ASME Transactions on Mechatronics 2005, 10, 455.

[40]. Rajabi AH, Jaffe M, Arinzeh TL, Acta Biomaterialia 2015, 24, 12. [PubMed: 26162587]

[41]. Hwang GT, Byun M, Jeong CK, Lee KJ, Advanced Healthcare Materials 2015, 4, 646. [PubMed: 25476410]

[42]. Il Park K, Lee M, Liu Y, Moon S, Hwang GT, Zhu G, Kim JE, Kim SO, Kim DK, Wang ZL, Lee KJ, Advanced Materials 2012, 24, 2999. [PubMed: 22549998]

[43]. Kim HW, Batra A, Priya S, Uchino K, Markley D, Newnham RE, Hofmann HF, Japanese Journal of Applied Physics, Part 1: Regular Papers and Short Notes and Review Papers 2004, 43, 6178.

[44]. Correia DM, Gonçalves R, Ribeiro C, Sencadas V, Botelho G, Ribelles JLG, Lanceros-Méndez S, RSC Adv. 2014.

[45]. Danti S, In Boron Nitride Nanotubes in Nanomedicine; 2016.

[46]. Morton WJ, Method of dispersing fluids. 1902.

[47]. Tucker N, Stanger JJ, Staiger MP, Razzaq H, Hofman K, Journal of Engineered Fibers and Fabrics 2012.

[48]. Ramakrishna S, Fujihara K, Teo WE, Yong T, Ma Z, Ramaseshan R, Materials Today 2006.

[49]. Haider A, Haider S, Kang IK, Arabian Journal of Chemistry 2015.

[50]. Chronakis IS, Journal of Materials Processing Technology 2005, 167, 283.

[51]. Greiner A, Wendorff JH, Electrospinning: A fascinating method for the preparation of ultrathin fibers. Angewandte Chemie - International Edition 2007.

[52]. Ribeiro C, Sencadas V, Correia DM, Lanceros-Méndez S, Piezoelectric polymers as biomaterials for tissue engineering applications. Colloids and Surfaces B: Biointerfaces 2015.

[53]. Telega R, Wojnar JJ, Journal of Theoretical and Applied mechanics 2002, 40, 723.

[54]. Wnek GL, Bowlin GE, Encyclopedia of biomaterials and biomedical engineering; 2008.

[55]. Shoichet MS, Macromolecules 2010, 43, 581.

[56]. Dhandayuthapani B, Yoshida Y, Maekawa T, Kumar DS, International Journal of Polymer Science 2011, 2011.

[57]. Sencadas V, Ribeiro C, Nunes-Pereira J, Correia V, Lanceros-Méndez S, Applied Physics A: Materials Science and Processing 2012, 109, 685.

[58]. Ribeiro C, Correia DM, Rodrigues I, Guardão L, Guimarães S, Soares R, Lanceros-Méndez S, Materials Letters 2017, 209, 118.

[59]. Kitsara M, Blanquer A, Murillo G, Humblot V, De Bragança Vieira S, Nogués C, Ibáñez E, Esteve J, Barrios L, Nanoscale 2019.

[60]. Szewczyk PK, Metwally S, Karbowniczek JE, Marzec MM, Stodolak-Zych E, Gruszczy ski A, Bernasik A, Stachewicz U, ACS Biomaterials Science and Engineering 2019.

[61]. Jeong H-G, Han Y-S, Jung K-H, Kim Y-J, Nanomaterials 2019.

[62]. Damaraju SM, Shen Y, Elele E, Khusid B, Eshghinejad A, Li J, Jaffe M, Arinzeh TL, Biomaterials 2017, 149, 51. [PubMed: 28992510]

[63]. Bahareh D. S. Azimi, D'Alessandro Delfo TL, Massimiliano Labardi, Andrea Lazzeri, In IPRS 2017; 2017.

[64]. Wang A, Hu M, Zhou L, Qiang X, Nanomaterials 2019.

[65]. Timin AS, Muslimov AR, Zyuzin MV, Peltek OO, Karpov TE, Sergeev IS, Dotsenko AI, Goncharenko AA, Yolshin ND, Sinelnik A, Krause B, Baumbach T, Surmeneva MA, Chernozem RV, Sukhorukov GB, Surmenev RA, ACS Applied Materials and Interfaces 2018.

[66]. Lins LC, Wianny F, Livi S, Dehay C, Duchet-Rumeau J, Gérard JF, Journal of Biomedical Materials Research - Part B Applied Biomaterials 2017, 105, 2376. [PubMed: 27571576]

[67]. Lhoste K, Département Chimie 2012, Doctor deg, 233.

[68]. Motamedi AS, Mirzadeh H, Hajiesmaeilbaigi F, Bagheri-Khoulenjani S, Shokrgozar MA, Journal of Biomedical Materials Research - Part A 2017, 105, 1984.

[69]. Mota C, Labardi M, Trombi L, Astolfi L, D'Acunto M, Puppi D, Gallone G, Chiellini F, Berrettini S, Bruschini L, Danti S, Materials and Design 2017, 122, 206.

[70]. Lee YS, Collins G, Livingston Arinzeh T, Acta Biomaterialia 2011, 7, 3877. [PubMed: 21810489]

[71]. Lee Y, Ph D, Arinzeh TL, 2012, 18, 1.

[72]. Lee YS, Collins G, Arinzeh TL, Proceedings of the 2010 IEEE 36th Annual Northeast Bioengineering Conference, NEBEC 2010 2010, 18.

[73]. Wu S, Chen MS, Maurel P, Lee YS, Bunge MB, Arinzeh TL, Journal of Neural Engineering 2018.

[74]. Martins PM, Ribeiro S, Ribeiro C, Sencadas V, Gomes AC, Gama FM, Lanceros-Méndez S, RSC Advances 2013.

[75]. Weber N, Lee YS, Shanmugasundaram S, Jaffe M, Arinzeh TL, Acta Biomaterialia 2010, 6, 3550. [PubMed: 20371302]

[76]. Guo HF, Li ZS, Dong SW, Chen WJ, Deng L, Wang YF, Ying DJ, Colloids and Surfaces B: Biointerfaces 2012, 96, 29. [PubMed: 22503631]

[77]. Hitscherich P, Wu S, Gordan R, Xie LH, Arinzeh T, Lee EJ, Biotechnology and Bioengineering 2016, 113, 1577. [PubMed: 26705272]

[78]. Bolbasov EN, Stankevich KS, Sudarev EA, Bouznik VM, Kudryavtseva VL, Antonova LV, Matveeva VG, Anissimov YG, Tverdokhlebov SI, Materials Chemistry and Physics 2016, 182, 338.

[79]. Augustine R, Dan P, Sosnik A, Kalarikkal N, Tran N, Vincent B, Thomas S, Menu P, Rouxel D, Nano Research 2017, 10, 3358.

[80]. Dias JC, Correia DC, Lopes AC, Ribeiro S, Ribeiro C, Sencadas V, Botelho G, Esperança JMSS, Laza JM, Vilas JL, León LM, Lanceros-Méndez S, Journal of Materials Science 2016, 51, 4442.

[81]. Fukada E, Yasuda I, Journal of the Physical Society of Japan 1957, 12, 1158.

[82]. Azimi B, Sorayani Bafqi MS, Uddin J, Trombi L, Danti S, Lazzeri A, In BiPoCo 2018 4th International Conference; Balatonfüred, Hungary, 2018; p. 134.

[83]. Bar-Cohen Y, Biomimetics using electroactive polymers (EAP) as artificial muscles - A review. Journal of Advanced Materials 2006.

[84]. Gouveia PJ, Rosa S, Ricotti L, Abecasis B, Almeida HV, Monteiro L, Nunes J, Carvalho FS, Serra M, Luchkin S, Kholkin AL, Alves PM, Oliveira PJ, Carvalho R, Menciassi A, das Neves RP, Ferreira LS, Biomaterials 2017.

[85]. Ciofani G, Mattoli V, Boron nitride nanotubes in nanomedicine; 2016.

[86]. Chorsi MT, Curry EJ, Chorsi HT, Das R, Baroody J, Purohit PK, Ilies H, Nguyen TD, Piezoelectric Biomaterials for Sensors and Actuators. Advanced Materials 2019.

[87]. Coté GL, Lec RM, Pishko MV, IEEE Sensors Journal 2003, 3, 251.

[88]. Hwang SH, Lee HJ, Yoon HN, Jung DW, Lee YJG, Lee YJ, Jeong DU, Park KS, IEEE Transactions on Biomedical Engineering 2014, 61, 2125. [PubMed: 24718565]

[89]. Baek HJ, Chung GS, Kim KK, Park KS, IEEE Transactions on Information Technology in Biomedicine 2012, 16, 150. [PubMed: 22086543]

[90]. Song A, Han Y, Hu H, Li J, IEEE Transactions on Instrumentation and Measurement 2014, 63, 1739.

[91]. Seminara L, Pinna L, Valle M, Basirico L, Loi A, Cosseddu P, Bonfiglio A, Ascia A, Biso M, Ansaldo A, Ricci D, Metta G, IEEE Sensors Journal 2013.

[92]. Lin Y, Leng H, Yang G, Cai H, IEEE Sensors Journal 2007, 7, 790.

[93]. Chen X, Han X, Shen QD, Advanced Electronic Materials 2017, 3.

[94]. Wang YR, Zheng JM, Ren GY, Zhang PH, Xu C, Smart Materials and Structures 2011, 20.

[95]. Zheng J, He A, Li J, Han CC, Macromolecular Rapid Communications 2007, 28, 2159.

[96]. Zheng GF, Wang X, Li WW, Lei TP, Tao W, Du J, Qiu QY, Chi XG, Sun DH, Dmf N, 2011, 2782.

[97]. Son HY, Nam YS, Kim WS, In Materials Research Society Symposium Proceedings; 2014.

[98]. Lang C, Fang J, Shao H, Ding X, Lin T, Nature Communications 2016, 7, 11108.

[99]. Ren G, Cai F, Li B, Zheng J, Xu C, Macromolecular Materials and Engineering 2013, 298, 541.

[100]. Beringer LT, Xu X, Shih W, Shih WH, Habas R, Schauer CL, Sensors and Actuators, A: Physical 2015.

[101]. Persano L, Dagdeviren C, Su Y, Zhang Y, Girardo S, Pisignano D, Huang Y, Rogers JA, Nature Communications 2013, 4, 1.

[102]. Mandal D, Yoon S, Kim KJ, Macromolecular Rapid Communications 2011, 32, 831. [PubMed: 21500300]

[103]. Park SH, Lee HB, Yeon SM, Park J, Lee NK, ACS Applied Materials and Interfaces 2016, 8, 24773.

[104]. Zampetti E, Bearzotti A, Macagnano A, Procedia Engineering 2014, 87, 1509.

[105]. Dhakras D, Borkar V, Ogale S, Jog J, Nanoscale 2012, 4, 752. [PubMed: 22234432]

[106]. Lee C, Wood D, Edmondson D, Yao D, Erickson AE, Tsao CT, Revia RA, Kim H, Zhang M, Ceramics International 2016, 42, 2734.

[107]. Ji SH, Cho JH, Jeong YH, Paik JH, Do Yun J, Yun JS, Sensors and Actuators, A: Physical 2016, 247, 316.

[108]. Augustine R, Sarry F, Kalarikkal N, Thomas S, Badie L, Rouxel D, Nano-Micro Letters 2016, 8, 282. [PubMed: 30460288]

[109]. Li B, Zheng J, Xu C, 2013, 8793, 879314.

[110]. Liu ZH, Pan CT, Yen CK, Lin LW, Huang JC, Ke CA, Applied Surface Science 2015, 346, 291.

[111]. Lou Z, Chen S, Wang L, Jiang K, Shen G, Nano Energy 2016, 23, 7.

[112]. Manesh KM, Santhosh P, Gopalan A, Lee KP, Analytical Biochemistry 2007, 360, 189. [PubMed: 17123457]

[113]. Sharma T, Naik S, Langevine J, Gill B, Zhang JXJ, IEEE Transactions on Biomedical Engineering 2015, 62, 188. [PubMed: 25095247]

[114]. Abreu M, Montañez S, Pinto NJ, Journal of Applied Polymer Science 2011, 119, 3640.

[115]. Martínez O, Bravos AG, Pinto NJ, Macromolecules 2009, 42, 7924.

[116]. Liu Z, Zhang S, Jin YM, Ouyang H, Zou Y, Wang XX, Xie LX, Li Z, Semiconductor Science and Technology 2017.

[117]. Fuh YK, Chen PC, Huang ZM, Ho HC, Nano Energy 2015, 11, 671.

[118]. Kato M, Kakimoto KI, Materials Letters 2015, 156, 183.

[119]. Ali F, Raza W, Li X, Gul H, Kim KH, Piezoelectric energy harvesters for biomedical applications. Nano Energy 2019.

[120]. Sun C, Shi J, Bayerl DJ, Wang X, Energy and Environmental Science 2011, 4, 4508.

[121]. Zhuang Y, Xu Z, Li F, Liao Z, Liu W, RSC Advances 2015, 5, 55269.

[122]. Shao H, Fang J, Wang H, Lin T, RSC Advances 2015, 5, 14345.

[123]. Baji A, Mai YW, Li Q, Liu Y, Nanoscale 2011, 3, 3068. [PubMed: 21713284]

[124]. Zandesh G, Gheibi A, Sorayani Bafqi MS, Bagherzadeh R, Ghoorchian M, Latifi M, Journal of Industrial Textiles 2017, 47, 348.

[125]. Liu X, Zhao H, Lu Y, Li S, Lin L, Du Y, Wang X, Nanoscale 2016, 8, 7278. [PubMed: 26976074]

[126]. Liu X, Wang X, Zhao H, Du Y, Journal of Physics: Conference Series 2014, 557.

[127]. He F, Sarkar M, Lau S, Fan J, Chan LH, Polymer Testing 2011, 30, 436.

[128]. Baniasadi M, Huang J, Xu Z, Moreno S, Yang X, Chang J, Quevedo-Lopez MA, Naraghi M, Minary-Jolandan M, ACS Applied Materials and Interfaces 2015, 7, 5358. [PubMed: 25691363]

[129]. Yang E, Xu Z, Chur LK, Behroozfar A, Baniasadi M, Moreno S, Huang J, Gilligan J, Minary-Jolandan M, ACS Applied Materials and Interfaces 2017, 9, 24220.

[130]. Yu B, Mao M, Yu H, Huang T, Zuo W, Wang H, Zhu M, Macromolecular Materials and Engineering 2017, 302, 1.

[131]. Corral-Flores V, Bueno-Baqués D, Ferroelectrics - Material Aspects 2009, 518.

[132]. Baji A, Mai YW, Li Q, Liu Y, Composites Science and Technology 2011, 71, 1435.

[133]. Zeng W, Tao XM, Chen S, Shang S, Chan HLW, Choy SH, Energy and Environmental Science 2013, 6, 2631.

[134]. Nunes-Pereira J, Sencadas V, Correia V, Rocha JG, Lanceros-Méndez S, Sensors and Actuators, A: Physical 2013.

[135]. Fashandi H, Abolhasani MM, Sandoghdar P, Zohdi N, Li Q, Naebe M, Cellulose 2016, 23, 3625.

[136]. Laxminarayana K, Jalili N, Textile Research Journal 2005, 75, 670.

[137]. B. Lee, B. Park, H. Yang, J. W. Han, C. Choong, J. Bae, K. Lee, W. Yu, U. Jeong, U. Chung, J. Park, O. Kim, 2014.

[138]. Gheibi A, Latifi M, Merati AA, Bagherzadeh R, Journal of Polymer Research 2014, 21.

[139]. Huang T, Wang C, Yu H, Wang H, Zhang Q, Zhu M, Nano Energy 2014, 14, 226.

[140]. Gheibi A, Bagherzadeh R, Merati AA, Latifi M, Journal of Polymer Research 2014, 21.

[141]. Fang J, Wang X, Lin T, Journal of Materials Chemistry 2011, 21, 11088.

[142]. Biomechanical H, Hansen BJ, Liu Y, Yang R, Wang ZL, 2010, 4, 3647.

[143]. Wang X, Yang B, Liu J, He Q, Guo H, Yang C, Chen X, Proceedings of the IEEE International Conference on Micro Electro Mechanical Systems (MEMS) 2015, 2015-Febru, 110.

[144]. Mokhtari F, Shamshirsaz M, Latifi M, Asadi S, Journal of the Textile Institute 2017, 108, 906.

[145]. Mokhtari F, Latifi M, Shamshirsaz M, Khelghatdoost M, Rahmani S, Journal of the Textile Institute 2017, 108, 1917.

[146]. Liu ZH, Pan CT, Lin LW, Huang JC, Ou ZY, Smart Materials and Structures 2014, 23.

[147]. Fuh YK, Ye JC, Chen PC, Ho HC, Huang ZM, ACS Applied Materials and Interfaces 2015, 7, 16923.

[148]. Pan CT, Yen CK, Wu HC, Lin L, Lu YS, Huang JCC, Kuo SW, Journal of Materials Chemistry A 2015.

[149]. Pu J, Yan X, Jiang Y, Chang C, Lin L, Sensors and Actuators, A: Physical 2010, 164, 131.

[150]. He YZ, Zheng XX, Yu J, You GF, Yu MH, Ning M, Long X, The Journal of Physical Chemistry C 2017, 121, 8663.

[151]. McCann JT, Chen JIL, Li D, Ye ZG, Xia Y, Chemical Physics Letters 2006, 424, 162.

[152]. Zhan S, Yu H, Li Y, Jiang B, Zhang X, Yan C, Ma S, Journal of Dispersion Science and Technology 2008, 29, 1345.

[153]. He Y, Zhang T, Zheng W, Wang R, Liu X, Xia Y, Zhao J, Sensors and Actuators, B: Chemical 2010, 146, 98.

[154]. Zhuang Y, Li F, Yang G, Xu Z, Li J, Fu B, Yang Y, Zhang S, Journal of the American Ceramic Society 2014, 97, 2725.

[155]. Yuh J, Perez L, Sigmund WM, Nino JC, Physica E: Low-Dimensional Systems and Nanostructures 2007, 37, 254.

[156]. Bauer MJ, Snyder CS, Bowland CC, Uhl AM, Budi MAK, Villancio-Wolter M, Sodano HA, Andrew JS, Journal of the American Ceramic Society 2016, 99, 3902.

[157]. Sá P, Bdikin I, Almeida B, Rolo AG, Isakov D, Ferroelectrics 2012, 429, 48.

[158]. Sá P, Barbosa J, Bdikin I, Almeida B, Rolo AG, Gomes EDM, Belsley M, Kholkin AL, Isakov D, Journal of Physics D: Applied Physics 2013, 46.

[159]. Li H, Wu H, Lin D, Pan W, Journal of the American Ceramic Society 2009, 92, 2162.

[160]. Wang F, Mai YW, Wang D, Ding R, Shi W, Sensors and Actuators, A: Physical 2015, 233, 195.

[161]. Yuh J, Perez L, Sigmund WM, Nino JC, Journal of Sol-Gel Science and Technology 2007, 42, 323.

[162]. Maensiri S, Nuansing W, Klinkaewnarong J, Laokul P, Khemprasit J, Journal of Colloid and Interface Science 2006, 297, 578. [PubMed: 16332372]

[163]. Lee DY, Lee KH, Lee MH, Cho NI, Kim BY, Journal of Sol-Gel Science and Technology 2010, 53, 43.

[164]. Xia Y, He Y, Wang R, Feng J, Zhang T, Materials Letters 2012, 88, 43.

[165]. Sr B, Nano T, ACS applied materials & interfaces 2014.

[166]. Jalalian A, Grishin AM, Wang XL, Cheng ZX, Dou SX, Applied Physics Letters 2014, 104, 0.

[167]. Jalalian A, Grishin AM, Dou SX, Journal of Physics: Conference Series 2012, 352, 1.

[168]. Sahoo B, Panda PK, Journal of Electronic Materials 2015, 44, 4563.

[169]. Wu W, Cheng L, Bai S, Dou W, Xu Q, Wei Z, Qin Y, Journal of Materials Chemistry A 2013, 1, 7332.

[170]. Zhou D, Zhou Y, Tian Y, Tu Y, Zheng G, Gu H, Journal of Materials Science and Technology 2015.

[171]. Chen YQ, Zheng XJ, Feng X, Dai SH, Zhang DZ, Materials Research Bulletin 2010, 45, 717.

[172]. Chen YQ, Zheng XJ, Li W, Materials Science and Engineering A 2010, 527, 5462.

[173]. Li P, Zheng X, Zhang Y, Yuan M, Jiang B, Deng S, Ceramics International 2015, 41, 14251.

[174]. Jiang B, Tang M, Li J, Xiao Y, Tao H, Zhou Y, He J, Journal of Electronic Materials 2012, 41, 651.

[175]. Liao M, Zhong XL, Wang JB, Xie SH, Zhou YC, Applied Physics Letters 2010, 96.

[176]. Tang M, Shu W, Yang F, Zhang J, Dong G, Hou J, Nanotechnology 2009, 20.

[177]. Liao M, Zhong XL, Wang JB, Yan HL, He JP, Qiao Y, Zhou YC, Journal of Crystal Growth 2007, 304, 69.

[178]. Hou D, Hu X, Hu P, Zhang W, Zhang M, Huang Y, Nanoscale 2013.

[179]. Xie SH, Li JY, Proksch R, Liu YM, Zhou YC, Liu YY, Ou Y, Lan LN, Qiao Y, Applied Physics Letters 2008, 93, 1.

[180]. Zhao Y, Fan H, Ren X, Long C, Liu G, Liu Z, Journal of Materials Chemistry C 2016, 4, 7324.

[181]. Maldonado-Orozco MC, Ochoa-Lara MT, Sosa-Márquez JE, Olive-Méndez SF, Espinosa-Magaña F, Ceramics International 2015, 41, 14886.

[182]. Jalalian A, Grishin AM, Applied Physics Letters 2012, 100.

[183]. Jalalian A, Grishin AM, Applied Physics Letters 2014, 104, 1.

[184]. Kang HB, Chang J, Koh K, Lin L, Cho YS, ACS Applied Materials and Interfaces 2014, 6, 10576.

[185]. Viswanathamurthi P, Bhattarai N, Kim HY, Lee DR, Kim SR, Morris MA, Chemical Physics Letters 2003.

[186]. W H Pan W, J. Am. Ceram. Soc, 2006, 89, 699.

[187]. Yang X, Shao C, Guan H, Li X, Gong J, Inorganic Chemistry Communications 2004, 7, 176.

[188]. Chen YQ, Zheng XJ, Mao SX, Li W, Journal of Applied Physics 2010, 107.

[189]. Chen YQ, Zheng XJ, Feng X, Nanotechnology 2010, 21.

[190]. Remant RB, Kim CK, Khil MS, Kim HY, Kim IS, Materials Science and Engineering C 2008, 28, 70.

[191]. Li D, Xia Y, Nano Letters 2004, 4, 933.

[192]. Ostermann R, Li D, Yin Y, McCann JT, Xia Y, Nano Letters 2006, 6, 1297. [PubMed: 16771598]

[193]. Wang N, Sun C, Zhao Y, Zhou S, Chen P, Jiang L, Journal of Materials Chemistry 2008, 18, 3909.

[194]. Li D, McCann JT, Xia Y, Marquez M, Journal of the American Ceramic Society 2006, 89, 1861.

[195]. Chen CY, Huang JH, Song J, Zhou Y, Lin L, Huang PC, Zhang Y, Liu CP, He JH, Wang ZL, ACS Nano 2011, 5, 6707. [PubMed: 21774517]

[196]. Zhang H, Jiang S, Kajiyoshi K, Applied Physics Letters 2011, 98.

[197]. Reichmann K, Feteira A, Li M, Materials 2015, 8, 8467. [PubMed: 28793724]

[198]. Huang Z, Wang GS, Li YC, Liang RH, Cao F, Dong XL, Physica Status Solidi (A) Applications and Materials Science 2011, 208, 1047.

[199]. Tellier J, Malic B, Dkhil B, Jenko D, Cilensek J, Kosec M, Solid State Sciences 2009, 11, 320.

[200]. Christman JA, Woolcott RR, Kingon AI, Nemanich RJ, Applied Physics Letters 1998, 73, 3851.

[201]. Ulubayram K, Calamak S, Shahbazi R, Eroglu I, Current Pharmaceutical Design 2015, 21, 1930. [PubMed: 25732666]

[202]. Peppas NA, Journal of Controlled Release 2000.

[203]. McCann JT, Li D, Xia Y, Journal of Materials Chemistry 2005, 15, 735.

[204]. Dai Y, Lu X, McKiernan M, Lee EP, Sun Y, Xia Y, Journal of Materials Chemistry 2010, 20, 3157.

[205]. Pukada E, IEEE Transactions on Ultrasonics, Ferroelectrics, and Frequency Control 2000.

[206]. Tasaka S, Miyata S, Journal of Applied Physics 1985, 57, 906.

[207]. Martins P, Lopes AC, Lanceros-Mendez S, Progress in Polymer Science 2014, 39, 683.

[208]. Sencadas V, Gregorio R, Lanceros-Méndez S, Journal of Macromolecular Science, Part B: Physics 2009, 48, 514.

[209]. Sharma S, Advanced Materials Letters 2013, 4, 522.

[210]. Ribeiro C, Correia DM, Ribeiro S, Sencadas V, Botelho G, Lanceros-Méndez S, Engineering in Life Sciences 2015, 15, 351.

[211]. Ribeiro C, Sencadas V, Ribelles JLG, Lanceros-Méndez S, Soft Materials 2010, 8, 274.

[212]. Liu ZH, Pan CT, Lin LW, Lai HW, Sensors and Actuators, A: Physical 2013, 193, 13.

[213]. Choi Sung Won, Kim Jeong Rae, Ahn Young Rack, Jo Seong Mu, Cairns Elton J, ACS publications 2006, 104.

[214]. Sencadas V, Ribeiro C, Bdikin IK, Kholkin AL, Lanceros-Mendez S, Physica Status Solidi (A) Applications and Materials Science 2012, 209, 2605.

[215]. Cozza ES, Monticelli O, Marsano E, Cebe P, Polymer International 2013, 62, 41.

[216]. Zhao Z, Li J, Yuan X, Li X, Zhang Y, Sheng J, Journal of Applied Polymer Science 2005, 97, 466.

[217]. Huang F, Wei Q, Cai Y, Wu N, International Journal of Polymer Analysis and Characterization 2008, 13, 292.

[218]. Andrew JS, Clarke DR, Langmuir 2008, 24, 670. [PubMed: 18189433]

[219]. Koombhongse S, Liu W, Reneker DH, Journal of Polymer Science, Part B: Polymer Physics 2001.

[220]. Costa LMM, Bretas RES, Gregorio R, Materials Sciences and Applications 2010, 01, 247.

[221]. Jiyong H, Yinda Z, Hele Z, Yuanyuan G, Xudong Y, Smart Materials and Structures 2017, 26, 085019.

[222]. Huang S, Aik Yee W, Chauhari Tiju W, Liu Y, Kotaki M, Freddy Boey YC, Langmuir 2008, 24, 13621.

[223]. Mokhtari F, Shamshirsaz M, Latifi M, Polymer Engineering and Science 2016.

[224]. S. Florczak, T. Lorson, T. Zheng, M. Mrlik, D. Hutmacher, M. Higgins, R. Luxenhofer, P. Dalton, M. Higgins, others, 2018.

[225]. Edmondson D, Cooper A, Jana S, Wood D, Zhang M, Journal of Materials Chemistry 2012, 22, 18646.

[226]. Yee WA, Kotaki M, Liu Y, Lu X, Polymer 2007, 48, 512.

[227]. Yee WA, Nguyen AC, Lee PS, Kotaki M, Liu Y, Tan BT, Mhaisalkar S, Lu X, Polymer 2008, 49, 4196.

[228]. Baji A, Mai YW, Du X, Wong SC, Macromolecular Materials and Engineering 2012, 297, 209.

[229]. Lagoudas NC, Ounaies Z, Proceedings of SPIE 2008, 6929, 69292N.

[230]. Shuakat MN, Lin T, Journal of the Textile Institute 2016, 107, 791.

[231]. Na H, Liu X, Li J, Zhao Y, Zhao C, Yuan X, Polymer 2009, 50, 6340.

[232]. Matabola KP, Moutloali RM, Journal of Materials Science 2013, 48, 5475.

[233]. Andrew JS, Clarke DR, Langmuir 2008, 24, 8435. [PubMed: 18646730]

[234]. Nasir M, Matsumoto H, Minagawa M, Tanioka A, Danno T, Horibe H, Polymer Journal 2007, 39, 670.

[235]. Wei K, Kim H-K, Kimura N, Suzuki H, Satou H, Lee K-H, Park Y-H, Kim I-S, Journal of Nanoscience and Nanotechnology 2013.

[236]. Shenoy SL, Bates WD, Frisch HL, Wnek GE, Polymer 2005.

[237]. Liao AG, Yuan, Wang, Tian Rong, Qiu Miao, Fane Changquan, Journal of Membrane Science 2013.

[238]. Yu L, Cebe P, Polymer 2009.

[239]. Li Z, Xu Y, Fan L, Kang W, Cheng B, Materials and Design 2016.

[240]. Bottino A, Capannelli G, Munari S, Turturro A, Journal of Polymer Science Part B: Polymer Physics 1988, 785.

[241]. Motamedi AS, Mirzadeh H, Hajiesmaeilbaigi F, Bagheri-Khoulenjani S, Shokrgozar M, Progress in Biomaterials 2017.

[242]. Gao K, Hu X, Dai C, Yi T, Materials Science and Engineering B: Solid-State Materials for Advanced Technology 2006.

[243]. Baqeri M, Abolhasani MM, Mozdianfard MR, Guo Q, Oroumei A, Naebe M, Journal of Applied Polymer Science 2015.

[244]. Ghafari E, Jiang X, Lu N, Advanced Composites and Hybrid Materials 2017.

[245]. Huang F, Wei Q, Wang J, Cai Y, Huang Y, E-Polymers 2008.

[246]. Brown P, Materials Research Bulletin 1989.

[247]. Larsen G, Velarde-Ortiz R, Minchow K, Barrero A, Loscertales IG, Journal of the American Chemical Society 2003, 125, 1154. [PubMed: 12553802]

[248]. Shao C, Kim HY, Gong J, Ding B, Lee DR, Park SJ, Materials Letters 2003, 57, 1579.

[249]. Viswanathamurthi P, Bhattarai N, Kim HY, Khil MS, Lee DR, Suh EK, Journal of Chemical Physics 2004, 121, 441. [PubMed: 15260565]

[250]. Dharmaraj N, Park HC, Lee BM, Viswanathamurthi P, Kim HY, Lee DR, Inorganic Chemistry Communications 2004, 7, 431.

[251]. Yuh J, Nino JC, Sigmund WM, Materials Letters 2005, 59, 3645.

[252]. Zhang Z, Li X, Wang C, Wei L, Liu Y, Shao C, Journal of Physical Chemistry C 2009, 113, 19397.

[253]. Chen WS, Huang DA, Chen HC, Shie TY, Hsieh CH, Der Liao J, Kuo C, Crystal Growth and Design 2009, 9, 4070.

[254]. Dai Y, Liu W, Formo E, Sun Y, Xia Y, Polymers for Advanced Technologies 2011, 22, 326.

[255]. Son WK, Cho D, Park WH, Nanotechnology 2006, 17, 439.

[256]. Wang Y, Santiago-Avil JJ??s, Nanotechnology 2004, 15, 32.

[257]. Choi SS, Lee SG, Im SS, Kim SH, Joo YL, Journal of Materials Science Letters 2003, 22, 891.

[258]. Chowdhury AR, Jaksik J, Hussain I, Tran P, Danti S, Uddin MJ, Energy Technology.

[259]. Ling S, Kaplan DL, Buehler MJ, Nature Reviews Materials 2018.

[260]. Cranford SW, Tarakanova A, Pugno NM, Buehler MJ, Nonlinear material behaviour of spider silk yields robust webs. Nature 2012.

[261]. Qin Z, Buehler MJ, Nature Communications 2013.

[262]. Qin Z, Compton BG, Lewis JA, Buehler MJ, Nature Communications 2015.

[263]. Ling S, Qin Z, Li C, Huang W, Kaplan DL, Buehler MJ, Nature Communications 2017.

[264]. Lin S, Ryu S, Tokareva O, Gronau G, Jacobsen MM, Huang W, Rizzo DJ, Li D, Staii C, Pugno NM, Wong JY, Kaplan DL, Buehler MJ, Nature Communications 2015.

[265]. Keten S, Xu Z, Ihle B, Buehler MJ, Nature Materials 2010.

[266]. Ling S, Qin Z, Huang W, Cao S, Kaplan DL, Buehler MJ, Science Advances 2017.

[267]. Baji A, Mai YW, Wong SC, Abtahi M, Chen P, Composites Science and Technology 2010, 70, 703.

[268]. Wang X, Ding B, Sun G, Wang M, Yu J, Progress in Materials Science 2013.

[269]. Fong H, Reneker DH, Structure formation in polymeric fibers 2001.

[270]. Latham J, Roxburgh IW, Proceedings of the Royal Society A: Mathematical, Physical and Engineering Sciences 1966.

[271]. Taylor G, Proceedings of the Royal Society A: Mathematical, Physical and Engineering Sciences 1966.

[272]. Taylor G, Proceedings of the Royal Society A: Mathematical, Physical and Engineering Sciences 1969.

[273]. Larrondo L, St R. Manley John, Journal of Polymer Science: Polymer Physics Edition 1981.

[274]. Larrondo L, St R. Manley John, Journal of Polymer Science: Polymer Physics Edition 1981.

[275]. Larrondo L, St R. Manley John, Journal of Polymer Science: Polymer Physics Edition 1981.

[276]. Hohman MM, Shin M, Rutledge G, Brenner MP, Physics of Fluids 2001.

[277]. Hohman MM, Shin M, Rutledge G, Brenner MP, Physics of Fluids 2001.

[278]. Reneker DH, Yarin AL, Fong H, Koombhongse S, Journal of Applied Physics 2000.

[279]. Shin YM, Hohman MM, Brenner MP, Rutledge GC, Applied Physics Letters 2001.

[280]. Shin YM, Hohman MM, Brenner MP, Rutledge GC, Polymer 2001.

[281]. Spivak AF, Dzenis YA, Reneker DH, Mechanics Research Communications 2000.

[282]. Yarin AL, Koombhongse S, Reneker DH, Journal of Applied Physics 2001.

[283]. Ederer C, Spaldin NA, Physical Review Letters 2005.

[284]. Bernardini F, Fiorentini V, Vanderbilt D, Physical Review B - Condensed Matter and Materials Physics 1997.

[285]. Crystallography Open Database.

[286]. Satta A, Fiorentini V, Bosin A, In Materials Research Society Symposium Proceedings; 1996; Vol. 395, p. 515.

[287]. Dal Corso A, Phys. Rev. B 1993, 47, 16252.

[288]. Dal Corso A, Posternak M, Resta R, Baldereschi A, Physical Review B 1994, 50, 10715.

[289]. de Gironcoli S, Baroni S, Resta R, Physical review letters 1989, 62, 2853. [PubMed: 10040108]

[290]. de Gironcoli S, Baroni S, Resta R, Ferroelectrics 1990, 111, 19.

[291]. Zhong W, Phys. Rev. Lett 1994, 72, 3618. [PubMed: 10056245]

[292]. Baptista FG, Budoya DE, de Almeida VAD, Ulson JAC, Sensors (Switzerland) 2014.

[293]. Caliò R, Rongala U, Camboni D, Milazzo M, Stefanini C, de Petris G, Oddo C, Sensors 2014, 14, 4755. [PubMed: 24618725]

[294]. Lefeuvre E, Badel A, Richard C, Petit L, Guyomar D, Sensors and Actuators, A: Physical 2006.

[295]. Huang ZM, Zhang YZ, Kotaki M, Ramakrishna S, Composites Science and Technology 2003.

[296]. Doucet JP, Weber J, Computer-aided molecular design: theory and applications; 1996.

[297]. Persano L, Dagdeviren C, Maruccio C, De Lorenzis L, Pisignano D, Advanced Materials 2014.

[298]. Hansen BJ, Liu Y, Yang R, Wang ZL, ACS Nano 2010.

[299]. Fuh YK, Chen SY, Ye JC, Applied Physics Letters 2013.

[300]. Wang P, Cheng L, Zhang Y, Wu H, Hou Y, Yuan W, Zheng L, Ceramics International 2017.

[301]. Francis L, Ghaffour N, Alsaadi AS, Nunes SP, Amy GL, Journal of Materials Science 2014, 49, 2045.

[302]. Lalia BS, Guillen-Burrieza E, Arafat HA, Hashaikeh R, Journal of Membrane Science 2013, 428, 104.

[303]. Lalia BS, Guillen E, Arafat HA, Hashaikeh R, Desalination 2014, 332, 134.

[304]. Prince JA, Singh G, Rana D, Matsuura T, Anbharasi V, Shanmugasundaram TS, Journal of Membrane Science 2012, 397–398, 80.

[305]. Correia DM, Ribeiro C, Sencadas V, Botelho G, Carabineiro SAC, Ribelles JLG, Lanceros-Méndez S, Progress in Organic Coatings 2015, 85, 151.

[306]. Wu CM, Chou MH, Composites Science and Technology 2016, 127, 127.

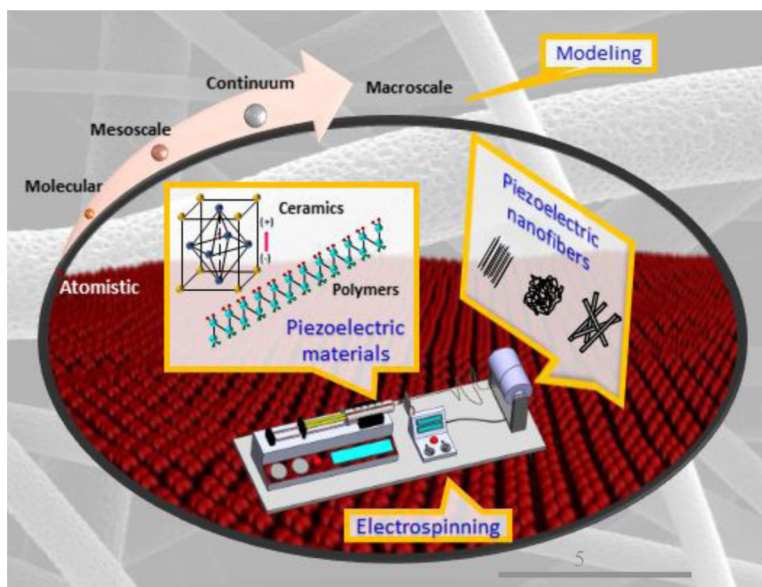[307]. Wu CM, Chou MH, European Polymer Journal 2016, 82, 35.

Figure 1.
Schematic depicting the topics covered in this review article: piezoelectric materials (ceramics and polymers) processed via electrospinning to produce piezoelectric nanofibers specific for different human body-related applications. Computational and mathematical modeling, ranging from atomistic to macroscale, represent very useful tools to tune the several parameters involved in the electrospinning of piezoelectric materials by modeling the electrospinning process, as well as the mechanical and electrical properties of the produced piezoelectric fibers and fiber meshes, thus greatly helping in reducing the experimental campaigns to achieve the desired goal.
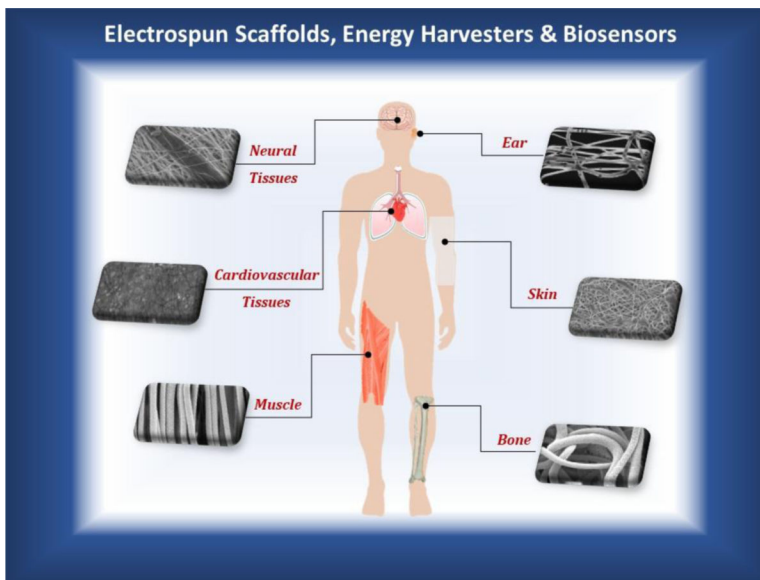
Figure 2.
Current studies on biomedical applications of electrospun tissue engineering scaffolds, energy harvesters and biosensors based on piezoelectric polymer fibers produced via electrospinning. Electrically responsive tissues targeted by researches are neural (brain), sensorineural (inner ear), cardiovascular (heart), skin (epidermis), musculoskeletal (striated muscle and bone). The piezoelectric fibrous materials serve for mechanical support and electrical stimulation of biological tissues and smart devices.
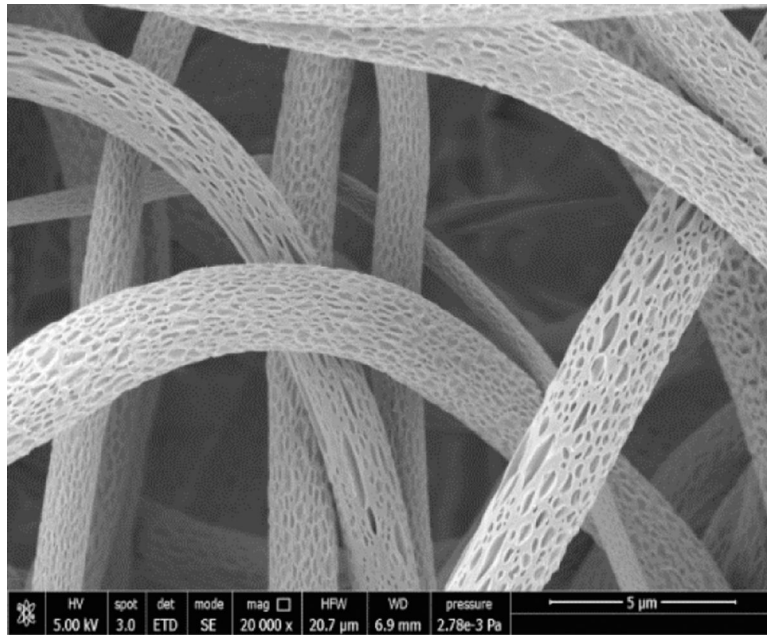
Figure 3.
SEM micrograph of nanoporous surface of P(VDF-TrFE) electrospun ultrafine fibers obtained by using MEK as a solvent and > 40% humidity. Unpublished original picture by the authors.
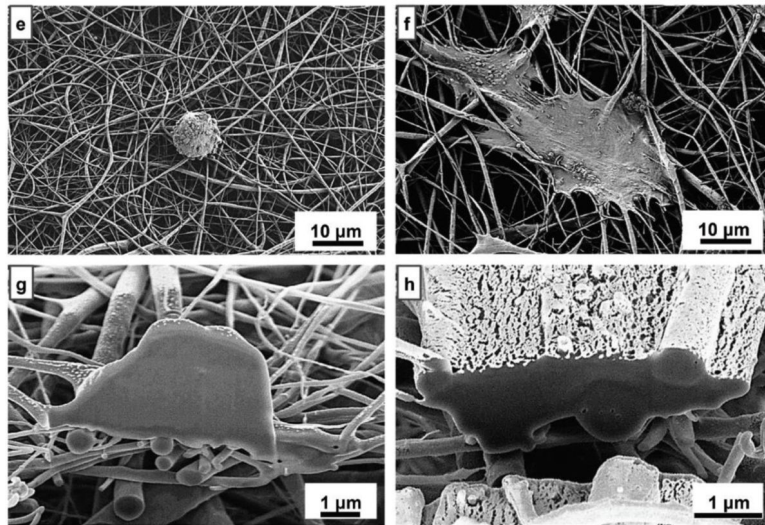
Figure 4.
Saos-2 cells cultured on PVDF electrospun samples: (e, f) hydrophobic and hydrophilic PVDF electrospun scaffolds, respectively; (g, h) SEM-FIB cross-sections of Saos-2 cells grown on hydrophobic and hydrophilic electrospun scaffolds, respectively. Adapted with permission.[59] Copyright 2019, The Royal Society of Chemistry.
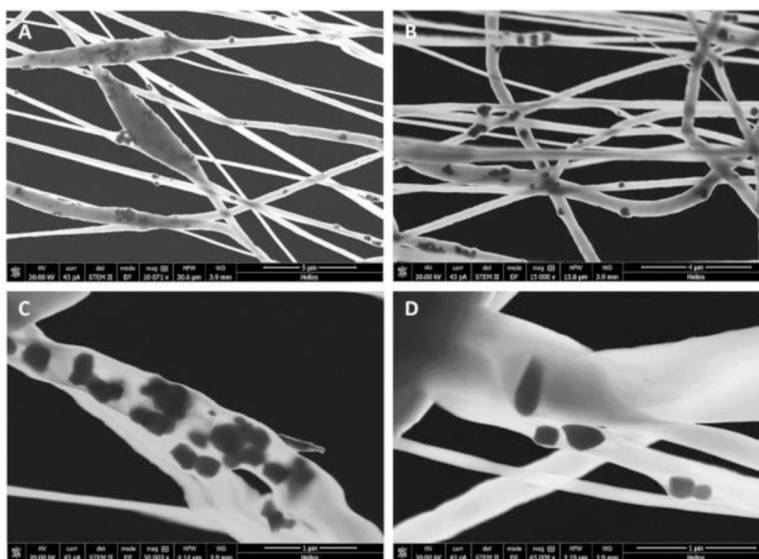
Figure 5.
STEM micrographs of BTNP/PVDF 10/90 electrospun fibers obtained with a collector tangential velocity of $3.7 \text{m} \cdot \text{s}^{-1}$ at different magnifications in the range of 10,000x to 65,000x. (A, B) dispersion of BTNPs inside the electrospun fibers; (A) beads induced by the presence of BTNP aggregates; (C) BTNP aggregates inside an electrospun fiber; and (D) BTNP dispersed inside an electrospun fiber. Reproduced with permission. [69] Copyright 2017, Elsevier.
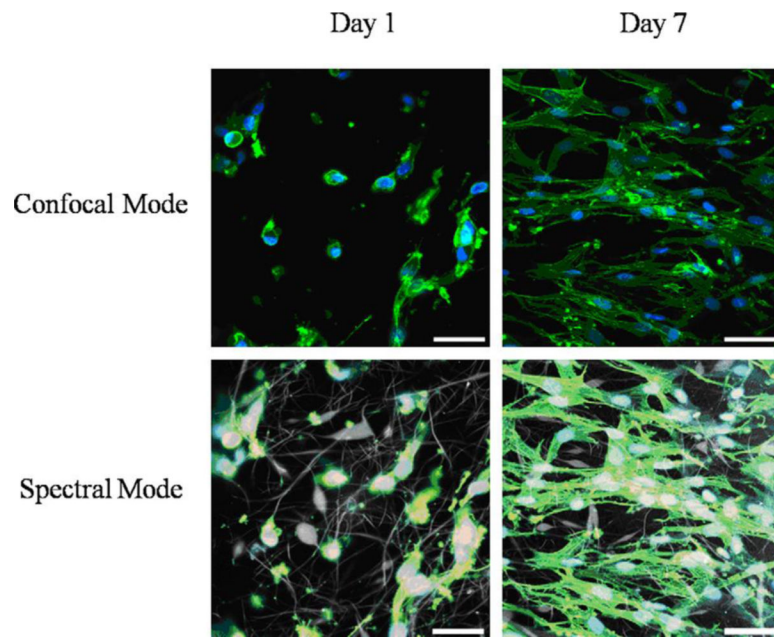
Day 1   Day 7

Confocal Mode

Spectral Mode

Figure 6.
Confocal fluorescence microscopy images of human skin fibroblasts attached to P(VDF-TrFE) fibers after 1 and 7 days of cell culture (40x objective; cytoskeleton, green; nucleus, blue; scale bar 50 μm). Reproduced with permission. [75] Copyright 2010, Elsevier.
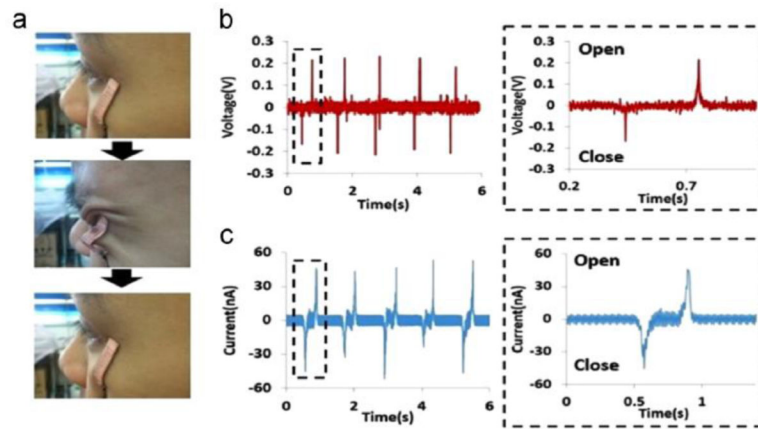
Figure 7.
Performance of the highly flexible self-powered sensing elements (SSE) to detect skin movement. Picture of the SSE on face skin (a). (b) Output voltage and (c) current generation of the sensors induced by one eye blinking. Adapted with permission. [117] Copyright 2015, Elsevier.
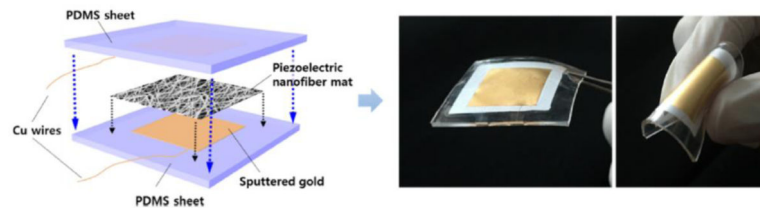
Figure 8.
The concept of a bendable piezoelectric sensor. Reproduced with permission. [103] Copyright 2016, American Chemical Society.
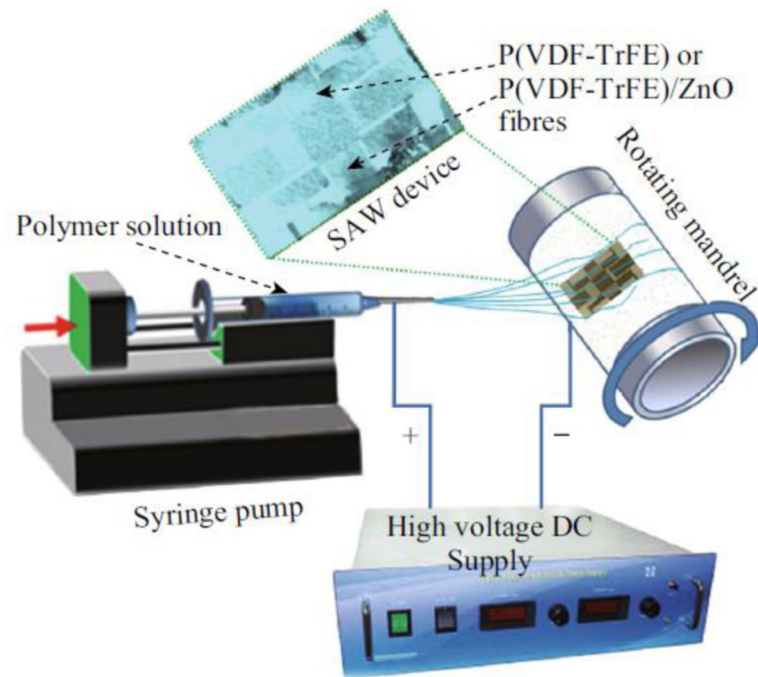
Figure 9.
Electrospinning process for P(VDF–TrFE) and P(VDF–TrFE)/ZnO nanocomposites on the SAW device. Reproduced with permission under the terms of the Creative Commons Attribution 4.0 International License. [108]. Copyright 2019, Published by Springer.

Figure 10.
Schematic of cell-dependent energy harvester including piezoelectric fiber mat applied on heart tissue. Reproduced with permission under the terms of the Creative Commons Attribution 4.0 International License. [126]. Copyright 2019, Published by IOP Publishing.
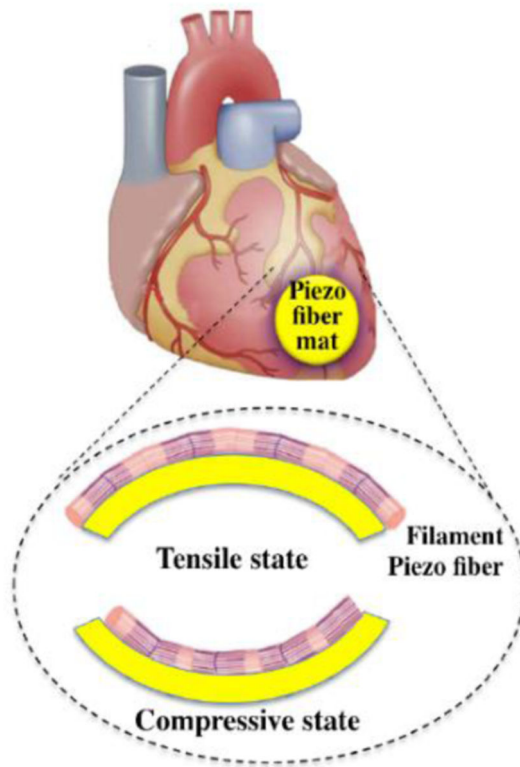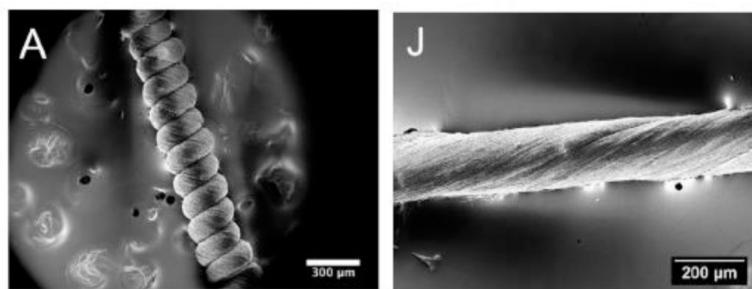
Figure 11.
Pictures from SEM of A) a coil and J) a twisted construct made of aligned nanofibers.
Reproduced with permission. [128] Copyright 2015. American Chemical Society
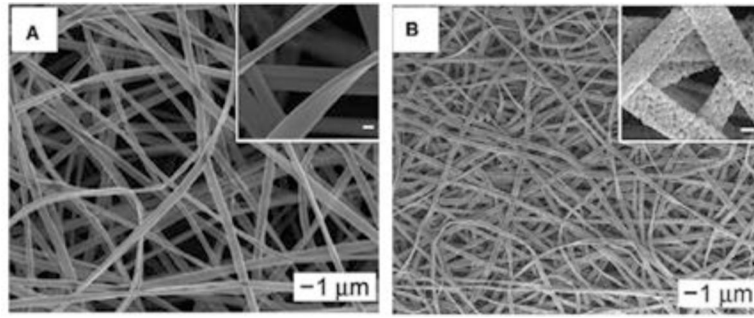
Figure 12.
(A) SEM image of BaTiO$_3$–PVP composite fibers prepared by electrospinning. (B) SEM image of the BaTiO$_3$ nanofibers after Calcination in air at 700 °C for 3 h. The scale bars in the insets are 250 nm. Reproduced with permission. [151] Copyright 2006, Elsevier.

Figure 13.
Rotating mandrel set-up for the electrospinning of aligned nanofibers showing the as-spun amorphous fibers aligned across the parallel copper wires on the rotating mandrel. Reproduced with permission. [156] Copyright 2016, The American Ceramic Society.
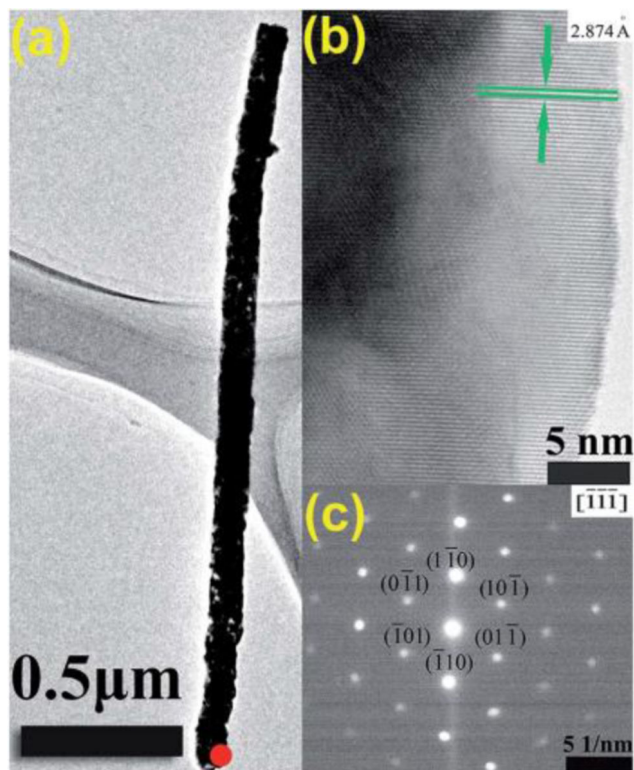
Figure 14.
TEM images and NBD pattern of a single BaTiO$_3$ nanofiber with Ce/Ba atomic ratio of 0.6%: (a) low magnification; (b) high-resolution TEM image of the red disk of (a); (c) NBD pattern of the red disk of (a). Reproduced with permission. [121]. Copyright 2015, The Royal Society of Chemistry.
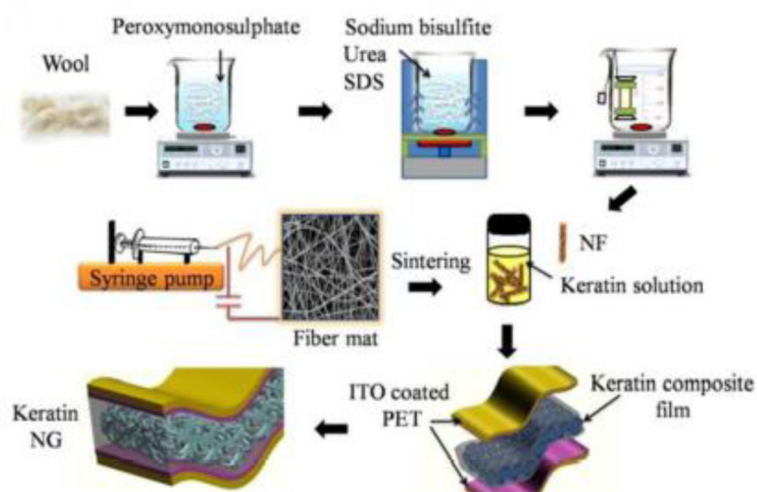
Figure 15.
Schematic diagram of the fabrication process of wool keratin-based Nano-generators with ferroelectric nanofibers. Reproduced with permission. [180] Copyright 2016, The Royal Society of Chemistry.
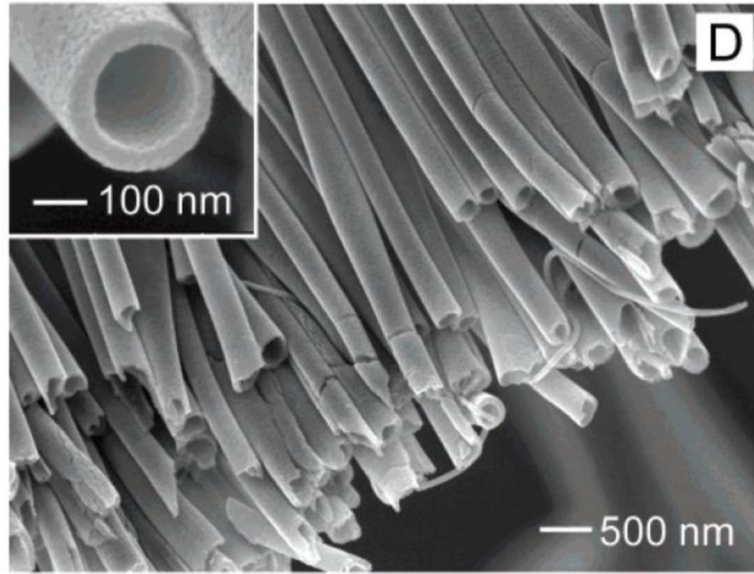
Figure 16.
SEM image of a uniaxially aligned array of TiO2 hollow fibers. Reproduced with permission. [191]. Copyright 2004, American Chemical Society.
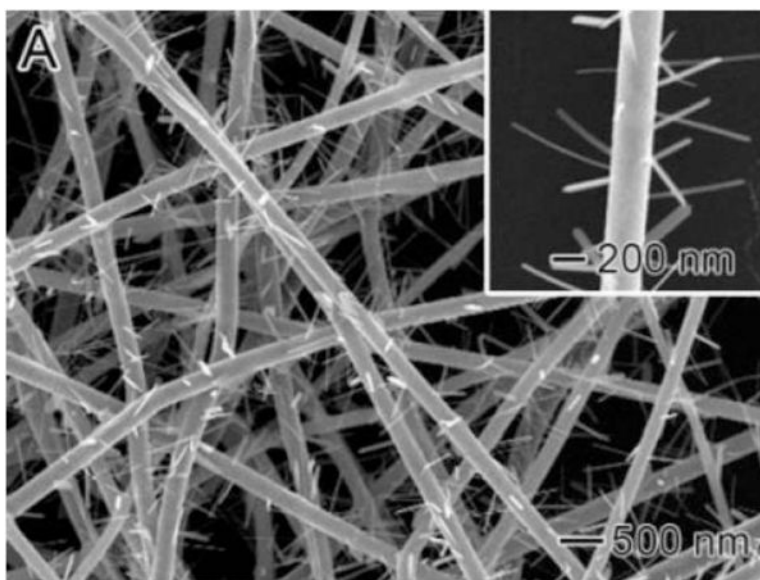
Figure 17.
SEM images of (A) V_2O_5-TiO_2-Ta_2O_5 nanofibers. Reproduced with permission. [192] Copyright 2006, American Chemical Society.
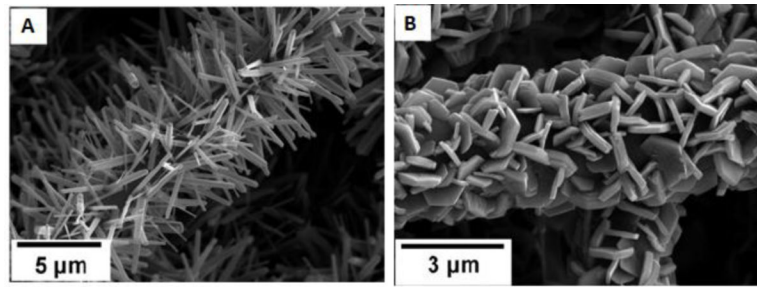
Figure 18.
SEM images of (A) high magnification ZnO/ TiO$_2$ heterojunctions with ZnO nanorods grown on TiO$_2$ fibers, (B) high magnification ZnO/TiO$_2$ heterojunctions with ZnO nanoplates grown on TiO$_2$ fibers. Reproduced with permission. [193] Copyright 2008, The Royal Society of Chemistry.
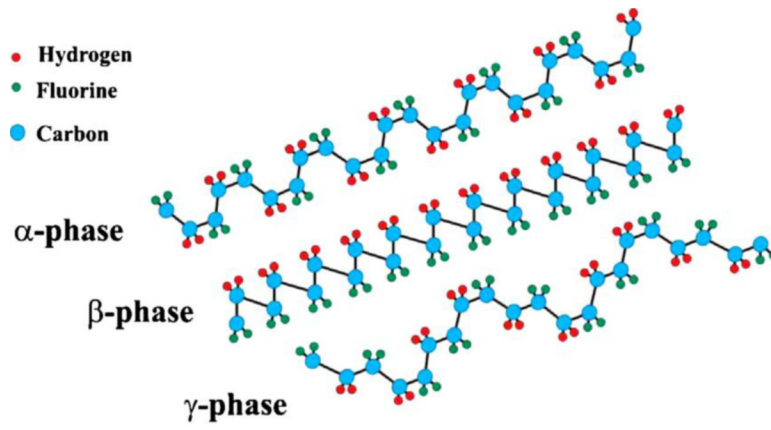
Figure 19.
Representation of the chain conformation for the α, β, and γ phases of PVDF. Adapted with permission. [207]. Copyright 2014, Elsevier.
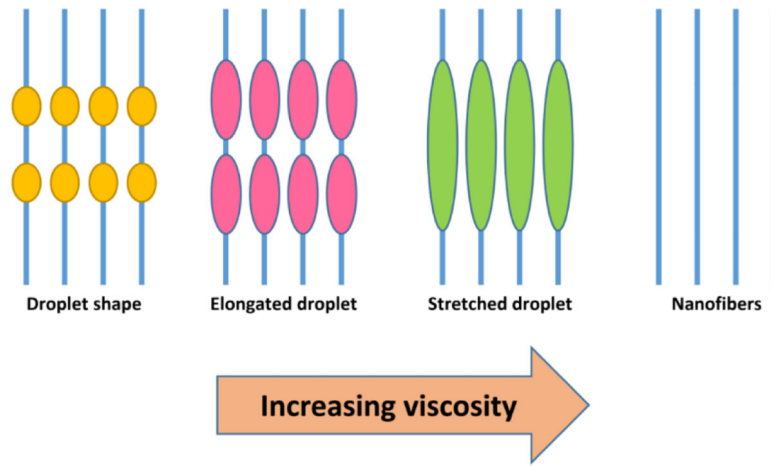
Figure 20.
Variation in morphology of electrospun nanofibers with viscosity.
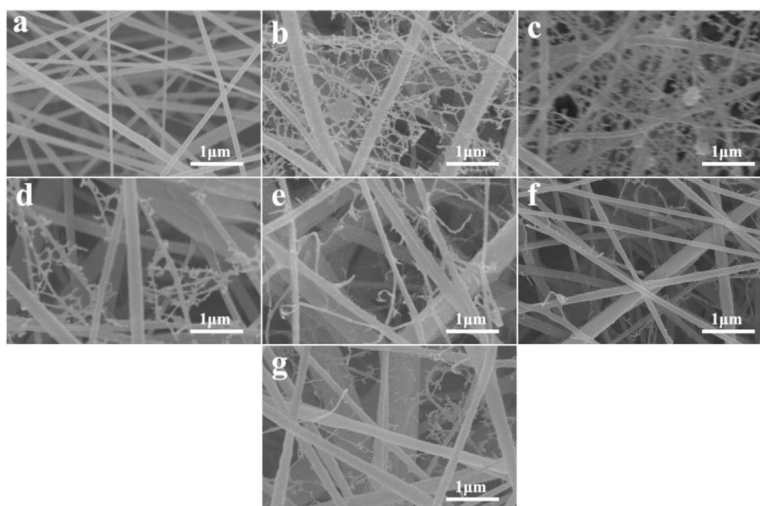
Figure 21.
FE-SEM images of PVDF nanofiber membranes with different types of salt: (a) no salt (pure PVDF), (b) 0.10 mol L^{-1} TBAC, (c) 0.10 mol L^{-1} TBAB, (d) 0.10 mol L^{-1} TEAC, (e) 0.10 mol L^{-1} LiCl, (f) 0.05 mol L^{-1} AlCl$_3$, (g) 0.05mol L^{-1} CaCl$_2$. Spinning parameter: applied voltage of 30 kV, tip to collector distance of 15 cm, extrusion rate of 1 mL h^{-1}. Reproduced with permission. [239] Copyright 2016, Elsevier.
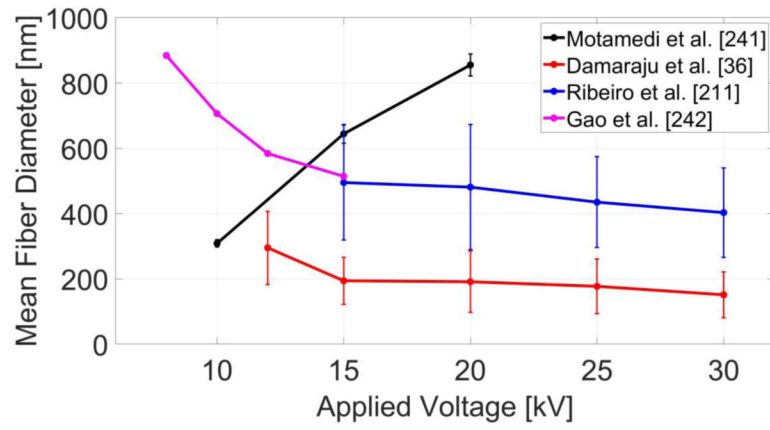
Figure 22.
Mean fiber diameter as a function of applied voltage. The graph representation was performed according to the values found in literature.
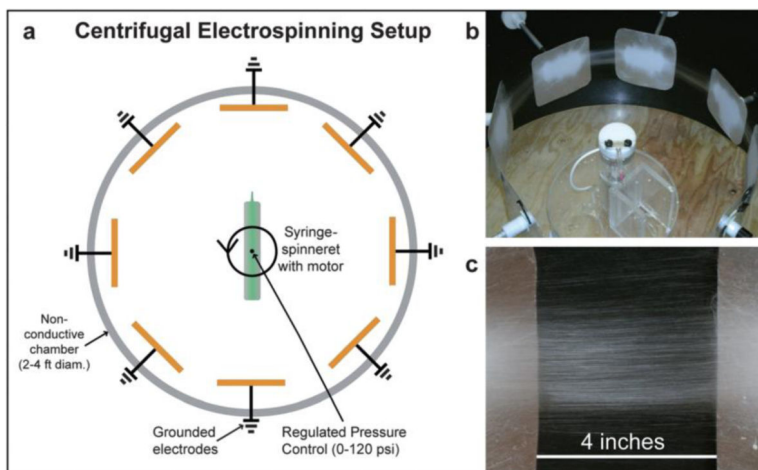
Figure 23.
Centrifugal electrospinning (CE) system for large-area production of aligned polymer nanofibers. (a) Schematic illustration of the system configuration. (b) Photograph of the CE system with deposited PVDF nanofibers. (c) Electrospun PVDF fibers deposited. Reproduced with permission. [225] Copyright 2012, The Royal Society of Chemistry.
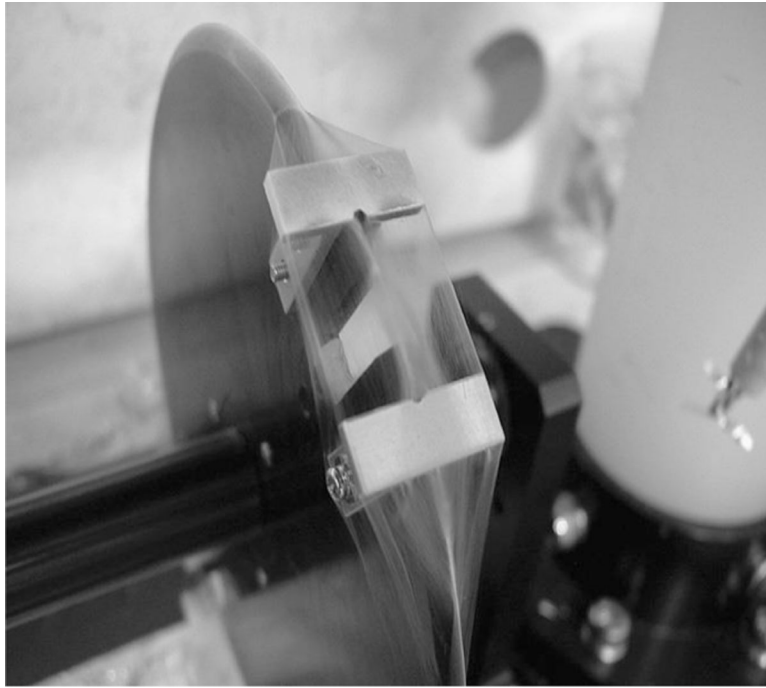
Figure 24.
A picture showing the fanning of the electrospun PVDF fibers on the modified rotating disk collector. No substrates were placed between the two aluminum electrodes. Reproduced with permission. [227] Copyright 2008, Elsevier.
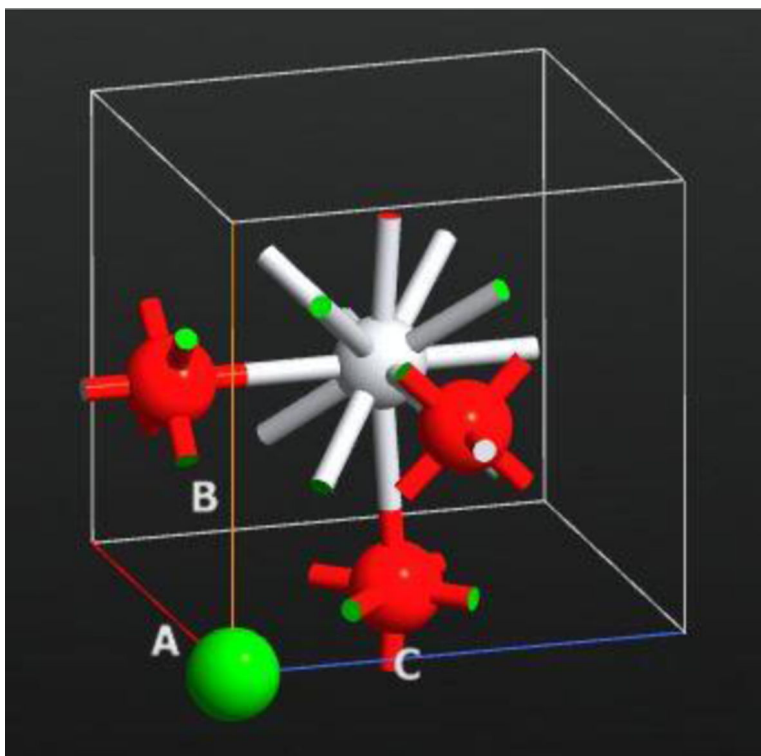
Figure 25.
A primitive cell of BaTiO$_3$ where Barium, Titanium and Oxygen atoms are displayed in white, green and red respectively. Primitive cells can be employed to develop ab initio studies. Reproduced from the open database [285].
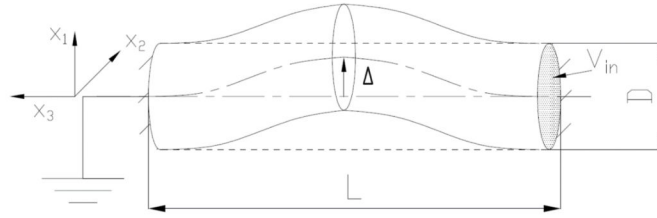
Figure 26.
Model of a single electrospun fiber. The boundary conditions (BC) are the following: mechanically, the structure has the two ends fixed to the frame while, from the electric point of view, an input voltage Vin is applied only to one end (the other one is grounded). Due to the BC, a transversal displacement is observed with the highest value   at the middle of the fiber.
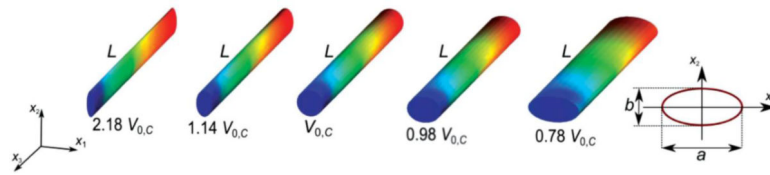
Figure 27.
Investigation on the sensitivity of the output voltage $V_{0,c}$ with respect to the variation of the ellipsoidal axes of the cross section of the piezoelectric fiber, by taking into account the circular section as baseline. Reproduced with permission under the terms of the Creative Commons Attribution 4.0 International License. [297] Copyright 2019, Published by WILEY-VCH.
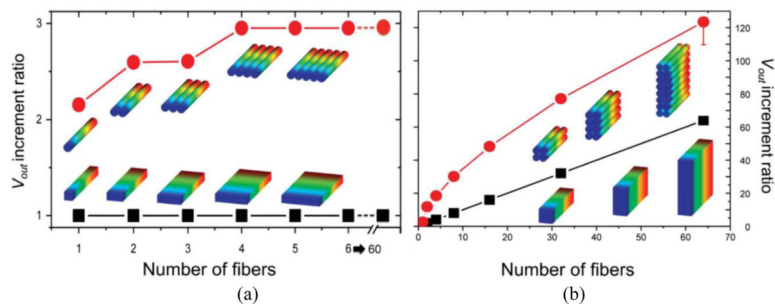
Figure 28.
Investigation on the enhancement of the piezoelectric effect, in terms of output voltage V_{out} increment ratio with respect to the increasing number of fibers of two different cross sections (squared – black squares and circular- red circles). Case of horizontal (a) and vertical (b) packing. Reproduced with permission under the terms of the Creative Commons Attribution 4.0 International License. [297] Copyright 2019, Published by WILEY-VCH.

Table 1.

A comprehensive list of piezoelectric polymeric fibers fabricated by electrospinning techniques for tissue engineering applications.

| Polymer	Solvent	Additives	Comments	Fiber properties	Ref.	Potential applications
PVDF (M_W= 275 000)	DMF:acetone (1:1 v/v)	-	C = 20% (w/w), V = 25 kV, d = 20 cm, flow rate = 0.5 ml h^{-1}	Fiber diameter: 177 ± 84 nm, β-phase fraction: 72%	[36]	Scaffold for bone tissue engineering
PVDF	DMF	-	C = 20% (w/w), V = 25 kV, d=15 cm, flow rate = 0.5 ml h^{-1}	Fiber diameter: 500 nm	[58]	Scaffold for bone tissue engineering
PVDF	DMF:acetone (40/60)	-	C=15%, V= 25 kV, d=15 cm, flow rate = 600 μl h^{-1}	-	[59]	Scaffold for bone tissue engineering
PVDF (Mm= 275000 g mol^{-1})	DMF:acetone (1:1 v/v)	-	C = 22 w%, V = ±15 kV, d = 18 cm, flow rate = 1.5 ml h^{-1}	Fiber diameters: PVDF(+) = 1.39 ± 0.58 μm and PVDF(−) = 1.37 ± 0.57 μm. Surface potential of PVDF(−) = −95 mV	[60]	Scaffolds for bone regeneration
PVDF (Mw = 275000 g mol^{-1})	DMF/THF (1:1 v/v)	POSS–EGCG Conjugate	C = 18 w/v%, V= 18 kV, d = 15 cm, flow rate = 2 ml h^{-1}	Fiber diameter= from 936 ± 223 nm to 1094± 394 nm	[61]	Scaffold for bone tissue engineering
PVDF–TrFE (65:35)	MEK	-	C=25% (w/v), V= 25–28 kV, d= 35 cm, flow rate: 15 ml h^{-1}, Annealing at 135 °C for 96 h followed by ice water quenching for few seconds	Fiber diameter: 6.9 ± 1.7 μm, porosity (%) = 92 ± 5.5, % relative β-phase fraction: 75 ± 3.2%	[62]	Scaffold for bone tissue engineering
PVDF–TrFE (70:30 mol%)	MEK	-	C = 20% (w/v), V = 35 kV, d = 15 cm, flow rate: 0.016 ml min^{-1}, rotating speed: 0 to 2500 rpm	Fiber diameter: 1.40 − 2.37 μm	[63]	Scaffold for bone tissue engineering
P(VDF-TrFE) (75/25 mol%)	DMF:acetone (6:4 v/v)	-	C = 20 w/v%, V = 15 kV, d = 10 cm, flow rate = 1 ml h^{-1}	d_{31} =22.88 pC/N, Maximum Voltage = −1.7 V, current output 41.5 nA	[64]	Scaffold for bone tissue engineering
PHB	Chloroform	Polyaniline (PANi)	C=6%, V= 6.5 kV, d = 8 cm, flow rate = 1.5 ml h^{-1}	-	[65]	Scaffold for bone tissue engineering
PVDF	DMF:acetone (3:1 v/v)	-	C=15% (w/v), V=30 kV, d=15 cm, flow rate = 10 ml h^{-1}, rotation speed = 50, 1000, 2000, and 3000 rpm	Fiber diameter: 1.51–1.98 μm	[66]	Scaffold for neural tissue engineering (NTE)
PVDF	DMF	-	C = 18% (w/w), V= 8 kV, d= 5 cm	Fiber diameter: 350 nm	[67]	Scaffold for neural tissue engineering
PVDF, M_W=584,000	DMAc/acetone (1:1 v/v)	Gold colloidal nanoparticles (Au NPs)	C = 30% (w/v), V=15 kV, d=18 cm, flow rate: 0.5 ml h^{-1}, rotating speed: 2500 rpm	Fiber diameter: 324 ± 18 nm	[68]	Scaffold for nerve tissue engineering
PVDF	DMF: acetone (1:1 v/v)	$BaTiO_3$	C= 20% (w/v), V=20 kV, d=15 cm, Flow rate: 1 ml h^{-1}, rotating speed: 500 to 3000 rpm	Fiber diameter: 400nm, d_{31}=130 ± 30 pmV^{-1}	[69]	Scaffold for nerve tissue engineering
PVDF–TrFE (65/35)	MEK	-	C = 15% and 25% (w/v)	Crystallinity (%): as-spun aligned fiber: 64.39%; annealed aligned fiber: 70.64%	[70,71]	Scaffold for neural tissue engineering

Polymer	Solvent	Additives	Comments	Fiber properties	Ref.	Potential applications
P(VDF-TrFE)	MEK	-	-	Average fiber diameter: 3.32 ± 0.2 μm	[72]	Scaffold for nervous tissue repair
PVDF-TrFE (70/30)	MEK	...	C = 20% (w/v), V =2 5 kV, flow rate: 3 ml h^{-1}, rotating speed: 2500 rpm, d = 30 cm, annaling at 135°C for 96 h	Average fiber diameter: 1.53 ± 0.39 μm	[73]	Scaffold for nerve tissue engineering
PVDF	DMF	-	C = 20 w%, V = 25 kV, d= 15 cm, flow rate = 0.5 ml h^{-1}	Fiber diameter: 200 ± 96 nm	[74]	Skeletal muscle tissue engineering (muscle regeneration)
P(VDF-TrFE) (65/35%)	MEK	-	C = 12%–18% (w/v), V= 15–35 kV	Average fiber diameter of 970 ± 480 nm, mean pore diameter of 1.7 μm	[75]	Scaffolds for skin tissue engineering
polyurethane/ polyvinylidene fluoride (PU/ PVDF) (1/1)	THF/DMF (1:1 v/v)	-	C= 12% (w/v, g ml^{-1}), V = 15 kV, d = 20 cm, flow rate = 0.8 ml h^{-1}	Fiber diameter: 1.41 ± 0.32 μm, pore size of the scaffolds: 11.47 ± 1.14 μm, d_{33} = 11.24 ± 1.2 pC N^{-1}	[76]	Skin tissue engineering, wound healing application
P(VDF-TrFE) (65:35)	MEK	-	C = 15% and 25% (w/v)	Fiber diameter: 575 ± 139 nm, fiber alignments: 89% ± 10%, elastic modulus: 359.77 MPa, tensile strength: 21.42 MPa	[77]	Cardiovascular tissues using stem cells
P(VDF-TrFE)	MEK:DMF (1:2 v/v)	-	C = 3%, 5%, 7%, 9%, 11% (w/w), V= 20 kV, d = 16 cm, flow rate = 10 ml h^{-1}	Fiber diameter: 0.38 − 1.71 μm, tensile strength:15.3 MPa, Relative elongation %= 122	[78]	Tissue engineering
P(VDF-TrFE) (60:40 molar ratio, MW = 500,000 g mol^{-1})	Acetone	ZnO: 0%,–4% (w/w)	C = 14% (w/v), V =1 8 kV, d = 10 cm, flow rate: 1.5 ml h^{-1}	Average diameter: 1035 – 1227 nm	[79]	Tissue engineering scaffold
PVDF, Mw = 700000 g mol^{-1}	DMF	Ionic liquid [C$_2$mim] [NTf$_2$] = 0, 5 and 10 (w/w)	C =15/85 (w/v), V= 1.3 kV cm^{-1}, d=15 cm, flow rate = 0.5 ml min^{-1}, collector speed = 1000 rpm	Fiber diameter: 500– 700 nm	[80]	Tissue engineering scaffold
P(VDF-TrFE)	DMF	Fe$_3$O$_4$ NPs (size 15 nm)	C = 18% (w/w), V = 10 kV, d = 5 cm, flow rate: 1 ml h^{-1}	Fiber diameter: 288 nm	[67]	Tissue engineering

[Mw = molecular weight; d = working distance; C = concentration (polymer/solvent), v = volume, w = weight, V = potential, NP = nanoparticles, rpm =rounds per minute; Methyl ethyl ketone (MEK); Dimethylformamide (DMF); Tetrahydrofuran (THF); Dimethylacetamide (DMAc)].

Table 2.

Comprehensive list of piezoelectric polymeric fibers fabricated by electrospinning techniques for biological sensor applications.

Polymer	Solvent	Additive	Comments	Fiber properties	Ref.	Potential applications
PVDF (Mw =534,000 g·mol^{-1})	DMF:acetone (2:3 w/w)	-	C = 12% (w/w), V = 9–18 kV, d = 15 cm, flow rate = 0.01–0.04 ml min^{-1}, T = 22°C, humidity = 50% −60%	Fiber diameter: 20–800 nm	[94]	Flexible force sensors for sensing garment pressure, blood pressure, heartbeat rate, respiration rate and accidental impact on the human body
PVDF (Mw: 275,000)	DMF:acetone (8:2 v/v)	-	C = 15% (w/w), V = 13 kV, d = 15 cm, flow rate = 50 μL min^{-1}	Fiber diameter: 150 nm	[95]	Nanosensors
PVDF (M$_W$=141,000 g·mol^{-1})	DMF:acetone (3:2 w/w)	-	C = 18%, V = 6 kV, d = 4 cm, flow rate= 100 μl h^{-1}	Fiber diameter: 332 nm, maximal piezoelectric output voltage: 100–300 mV	[96]	Vibration sensor
PVDF (Mw~180 kDa)	DMF:acetone (7:3 v/v)	-	C = 27% (w/w), V = 15 kV, d = 15 cm, flow rate = 0.3 ml h^{-1}, rotating speed = 800 rpm	Average diameter: 417 ± 88 nm	[97]	Piezoelectric Sensors
PVDF (M$_W$: 275,000 g·mol^{-1})	DMF:acetone (4:6 v/v)	-	C = 20% (w/w), V = 15 kV, d = 15 cm, flow rate = 1 ml h^{-1}, speed = 100 rpm	Fiber diameter: 310 ± 60 nm	[98]	High-sensitivity acoustic sensors
P(VDF-TrFE) (55:45 and 77:23 molar ratios)	DMF:acetone (3:2 w/w)	-	C = 12% (w/v), V = 12 kV, flow rate = 1.6 ml h^{-1}	-	[99]	Flexible pressure sensors
P(VDF-TrFE) (65:35%)	MEK	-	C = 15% (w/w), V = 10 kV, d= 10 cm, flow rate = 0.5–0.9 ml h^{-1}	Fiber diameter: 360 nm, voltage response sensitivity = 50 V N^{-1}	[100]	Biosensor
P(VDF-TrFE) (75:25 w/w)	DMF:acetone (3:2 v/v)	-	C = 21% (w/w), V=30 kV, d= 6 cm, flow rate = 1 ml h^{-1}, speed = 4000 rpm	Fiber diameter: 260 nm, overall porosity of 65%	[101]	Flexible piezoelectric sensors
P(VDF-TrFE) (77:23 mol %)	-	-	V = 20 kV, flow rate = 1 ml h^{-1}, rotational speed = 1000 rpm	-	[102]	Flexible nano-generators and nano-pressure sensors
P(VDF-TrFE) (70:30 mol %)	DMF:acetone (40:60 v/v)	-	C = 14%, 18%, and 22% (w/v), V = 15 kV, d = 20 cm, flow rate = 0.2 ml min^{-1}	Fiber diameter= 520 nm to 1.5 μm	[103]	Flexible and stretchable piezoelectric sensor for wearable devices, medical monitoring

Polymer	Solvent	Additive	Comments	Fiber properties	Ref.	Potential applications
						systems, and electronic skin
P(VDF-TrFE)	MEK	-	V = 5 kV, d = 10 cm, flow rate = 300 μl h^{-1}	Average fiber diameter = 500 nm	[104]	Transducer for sensing application
PVDF (Mw=100,000 g·mol^{-1})	DMF	hydrated salt NiCl$_2$.6H$_2$O (NC) 0.5 (w/w)	C = 25% (w/w), V = 15 kV, d= 15 cm, flow rate = 0.9 ml h^{-1}	β phase fraction of (PVDF NC): 0.92	[105]	Sensors which can be used in health monitoring and, biomedical applications
PVDF	DMF:acetone (60:40 w/w)	BaTiO3 NPs	C = 20% (w/w), V = 8 kV, d = 22 cm, rotating speed = 162 rpm	Fiber diameter: 200 nm	[106]	Wearable smart textiles and implantable biosensors
P(VDF-TrFE) (75:25)	DMF:acetone (1:1 v/v)	(0.78Bi0.5Na0.5TiO$_3$– 0.22SrTiO$_3$) ceramic	V = 10 ~ 15 kV, d =10 cm, flow rate = 1.0 ml h^{-1}	Fiber diameter: 100– 300 nm.	[107]	Frequency sensor applications
P(VDF–TrFE) (60:40) (Mw= 500,000 g·mol^{-1})	Acetone	ZnO NPs (1%, 2% and 4% w/w)	C = 14% (w/w), V = 18 kV d= 10 cm, flow rate = 1.5 ml h^{-1}, rotating velocity = 1000 rpm	Incorporation of ZnO NPs enhanced the formation of β phase	[108]	Acoustic biosensors
PVDF (Mn=543,600)	DMF:acetone (2:3 w/w)	Silver nanowires (1.5%)	C = 15% (w/v), V = 12 kV, d = 16 cm, flow rate = 1 ml h^{-1}	Fiber diameter: 200– 500 nm, d$_{33}$ = 29.8 pC N^{-1}	[109]	Human-related applications such as force sensors
PVDF	DMSO:acetone (1:1 w/w)	MWCNTs (0.03% and 0.05% w/w)	C =1 6%, 18%, 20% (w/w), V = 1×10^7 V m^{-1}, flow rate = 0.001 ml min^{-1}, rotating velocity = 900 rpm	Fiber diameter: from 200 nm to few μm	[110]	Highly durable wearable sensor applications
P(VDF-TrFE)	DMF:acetone (1:1 v/v)	Grapheme (rGO) (80:20 w/w)	C = 20% (w/w), V = 10 kV, d = 10 cm	High sensitivity (15.6 kPa^{-1}), low detection limit (1.2 Pa)	[111]	Highly sensitive piezo-resistive pressure sensors
Composite of (PVDF) and poly(aminophenylboronic acid) (PAPBA)	DMF:acetone (7:3 v/v)		Flow rate = 10 ml h^{-1}, V = 25 kV, d = 15 cm	Fiber diameter 150 nm	[112]	Biosensor
Core-shell: The core = (poly(3,4-ethylene dioxy thiophene) poly(styrene sulfonate) and poly vinyl pyrrolidone (PVP), The shell: P(VDF-TrFE) (70:30)	DMF for core and DMF:MEK (25:75) for shell	-	The core and shell solutions were kept at flow rates of 1 and 3 ml h^{-1}, respectively. Shell concentration: 14% (w/v)	-	[113]	Sensors for endovascular applications
P(VDF-TrFE) (75:25), polyaniline-polystyrene sulfonic acid Marı (PEDOT-PSS)	DMF	-	C = 1%, 3%, 5%, 7%, 9%, 11%, 13%, 15% (w/w), V = 10 kV and d = 15 cm.	-	[114]	Sensor
PVF2-TrFE (75:25), poly(3,4-thylenedioxthiophene)-poly(styrene sulfonate), (PEDOT-PSS)	DMF	-	C = 13%, 10%, 7%, 5%, 3% (w/w), V= 8–10 kV	-	[115]	Supersensitive sensors

Polymer	Solvent	Additive	Comments	Fiber properties	Ref.	Potential applications
PVDF	DMF:acetone (3:1 v/v)	-	C = 15 w%, d = 3 cm, V = 10 kV, rotating velocity = 60 rpm	Open-circuit voltage generated from active sensor was around 70 mV	[116]	Wearable self-powered sensor

[Mw = molecular weight; d = working distance; C = concentration (polymer/solvent), v = volume, w = weight, V = potential, NP = nanoparticles, rpm =rounds per minute; Methyl ethyl ketone (MEK); Dimethylformamide (DMF); Dimethylsulfoxide (DMSO)].

Table 3.

Comprehensive list of piezoelectric polymeric fibers fabricated by electrospinning techniques for energy harvesting applications.

Polymer	Solvent	Additive	Comments	Fiber properties	Ref.	Potential applications
PVDF(Mw = 172,000)	DMF:acetone (4:6 v/v)	-	C = 16% (w/w), V = 40–60 kV, d = 16 cm, rotating speed = 100 rpm	Fiber diameter: 539 nm	[19]	Energy harvesting application
PVDF (Mw = 275,000)	DMF:acetone (4:6 v/v)	-	C = 16%, 20%, 26%, V=9, 15, 21 kV, d = 15 and 17 cm, flow rate = 1 ml h^{-1}	Fiber diameter: 230–810 nm	[122]	Energy harvesting application
PVDF	DMF:acetone (6:4 w/w)	-	C = 12%, 18%, 22% (w/w), V=15 kV, d = 20 cm, feed rate = 0.05 ml min^{-1}.	Fiber diameter: 70– 400 nm	[123]	Energy generators and harvesters
PVDF (Mw = 46,000 g·mol^{-1})	DMF:acetone	-	V = 18 kV, d = 15 cm, flow rate = 0.5 ml h^{-1}, speed = 400 rpm	Fiber diameter: 124 nm	[124]	Energy harvesting application
PVDF	DMAC:acetone (4:6 v/v)	-	C = 16% (w/w), V = 30 kV, d = 12 cm, flow rate = 1.0 ml h^{-1}	PVDF	[125,126]	*In vivo* biomechanical energy harvesting and human motion monitoring
P(VDF-TrFE) (70:30)	DMF:acetone	-	P(VDF-TrFE):DMF:acetone 20:56:24 (w/w/w), V = 28 kV, d = 14 cm, flow rate = 150 μl h^{-1}, speed= 4100 rpm	Fiber diameter: 509 nm	[12]	Energy harvesting devices
P(VDF–TrFE) (70:30)	DMF:acetone (3:7 v/v)	-	C = 20%, V= 25 kV, d = 25 cm, speed: 120 and 4300 rpm	Fiber diameter: 200–600 nm, coil diameter: 306 μm, yarn diameter: 175 μm, d$_{33}$ = 37–48 pmV^{-1}	[128]	Energy harvesting application
P(VDF–TrFE) (70:30)	-	-	C = 20 w%, V = 28 kV, d = 20 cm, flow rate = 170 μl h^{-1}, rotational speed: 5500 rpm	-	[129]	Energy harvesting application
P(VDF–TrFE) (70:30)	DMF:acetone (8:2)	-	Electrospinning + hot-pressing, C = 12% and 18% (w/w), V = 15 kV, d = 15 cm	Porous membranes with d$_{33}$: 13.7 for C = 18% (w/w) and d$_{33}$: 11.2 for C = 12% (w/w)	[127]	Energy harvesting application
PVDF	DMF:acetone (6:4 w/w)	Inorganic salts	C = 10% (w/w), V = 18 kV, d = 15 cm, flow rate = 1 ml h^{-1}	-	[130]	Energy-scavenging devices and portable sensors
PVDF	DMF	BaTiO$_3$/PVDF 1:10 (w/w)	V = 15 kV, d = 10–15 cm, feeding rate = 0.5 ml h^{-1}	Fiber diameter: 110.4 ± 48.2 nm	[131]	Energy harvesting application
PVDF	DMF	BaTiO$_3$ 30% (w/w) of the total PVDF	C = 18% (w/w), V = 18 kV, d = 15 cm, flow rate= 0.12 ml min^{-1}	Fiber diameter of BaTiO$_3$: 110 ± 40 nm, d$_{33}$= 50 pmV^{-1}	[132]	Energy harvesting application
PVDF (Mw = 172,000)	DMF:acetone (8:2 w/w)	NaNbO$_3$ (mass ratio 5:100)	C = 18% (w/w), V = 25 kV, d = 15 cm	-	[133]	Energy harvesting application

Polymer	Solvent	Additive	Comments	Fiber properties	Ref.	Potential applications
PVDF	DMSO	$(Na0.5K0.5)NbO_3$ (NKN) 50wt%	V = 18 kV, d = 10 cm, flow rate: 1.5 ml h^{-1}	d_{33} after poiling: 25 pC N^{-1}	[118]	Sensors in ubiquitous networks
P(VDF-TrFE) (70:30)	DMF:MEK (7:3 v/v)	0 up to 20% ceramic content (w/w)	C = 15% (w/w), V = 20 and 35 kV, d = 10–30 cm, flow rate: 0.5–8.0 ml h^{-1}	Fiber diameter: 469 ± 136 nm	[134]	Energy harvesting application
PVDF (Mw = 495,000 g·mol^{-1})	DMF	Cellulose nanocrystal PVDF/CN (C = 0%, 1%, 3%, 5% w/w)	C = 13% (w/w), V = 15 kV, d = 15 cm, flow rate = 1 ml h^{-1}	Average diameter: 0.439–0.559 μm, electrical conductivity: 5.82–60.17 μS	[135]	Energy harvester application
P(VDF-TrFE) 65:35 (w/w%)	DMF	MWNTs	V = 20 kV, d = 7 cm	Fiber diameter: 500 nm to 1 μm, of MWNTs	[136]	Smart fabric with applications in energy harvesting
PVDF (Mw = 534,000 g·mol^{-1})	DMF:acetone (4:6)	ZonylUR as fluoro surfactant	C = 4%, 16%, 80% (w/w), V = 15 kV, d = 15 cm, flow rate = 0.5 ml h^{-1}, rotating speed = 800 rpm	Fiber diameter: 84.6 ± 23.5 nm, β-phase fraction: 80%, d_{33} = −33 pC N^{-1}	[137]	Energy generator
PVDF (Mw = 46,000)	DMF:acetone (70:30 v/v)	-	C = 20 % w/w, V = 15 kV, d = 15 cm, flow rate = 0.5 ml h^{-1}, rotational speed = 180 rpm	Fiber diameter: 124 nm, electrical output: 1 V	[138]	Nano generator for designing flexible power source for smart and wearable electronic textiles applications
PVDF	DMF:acetone (6:4 w/w)	-	C = 10% (w/w), V = 20 kV, d: 15 cm, flow rate = 1 ml h^{-1}	-	[139]	Nano-generator
PVDF (Mw = 46,000 g.mol^{-1})	Acetone:DMF (4:6 v/v)	-	C = 26% (w/w), V=20 kV, d = 15 cm, flow rate = 0.5 ml h^{-1}, rotating speed: 216 rpm	Fiber diameter: 812 ± 123 nm, output voltage: 0.028 V	[140]	Nano-generator
PVDF	DMF	-	-	Fiber diameter: 183 ± 37 nm, voltage output: 4 V	[141]	Nano-generator
PVDF (Mw = 534000)	DMF:acetone (3:7 v/v)	-	C = 15% (w/w), V = 12 kV, d = 15 cm, feed rate: 50 ml min^{-1}	-	[142]	Nano-generator for concurrently harvesting biomechanical and biochemical Energy
P(VDF-TrFE) (55:45)	DMF:acetone (45:55 w/w)	-	C = 15% (w/w), V = 10 kV, d = 10 cm, flow rate = 0.4 ml h^{-1}.	-	[143]	Nano-generator
PVDF (Mw = 534,000 g·mol^{-1})	DMF:acetone (4:6 v/v)	(ZnO, CNT, LiCl, PANI)	C = 16% (w/w), d = 20 cm, flow rate= 0.3 ml h^{-1}, rotational speed: 180 rpm	Fiber diameter: 504.89 nm-39.69 μm	[144]	Nano-generator
PVDF (Mw = 534,000 g mol^{-1})	DMF:Acetone (6:4 v/v)	LiCl	C = 16% (w/w), V = 20 kV, d = 20 cm, flow rate = 0.3 ml h^{-1}	Coupling coefficient e_{31} = 189.68 and e_{33}= 534.36	[145]	Nano-generator
PVDF	-	-	Near-field electrospinning	Fiber diameter: 500 nm to 6.5 μm	[146]	Nano-generator

Polymer	Solvent	Additive	Comments	Fiber properties	Ref.	Potential applications
PVDF	-	-	Near-field electrospinning	Fiber diameter: 900 nm to 2.5 μm	[147]	Nano-generator
PVDF/ PMLG (poly (γ-methyl L-glutamate))	-	-	Near-field electrospinning V=10–16 kV, d= 1–2 mm	Output voltage: 0.019–0.185 V, energy conversion efficiency is 3.3%	[148]	Energy harvester
PVDF	DMF	-	Hollow cylindrical near-field electrospinning (HCNFES), C = 18% (w/w), V = 10–16 kV, d = 0.5 mm, rotational speed = 900 and 1900 rpm	200 nm to 1.16 μm	[146]	Energy harvester

[Mw = molecular weight; d = working distance; C = concentration (polymer/solvent), v = volume, w = weight, V = potential, NP = nanoparticles, rpm =rounds per minute; Dimethylformamide (DMF); Dimethylsulfoxide (DMSO)].

Table 4.

Overview of piezoelectric ceramic nanofibers for bio-applications.

Ceramic	Precursor, polymer	Fabrication method	Fiber properties	Ref.	Potential applications
$BaTiO_3$	Barium titanium, ethylhexano-propoxide, acetyl acetone, PVP	Sol-gel calcination in air at 500 °C and 700 °C for 3 h	Ribbon-like nanofibers ~200 nm in width and ~75 nm in thickness with grain sizes < 30 nm	[151]	Ferroelectric and piezoelectric sensors
$BaTiO_3$	Barium acetate hydrate and titanium n-butyloxide, catechol $(C_6H_4(OH)_2)$ as the stabilized agent to reduce hydrolysis of titanium n-butyloxide	Co-electrospinning, Sol-gel, aging for 1–2 days, calcination at 1000°C for 2 h in air	Fiber diameters: 500 nm to 4 µm	[152]	Actuator and sensor applications in composite materials
$BaTiO_3$	Barium acetate, tetrabutyl titanium, PVP	Sol-gel, annealing at 800 °C for 2 h in open air	Fiber diameter: 80–200 nm	[153]	Humidity sensor
$BaTiO_3$	Barium acetate, tetrabutyl titanate, PVP	Sol–gel, calcination at 750°C for 2 h	Fiber diameter: hundreds nanometers, $d_{33} = 20$ pmV^{-1}	[154]	Transducers
$BaTiO_3$	Barium acetate, titanium isopropoxide, PVP	Sol-gel, annealing at 750 °C for 12–16 h	Fiber diameter: 30 nm	[155]	Transducers
$BaTiO_3$	Barium carbonate, titaniumisopropoxide, PVP	Sol-gel, calcination at 1000 °C	Fiber diameter: 50–400 nm	[30]	Ferroelectric random access memory
$BaTiO_3$	Barium acetate, titanium isopropoxide, PVP	Sol-gel	Fiber diameter: 180 nm, $d_{33} = 15.5$ pmV^{-1}	[156]	High-density ferroelectric random access memories
$BaTiO_3$	Barium acetate, titanium isopropoxide, PVP	Sol-gel, annealing at (700, 800 and 900 °C) for 1 h	Fiber diameter: 100–300 nm	[157]	Ferroelectric random access memory
$BaTiO_3$	Barium acetate, titanium isopropoxide, PVP	Sol-gel	Fiber diameter: 150–400 nm, effective piezoelectric coefficient: 20 pmV^{-1} for a 250 nm fiber	[158]	Ferroelectric random access memory cells, tissue bio-imaging
$BaTiO_3$	Barium acetate, tetrabutyl titanate, PVP	Sol-gel annealing at500, to 800°C for 10 h, as well as at 600°C for 1, 2, 5, 8, 10, 15, and 20 h	Fiber diameters: 92 nm to 182 nm	[159]	-
$BaTiO_3$	Barium acetate, titanium isopropoxide, PVP	Sol-gel, annealing at 750 °C for 2 h	Fiber diameters ~ 100–200 nm, Effective piezoelectric constant ~40 pmV^{-1}	[160]	-

Ceramic	Precursor, polymer	Fabrication method	Fiber properties	Ref.	Potential applications
$BaTiO_3$	Barium acetate, titanium isopropoxide, PVP	Sol-gel, first annealing at 450°C for 3 h and second annealing at 580 °C to 750 °C for 6 to 48 h	Fibers diameter: 50 nm	[161]	-
Ce-doped $BaTiO_3$	Stoichiometric barium acetate, tetrabutyl titanate, cerium nitrate hexahydrate, PVP	Sol–gel, annealing at 750 °C for 10 h	Fiber diameter: 100 − 200 nm, d_{33}: 42 pm V^{-1}	[121]	Energy harvesting device
$Ba_{0.6}Sr_{0.4}TiO_3$ (BST)	Titanium(diisopropoxide) bis(2,4-pentanedionate), barium acetate, strontium acetate, PVP	Sol-gel, calcination at 700 °C in air for 2 h	Fiber diameter: 188 ± 25 nm	[162]	Nanosensors
$BaSrTiO_3$	Barium strontium titanate, PVP	Sol-gel, calcination at 650–800 °C for 2 h	Fiber diameter: 150–210 nm	[163]	Nanoscale capacitors for high density dynamic random access memory and ferroelectric random access memory
$Ba_{0.8}Sr_{0.2}TiO_3$	Barium acetate, strontium acetate, PVP	Sol-gel, calcination at 800 °C for 2 h	Fiber diameter: 100 nm	[164]	Humidity sensor
$Ba_{0.6}Sr_{0.4}TIO_3$	Barium acetate, strontium acetate hemihydrate, PVP	Sol-gel, annealing at 650 °C for 3 h	Fiber diameter: 100–200 nm	[165]	-
$Ba(Ti_{0.8}Zr_{0.2})O_3$-0.5($Ba_{0.7}Ca_{0.3}$)TiO_3	-	-	Fiber diameter: 200 nm d_{33} = 180 pmV^{-1}	[166]	Low-dimensional piezoelectric devices
$(Ba_{0.85}Ca_{0.15})(Ti_{0.9}Zr_{0.1})O_3$ (BCTZ)	Barium acetate, calcium acetate, titanium isopropoxide, zirconiumpropoxide, PVP	Sol-gel, calcination in air at 800°C for 1 h in air	Fiber diameter: 200 nm	[167]	Piezoelectric nano-generators and nano-sensors in nano-devices for energy harvesting
$(Ba_{0.95}Ca_{0.05})(Ti_{0.92}Sn_{0.08})O_3$ (BCTS)	Barium carbonate, calcium acetate, tin chloride, titanium-isopropoxide, PVP	Sol-gel, calcination at 1150°C for 2 h	Fiber diameter: 80–275 nm, d_{33} = 398 pC N^{-1}	[168]	Humidity sensors
$0.5Ba(Zr_{0.2}Ti0.8)O_3–0.5(Ba_{0.7}Ca_{0.3})TiO_3$	Tetrabutyl titanate, barium hydroxide, calcium hydroxide, zirconium acetylacetonate, PVP	Sol-gel, sintering at 700 °C for 3 h	Fiber diameter: 175 nm	[169]	High performance nano-generators (NGs), energy harvesting
$(Na_{0.5}Bi_{0.5})0.94TiO_3–Ba_{0.06}TiO_3$ (NBT-BT6)	Barium acetate, bismuth acetate, sodium acetate, tetrabutyl titanium, PVP	Sol-gel, calcination at 700 °C for 1 h	Fiber diameter: 150– 300 nm, d_{33} = 102 pmV^{-1}	[31]	Nanoscale lead-free piezoelectric devices in MEMS applications.
$Na_{0.5}Bi_{0.5}TiO_3$ (NBT)	PVP	Sol-gel, calcination at 800 °C in air for 90 min	Fiber diameter: 30–200 nm, d_{33} = 89 pmV^{-1}	[170]	Transducers
$(Na_{0.82}K_{0.18})0.5Bi_{0.5}TiO_3$	Bismuth nitrate, potassium nitrate, natrium acetum, titanium butoxide, PVP	Sol-gel, nanofibers dried at 120 °C for 8 h, followed by heating at 400°C	Fiber diameter: 150–600 nm,	[171]	Micro-electro-mechanical systems (MEMS)

Ceramic	Precursor, polymer	Fabrication method	Fiber properties	Ref.	Potential applications
		for 1 h and then calcining at 700 °C	average d_{33} = 96 pmV^{-1}		
$(Na_{0.82}K_{0.18})0.5Bi_{0.5}TiO_3$	Bismuth nitrate, potassium nitrate, natrium acetum, titanium butoxide, PVP	Sol–gel, nanofibers were dried at 120 °C for 8 h, followed by heating at 400 °C for 1 h and then thermal calcined at 700 °C for 1 h	Fiber diameter: 100–500 nm	[172]	MEMS application
$Na_{0.5}Bi_{0.5})0.94TiO_3–Ba_{0.06}TiO_3$ (NBT–BT6)	Barium acetate, bismuth acetate, sodium acetate, tetrabutyl titanium, PVP	Sol–gel, calcination in air at 700 °C for1 h	Fiber diameter: 110 nm	[173]	Humidity sensor
Cerium-substituted bismuth titanate (BCT)	Bismuth nitrate, cerium nitrate, and titanium butoxide, PVP	Sol–gel, annealing in air for 1 h at 750 °C	Fiber diameter: 100 nm to 200 nm, d_{33} = 158 pmV^{-1}	[174]	Energy harvesting devices, lead-free nonvolatile memory devices.
$Bi_{3.15}Nd_{0.85}Ti_3O_{12}$ (BNT)	BNT precursor, PVP	Sol-gel, Calcination at 800 °C in air for 90 min	Fiber diameter: 30–200 nm, d_{33} = 89 pmV^{-1}	[175]	Transducers
$Bi_{3.25}La_{0.75}Ti_3O_{12}$, (BLT)	Bismuth nitrate, lanthanum nitrate, Tetrabutyl titanate, PVP	Sol–gel, annealing at 700 °C in air for 1 h	Fiber diameter: 100–300 nm, d_{33} = 101 pmV^{-1}	[176]	Nanoscale nonvolatile memory devices.
$Bi_{3.15}Nd_{0.85}Ti_3O_{12}$, (BNT)	Bismuth nitrate, neodymium nitrate, titanium butoxide, PVP	Sol-gel, Calcination in air for 1 h at 700°C	Fiber diameter: 70–160 nm	[177]	Memory applications
$Bi_4Ti_3O_{12}$	$Bi(NO_3)3.5H_2O$, tetrabutyltitanate (TBT), PVP	Sol-gel, calcination at 400, 500, 600, 700 and 800 °C in air for 30 min	Fiber diameter: 30–50 nm	[178]	Semiconductor photocatalysts
$BiFeO_3$	Bismuth nitrate, iron nitrate, PVP	Sol-gel, thermal annealing at 550 °C for 2 h in air	Fiber diameter: 100–300 nm	[179]	-
$Bi_5Ti_3FeO_{15}$ and $Bi_5-xLa_xTi_3FeO_{15}$ (x=0, 1)	$Bi(NO_3)_3·5H_2O$, TBT, $La(NO_3)_3·6H_2O$, $Fe(NO_3)_3·9H_2O$, PVP	Sol-gel, Calcination at 300 °C for 2 h in oxygen atmosphere and 600 °C for 2 h in the protection of nitrogen atmosphere	d_{33} = 39.11 pmV^{-1}	[180]	Biocompatible piezoelectric nano-generators *in vivo* applications
$LiNbO_3$	Niobium ethoxide, lithium hydro-xide, PVP	Sol-gel, annealing at 700 °C for 6h	Fiber diameter: 100–300 nm	[181]	-
$(Na_{0.5}K_{0.5})NbO_3$ (NKN)	Potassium acetate and sodium acetate, niobium ethoxide, PVP	Sol-gel, annealing at 800°C for 1 hour in air	Fiber diameter: 50–100 nm	[166]	Scaffolds for engineering, repair, and regeneration of damaged tissue.
$(Na,K)NbO_3$	Sodium acetate, potassium acetate, niobium ethoxide, PVP	Sol-gel, annealing at 800 °C for 1 h	Fiber diameter: 50–200 nm	[182]	Biocompatible material for implants
$(Na,K)NbO_3$	Sodium and potassium acetates, niobium ethoxide, PVP	Sol-gel, drying at 100 °C in nitrogen atmosphere for 12	d_{33} = 18.3 – 75.8 pmV^{-1}	[183]	Scaffolds for tissue engineering and

Ceramic	Precursor, polymer	Fabrication method	Fiber properties	Ref.	Potential applications
		h, and annealing at 800 °C for 1 h in air			for energy harvesting biocompatible nano-generators
Mn-doped $(Na_{0.5}K_{0.5})NbO_3$ (NKN)	Potassium acetate, sodium acetate, niobium ethoxide, manganese acetate tetrahydrate, PVP	Sol-gel, annealing at 750 °C for 1 h.	Fiber diameter ~130 nm, d_{33} = 40.06 pmV^{-1}	[184]	Nano-generators
Nb_2O_5	Niobium ethoxide, acetic acid in ethanol, PVAC	Sol–gel, high temperature calcination	Fiber diameter: 0.5–1 μm	[185]	-
ZnO	Zinc acetate, PVA, H_2O	Sol-gel, calcination at 500°C in air for 4,6, 8, and 10 h	Fiber diameter: 300–800 nm	[186]	-
ZnO	PVA, H_2O, Zinc acetate	Sol-gel, calcination at 700 °C for 5 h	Fiber diameter: 50–100 nm	[187]	-
$Zn_{0.975}V_{0.025}O$ V-ZnO	Zinc acetate, vanadyl acetylacetonate, PVP	Sol-gel, calcination at 700 °C	Fiber diameter: 50–300 nm	[188,189]	MEMS
Hydroxy apatite on TiO_2	Titanium isopropoxide, PVAc, SBF.	On TiO_2 nanofiber SBF fluid treated	-	[190]	Biomedical applications such as dental and bone implants
TiO_2	$Ti(OiPr)_4$, PVP	Sol–gel, removal of PVP by calcination makes hollow anatase nanofibers	Hollow fibers	[191]	-
V_2O_5-TiO_2-Ta_2O_5	$Ti(OiPr)_4$, $VO(OiPr)_3$, hexadecyltrimethylammonium bromide (HTAB), PVP	Calcination at 425 °C for 6 h	Nanofibers with hierarchical structures	[192]	-
ZnO/ TiO_2	$Ti(OBu)_4$, $Zn(Ac)_2$–$C_6H_{12}N_4$–H_2O	Sol, calcination at 500 °C	Hierarchical structure nanofibers	[193]	Supercapacitors

[PVA = polyvinyl alcohol; PVP = polyvinylpyrrolidone; SBF = simulated body fluid].

Table 5.

List of piezoelectric polymeric fibers fabricated by different electrospinning approaches.

Polymer	Solvent	Additive	Production condition	Fiber properties	Ref.	Electrospinning Method
PVDF (Mw= 534.000)	Dimethyl sulfoxide (DMSO:acetone 1:1 w/w)	-	C=16% (w/w), V=1.1 kV, d=1-mm, flow rate = 35 mm s^{-1}	Single fiber diameter: 550 nm, d$_{33}$ = −57.6 pmV^{-1}	[149]	Near-field electrospinning
PVDF (Mw = 534,.000)	DMSO:acetone	MWCNT	C = 16%, 18 %, 20% (w/w), V = 1.2 kV, d = 0.5–1.0 mm	Fiber diameter: 0.7–1 μm	[212]	Near-field electrospinning
PVDF	-	-		Flow sensing sensitivity: 83.3 mV/(m/s)	[117]	Near-field electrospinning
PVDF (Mw = 5.2·10^5)	Acetone: N,N-dimethylacetamide (DMAc)	--	C = 17% (w/w), V = 15 kV, d = 12 cm	Porous fiber diameter: (0.75 − 1.63 μm)	[213]	Far-field electrospinning
PVDF	DMF	-	C = 20% (w/w), V= 25 kV, d = 15 cm	Fiber diameter: 400 nm, fraction of β phase: 70%	[214]	Far-field electrospinning
PVDF (Mw = 4·10^5 g·mol^{-1})	DMF:acetone	-	C = 15% (w/w), V = 1 5, 20 kV, flow rate: 0.003 ml min^{-1}	Fiber diameter: 127–244 nm	[215]	Far-field electrospinning
PVDF (Mw= 107,000)	DMF:DMAc (1:1)	-	C = 20%, V = 20 kV, d = 20 cm	-	[219]	Far-field electrospinning
PVDF	DMF:acetone (8:2 v/v)	-	C = 15% (w v^{-1}), V = 5 kV, d = 10 −20 cm, flow rate = 0.3 ml h^{-1}	The average fiber diameter: 172 ± 89 nm	[216]	Far-field electrospinning
PVDF	DMF:acetone (1:4 v/v)	-	C = 15% (w/w), V = 10, 13, 16, 19, 22 kV, d = 15 cm	Fiber diameter: 578.4 to 978.6 nm	[217]	Far-field electrospinning
PVDF (Mw=687000)	DMF	-	C = 10%−20% (w/w), V = 7 and 20 kV, d = 15 cm, flow rates: 0.8 to 1.5 ml h^{-1}	Fiber diameter: 120–1000 nm Maximum fraction of β phase: 0.75	[218]	Far-field electrospinning
PVDF	DMF and DMF: acetone (3:1 v/v)	-	C = 5%, 7%, 10%, 15% (w/w), d = 3 cm, V = 10 kV, angular velocity: 60 rpm	Fiber diameter: 330 to 540 nm	[220]	Far-field electrospinning
PVDF (Mw= 172 000)	DMF:acetone (4:6 v/v)	-	C = 10% (w/w), rotating speed = 300 rpm, d = 15 cm, V =1 4–18 kV, flow rate: 0.5–3 ml h^{-1}	-	[221]	Far-field electrospinning
PVDF(Mw = 115 000)	DMF:acetone (60:40 w/w)	Surface-oxidized SWCNTs and MWCNTs	C = 20/80 (w/w), v = 15 kV, flow rate:0.25 ml h $^{-1}$, rotating speed = 1500 rpm.	-	[222]	Far-field electrospinning
PVDF (534,000 g mol^{-1})	DMF:acetone (6:4 v/v)	LiCl (0.00133 wt%)	C=16% (w/w), V=20 kV, d = 20 cm, flow rate = 0.3 ml h^{-1}, rotating speed: 800, 1000, 1500, and 2000 rpm	Fiber diameter: 65 nm	[223]	Far-field electrospinning
PVDF(Mw =172 000)	DMF:acetone (4:6 v/v)	-	C = 16% (w/w), V = 40 to 60 kV, d = 16 cm, rotating speed: 100 rpm	Fiber diameter: 539 nm	[19]	Needleless electrospinning

Polymer	Solvent	Additive	Production condition	Fiber properties	Ref.	Electrospinning Method
PVDF	-	-	Temperature of fluid: 189 ± 2 °C, V: $+2.70 \pm 0.08$ kV, working distance: 4.0 ± 0.5 mm, collector speeds: 1800 to 5000 mm min^{-1} (at 400 mm min^{-1} increments)	Fiber diameter: 17–55 μm, d_{33} ~19 pmV^{-1}	[224]	Melt-electrospinning
PVDF	DMF:acetone (60:40 w/w)	-	C = 20% (w/w), V = 12 kV dc, d= 20 cm, speed= 200 rpm	Fiber diameter =224 nm	[225]	Centrifugal electrospinning system
PVDF	DMF:acetone (60:40, 70:30 and 80:20 (w/w))	Tetrabutyl ammonium chloride (TBAC)	C = 15 and 20 %w, V=15 or 21 kV, d=15 cm	The addition of 3% (w/w) of TBAC into the polymer solution led to almost pure β-phase in the fibers.	[226]	Far-field electrospinning with rotating ring collector
PVDF, P(VDF-TrFE) 70:30 mol%	DMF:acetone (60:40 w/w)	MWCNT	C = 20% (w/w), V = 15 kV, flow rate: 0.25 ml h^{-1}, rotating speed: 1500 rpm	-	[227]	Electrospinning with rotating ring collector
PVDF	DMF:acetone (6:4 w/w)	-	C = 15% (w/w), V= 20 kV, d = 15 cm, flow rate = 0.033 ml min^{-1}	Fiber diameter: 100 nm, β content = 80.67%	[228]	Electrospinning on water method
PVDF (Mw =500,000)	DMAc	-	C = 20%, 25% (w/w), V = 6–12 kV, d = 3–6 in, flow rate = 3–5 ml h^{-1}	Yarn diameter: 5–200 μm	[229]	Electrospinning on water method
PVDF-co-hexafluoropropylene) (PVDFHFP)	DMF:acetone (1:1 v/v)	-	C = 17.0%, V = 7 kV, flow rate: 3.0 ml h^{-1}, winding speed= 72 m h^{-1}	Tensile strength: 93.6 MPa elongation at break: 242.6%	[230]	-
The core = poly(3,4-ethylene dioxy thiophene), poly(styrene sulfonate) and poly vinyl pyrrolidone (PVP), The shell: P(VDF-TrFE) (70:30)	DMF for core and DMF:MEK (25:75) for shell	-	The core and shell solutions were kept at flow rates of 1 and 3 ml h^{-1}, respectively. Shell concentration: 14% w/v	-	[113]	Co-electrospinning
(PVDF)/polycarbonate	DMF:THF	-	V = 12 kV, d = 15 cm, flow rate: 0.4 ml h^{-1}	-	[231]	Co-electrospinning
PVDF	DMAc	NaCl	C = 22% - 28% (w/w), V = 12– 18 kV, d = 15 cm, flow rate: 0.050 mm min^{-1}	Addition of NaCl improved the morphology and uniformity of the resultant PVDF fibers	[232]	Far-field electrospinning
PVDF (Mw=687 000)	DMF	$Ni_{0.5}Zn_{0.5}Fe_2O_4$ nanoparticles	C = 10%–20% (w/w), V = 7 and 20 kV, d = 15 cm, flow rate = 0.4 to 1.5 ml h^{-1}	-	[233]	Far-field electrospinning
PVDF (Mw = 141000)	DMAc	Anionic and cationic fluorinated surfactant (0 to 0.5 w %)	C = 26% (w/w), V = 15 kV, d = 12 cm, , flow rate = 2 ml min^{-1}	-	[234]	Electrospinning

[Mw = molecular weight; d = working distance; C = concentration (polymer/solvent), v = volume, w = weight, V = potential, NP = nanoparticles, rpm =rounds per minute; Dimethylformamide (DMF); Dimethylacetamide(DMAc, Dimethylsulfoxide (DMSO), Tetrahydrofuran (THF); Methylethylketone (MEK)].